

Lawrence Berkeley National Laboratory

Recent Work

Title

THE EFFECT OF STACKING FAULT ENERGY ON THE STRAIN INDUCED MARTENSITE TRANSFORMATION AND TENSILE CHARACTERISTICS IN IRON BASED ALLOYS

Permalink

<https://escholarship.org/uc/item/9hj815cn>

Author

Dunning, John S.

Publication Date

1969-12-01

c.2

RECEIVED
LAWRENCE
RADIATION LABORATORY
FEB 3 1970
LIBRARY AND
DOCUMENTS SECTION

THE EFFECT OF STACKING FAULT ENERGY ON THE STRAIN
INDUCED MARTENSITE TRANSFORMATION AND TENSILE
CHARACTERISTICS IN IRON BASED ALLOYS

John S. Dunning
(Ph. D. Thesis)

December 1969

AEC Contract No. W-7405-eng-48

TWO-WEEK LOAN COPY

*This is a Library Circulating Copy
which may be borrowed for two weeks.
For a personal retention copy, call
Tech. Info. Division, Ext. 5545*

LAWRENCE RADIATION LABORATORY
UNIVERSITY of CALIFORNIA BERKELEY

1970

DISCLAIMER

This document was prepared as an account of work sponsored by the United States Government. While this document is believed to contain correct information, neither the United States Government nor any agency thereof, nor the Regents of the University of California, nor any of their employees, makes any warranty, express or implied, or assumes any legal responsibility for the accuracy, completeness, or usefulness of any information, apparatus, product, or process disclosed, or represents that its use would not infringe privately owned rights. Reference herein to any specific commercial product, process, or service by its trade name, trademark, manufacturer, or otherwise, does not necessarily constitute or imply its endorsement, recommendation, or favoring by the United States Government or any agency thereof, or the Regents of the University of California. The views and opinions of authors expressed herein do not necessarily state or reflect those of the United States Government or any agency thereof or the Regents of the University of California.

RECEIVED
LAWRENCE
RADIATION LABORATORY

FFB 3 1970

LIBRARY AND
DOCUMENTS SECTION

THE EFFECT OF STACKING FAULT ENERGY ON THE STRAIN
INDUCED MARTENSITE TRANSFORMATION AND TENSILE
CHARACTERISTICS IN IRON BASED ALLOYS

John S. Dunning
(Ph. D. Thesis)

December 1969

AEC Contract No. W-7405-eng-48

TWO-WEEK LOAN COPY

*This is a Library Circulating Copy
which may be borrowed for two weeks.
For a personal retention copy, call
Tech. Info. Division, Ext. 5545*

LAWRENCE RADIATION LABORATORY
UNIVERSITY of CALIFORNIA BERKELEY

247

THE EFFECT OF STACKING FAULT ENERGY ON THE STRAIN INDUCED MARTENSITE TRANSFORMATION AND TENSILE CHARACTERISTICS IN IRON BASED ALLOYS

John S. Dunning

Inorganic Materials Research Division, Lawrence Radiation Laboratory
Department of Materials Science and Engineering of the College of Engineering
University of California, Berkeley, California

ABSTRACT

Two series of iron based alloys, one carbonless the second containing carbon were designed such that a regular variation of stacking fault energy (S.F.E.) in the range 10-50 ergs cm⁻² was obtained while maintaining a constant M_s temperature within each series.

The austenitic alloys were transformed to martensite under the influence of tensile strain at cryogenic temperatures. Transformation characteristics were found to vary in a consistent fashion within each series of alloys. In alloys with high S.F.E. the martensite formed during tensile straining formed in massive blocks or large fragmented plates. In low S.F.E. alloys, however the transformation products observed were extremely fine. In the carbonless series of alloys the presence of ϵ - (hcp) phase was detected together with α - (bcc) martensite after transformation, in the alloy with lowest stacking fault energy. This indicated the possibility that the sequence of transformation is $\gamma \rightarrow \epsilon \rightarrow \alpha'$ in alloys of low S.F.E. as opposed to $\gamma \rightarrow \alpha'$ in alloys with high S.F.E.

The effect of prior deformation on subsequent strain induced transformation varied considerably between the two alloy series. Differences in composition both within and between the two series of alloys resulted in a variation in response to prior deformation. In addition the variation in S.F.E. within each series resulted in the development of different textures after deformation. In carbonless alloys prior deformation did not affect the rate of subsequent transformation. In carbon containing

alloys prior deformation resulted in a stimulation of the transformation. The degree of stimulation increased uniformly with increasing S.F.E. in the carbon containing alloys. Transformation rates and the size and distribution of the transformation products were related to the abundance of favorable nucleation points.

The nature of the transformation products, and superior deformation characteristics were correlated with superior tensile behavior and TRIP responses in alloys with low S.F.E. In low S.F.E. carbon containing alloys tensile strengths of 250,000 - 320,000 psi with elongations of 66 and 31% were recorded at cryogenic temperatures.

TABLES OF CONTENTS

ABSTRACT

I. INTRODUCTION----- 1

II. EXPERIMENTAL PROCEDURE----- 5

 A. Alloy Composition----- 5

 B. Thermal Mechanical Treatment----- 7

 C. Measurement of Transformation to Martensite in Tensile Samples 7

 D. Optical Microscopy and Electron Microscopy Techniques----- 9

 E. X-ray Techniques----- 11

III. EXPERIMENTAL RESULTS----- 14

 A. Series I Carbonless Alloys----- 14

 1. Tensile strength data

 2. Ductility

 3. Phase transformation

 4. Metallographic studies

 5. X-ray studies

 B. Series II Carbon Containing Alloys-----19

 1. Tensile strength data

 2. Ductility and phase transformation

 3. Metallographic studies

 C. The Strain Induced Martensite Transformation----- 25

IV. DISCUSSION----- 29

 A. The Strain Induced Martensite Transformation----- 30

 1. Transformation in austenite with us prior deformation

 2. Transformation in alloys with prior deformation.

 B. Tensile Characteristics----- 42

1. Carbonless Alloys	
2. Carbon containing alloys	
IV. SUMMARY AND CONCLUSIONS-----	53
A. The Strain Induced Martensite Transformation and the 'TRIP' Mechanism-----	53
B. Carbonless Alloys-----	54
C. Alloys Containing Carbon-----	55
ACKNOWLEDGEMENTS-----	58
REFERENCES-----	59
TABLES-----	62
FIGURE CAPTIONS-----	70
FIGURES-----	76

I. INTRODUCTION

In recent years in the field of alloy design, metastable austenitic steels which transform to martensite during straining have shown good potential for strength, ductility, and toughness.^{1,2} Considerable development work, much of it conducted on a trial and error basis, has been carried out in order to optimize compositional and processing parameters. However, very little is known about the relative importance of factors effecting the strain induced transformation to martensite during tensile straining. This study was designed to determine the effect of stacking fault energy S.F.E. on the strain induced transformation in iron based alloys.

Breedis³ has shown that in single crystal Fe-Cr-Ni alloys the S.F.E. (stacking fault energy) of the alloys has a marked effect on the deformation substructure of austenite and that the substructure has an effect on subsequent nucleation of martensite on cooling these alloys below the M_s temperature. In alloys with high S.F.E., separation of partials is restricted and cross slip of dislocations takes place relatively easily. Three dimensional, cellular dislocation arrays predominate and local stress concentrations tend to be dissipated through cross slip. Conversely, in alloys with low S.F.E., linear dislocation arrays were observed at low deformations and dissipation of the stress concentrations by cross slip was more limited. Several authors³⁻⁵ have suggested that local stress concentrations and dislocation pile-ups act as nuclei for subsequent transformation to martensite. It may be suggested therefore that in alloys with high S.F.E. where local stress concentrations can be dissipated by cross slip subsequent strain induced transformation to marten-

site might be inhibited. In alloys with low S.F.E., however where dislocations are more restricted to their slip planes, and new nucleation sites can be produced readily by dislocations piling up behind barriers during deformation.

While the deformation substructures in carbonless alloys have received considerable attention and the behavior after small amounts of deformation is well established, the same effect is not observed in carbon containing alloys. Swann⁶ and Fawley et al.⁷ have observed that in carbon containing alloys, regardless of S.F.E., small degrees of plastic deformation result in highly tangled dislocation substructures. It appears as if pinning and multiplication of dislocations around carbide precipitates is a likely cause of these tangled dislocation structures.

In addition to differences in dislocation substructure a number of workers⁸⁻¹¹ have detected a consistent variation in rolling texture with S.F.E. in fcc metals and alloys. Considering the simplest deformation texture, the fibre texture produced by rolling or drawing operations, in fcc metals there is generally a dual texture with [111] and [100] parallel to the deformation axis. The proportions of texture vary with different metals depending on the ease of cross slip and hence on the S.F.E. Dillamore and Smallman¹² have recently used the nature of rolling textures to establish values of S.F.E.'s for pure metals. In the range of S.F.E.'s considered in the two alloy series used in this study a distinct cube texture was anticipated in alloys with low S.F.E. In the case of alloys with high S.F.E. a dual texture with a mixture of grains having [111] and [100] parallel to the rolling direction and random direction orientations around the axis was anticipated. The nature of deformation textures obtained in deformed austenites used in this work was studied using X-ray metallographic techniques.

It can be seen from the above discussion that the variation in composition and S.F.E. within the two alloy series can have marked effects on orientation and substructure after deformation. This variation in substructure within the series must be considered when discussing subsequent transformation to martensite.

The variation of S.F.E. can affect not only the substructure of the alloys but also the transformation products. The transformation structure of metastable Fe-Cr-Ni austenites obtained by thermally induced or strain induced transformation have been widely investigated by both optical¹³⁻¹⁶ and electron microscopy¹⁷⁻²⁰ in conjunction with X-ray techniques. In almost all of these investigations, the presence of an ϵ - (hcp) phase which is closely associated with the α -martensite phase has been reported in alloys with low S.F.E. In the light of a number of recent studies²¹⁻²⁴ it is concluded that in these low S.F.E. alloys ϵ is an intermediate phase and that the sequence of events in the transformation is $\gamma \rightarrow \epsilon \rightarrow \alpha'$. Thus in alloys of low S.F.E. a three phase situation must be considered together with fact that the presence of an intermediate phase in the $\gamma \rightarrow \alpha'$ transformation must inevitably affect the resulting transformation products.

In the present study two alloy series with a regular variation in S.F.E. were selected, one series carbonless the other series containing nominally 0.3% carbon. X-ray, optical, magnetic and scanning electron microscope techniques were used to study the structure and transformation characteristics in both series of alloys and efforts were made to correlate these characteristics with the tensile properties of the alloys at a number of test temperatures. Of particular interest in this study was the observation of TRIP or transformation induced plasticity during tensile straining of the alloys at cryogenic temperatures. When transformation to martensite

occurs during the tensile straining of a metastable austenitic alloy at a temperature below M_d (the temperature above which no martensite transformation can be induced by deformation) excellent ductility as represented by high uniform elongation values can be achieved. In both carbonless and carbon containing alloys the transformation product, either B.C.C. martensite or B.C.T. martensite respectively, can have a marked strengthening effect on the parent austenite. If this transformation can be controlled such that, as the austenite yields and incipient necking begins, the transformation to martensite occurs in the necked region, strengthening of the necked region occurs. Since the necked region is strengthened, subsequent deformation is forced into adjacent material, fracture is prevented and uniform elongation of austenite is promoted. Increased ductility obtained in this manner, essentially preventing fracture by means of a controlled phase transformation, has been termed transformation induced plasticity or TRIP. Steels exhibiting these characteristics have been classed as TRIP steels. One purpose of the present study was to relate structural and transformation data to the TRIP response of the metastable austenitic alloys in each of the two alloy series.

In terms of response of prior deformation at elevated temperatures and transformation characteristics during tensile straining, the two alloys series must initially be considered separately. The phase transformation of interest is F.C.C. austenite to B.C.C. martensite in the case of carbonless alloys and F.C.C. austenite to B.C.T. martensite in the case of carbon containing alloys. When the S.F.E. is low an intermediate step involving formation of ϵ (hcp) martensite is also likely. However, comparison of data obtained from the two alloys series was useful from a number of standpoints to be discussed and it was possible to draw a number of interesting conclusions by comparison of the two sets of data.

II. EXPERIMENTAL PROCEDURE

A. Alloy Composition

Two main series of alloys were tested. Compositions and estimations of the stacking fault energies of each alloy are shown below.

SERIES I

Carbonless Alloys

Composition	Estimated S.F.E. (ergs cm ⁻²)
1. Fe - 35 Ni	50
2. Fe - 23 Ni - 10 Cr	30
3. Fe - 15 Ni - 15 Cr	15 to 20
4. Fe - 12 Ni - 22 Cr	10 to 13

SERIES II

Alloys with carbon

Composition	Estimated Stacking Fault Energy (ergs cm ⁻²)
1. Fe - 25 Ni - 4 Mo - 0.28 C	50
2. Fe - 12 Ni - 12 Cr - 4 Mo - 0.30 C	12 - 17
3. Fe - 8 Ni - 15.5 Cr - 4 Mo - 0.32 C	7 - 10

A considerable amount of work has been carried out measuring the stacking fault energies of iron nickel chromium austenites and austenitic stainless steels. The determination of stacking fault energies has usually been through the determination of node curvatures.^{25,26} The method has limitations due to formula approximations²⁷ and necessitates extremely meticulous experimental techniques. The values of S.F.E. given for the austenitic alloys represent average values from a large body of data referenced above. The values are believed to represent very good approximations and give an excellent representation of the change of S.F.E. with composi-

tion within each alloy series.

Nickel increases the S.F.E. of iron alloys, chromium has the reverse effect in the composition range selected and decreases the S.F.E. Thus the composition of alloys could be arranged such that by varying the balance of Ni and Cr the S.F.E. could be varied in a regular fashion while keeping M_s temperatures of all alloys in a given series in the same range.

The M_s temperatures were calculated from formulas developed by Andrews²⁸ which were reported as accounting for interaction between alloy elements. The M_s temperatures were all designed to be below -196°C and both M_s and M_d were below R.T. In this manner R.T. tensile tests could be carried out with no strain induced transformation occurring and tensile characteristics could be compared with data for cryogenic tests where strain induced martensite was formed during testing.

In high chromium alloys in addition to controlling the M_s temperature and the S.F.E. energy it was also important that the proportion of Cr and Ni were such that the delta ferrite region of the phase diagram was avoided. The schematic shown in Fig. 1²⁹ was particularly helpful in determining the suitable alloy compositions.

In carbon containing alloys (Series II) sufficient molybdenum was included in the composition to tie up carbon as molybdenum carbides. Molybdenum has a higher diffusivity than chromium in austenite, particularly when the austenite is highly deformed.³⁴ However, in alloys containing high percentages of chromium, some chromium carbides will be present in addition to molybdenum carbides as chromium is the stronger carbide former of the two elements.

In addition to the two main alloys series, one additional composition was studied. Series II(a), (Carbon Containing) 1. Fe - 24 Ni - 4 Mo - 0.25 C

The small variation in composition from alloy 1 in Series II was sufficient to bring the M_d of this alloy slightly above room temperature. The room temperature tensile characteristics of this alloy where a low rate of transformation to martensite was observed during testing at R.T. could thus be compared directly to the Fe - 25 Ni - 4 Mo - 0.28 C alloy where no transformation to martensite occurred at room temperature.

B. Thermal Mechanical Treatment

The thermal mechanical treatment selected for all the alloys was selected from a backlog of data^{1,2} on similar TRIP steels to those used in Series II. While no attempt was made to optimize processing parameters the parameters selected were known to be of the type that would tend to maximize any TRIP characteristics of alloys. The thermal mechanical treatment may be outlined as follows:

1. Homogenized alloys at 1100°C for three days.
2. Forge at 1100°C and roll between 600-1000°C to suitable size.
3. Austenitize 1 hour at 1175°C, water quenched.
4. Deform varying amounts at 450°C.
5. Cut tensile specimens to specifications shown in Fig. 2.
6. Tests specimens in tension at (a) R.T. (b) -72°C and (c) -196°C.

Deformed austenite was thus tested in tension at a number of test temperature. At cryogenic temperatures strain induced martensite was formed during testing. The austenite - martensite transformation was observed by a number of techniques including metallographic studies, magnetic studies and scanning electron microscope studies.

C. Measurement of Transformation to Martensite in Tensile Samples

The austenite-martensite phase transformation was measured magnetically. Magnetic measurement of the martensite transformation is possible

since the α martensite phase is ferromagnetic while austenite and the ϵ -hcp phase are both paramagnetic. Magnetic measurements were checked by optical and X-ray metallographic techniques and gave an excellent one-to-one correlation.

The saturation induction of specimens was measured using a permeameter. Two detecting coils bucking each other were situated between the poles of an electromagnet. The resulting current from the detecting coils was first integrated, then read on a chart recorder.

The energizing current in the large coils of the electromagnet could be switched continuously from a negative value to a positive value so that the magnetic field between the poles could be reversed from about -6,000 oersted to +6,000 oersted to measure the saturated induction B_s in the specimen.

1. With the specimen removed, search coils A and B were balanced with a divider, to give a minimum signal on the recorder.

2. With the specimen in one of the search coils, any increase, n volts, in the signal on the recorder was due to an additional flux in the specimen.

$$\Delta\phi_{\text{spec}} = \Delta(B-H) NA_{\text{spec}} = B_s NA_{\text{spec}}$$

where

ϕ_{spec} is the flux in the specimen (Maxwells)

B is the induction (gauss)

B_s is the saturation induction

H is the magnetic field (oersteds)

A_{spec} is the cross-section area of the specimen.

To calibrate the integrated signal, a square loop flux standard was used; a known variation in the flux $\Delta\phi_{\text{SLFS}}$ given by the flux standard gave an integrated voltage read on the recorder.

$$\Delta\phi_{\text{SLFS}} \rightarrow n_0 \text{ volts on the recorder}$$

The saturation induction is related to the measured voltage from the integrated signal by:

$$B_s = \frac{l}{2 NA_{\text{spec}}} \times \Delta\phi_{\text{SLFS}} \times n/n_0 \quad (1)$$

The factor $l/2$ is due to the fact that the magnetic field was switched from a negative value to a positive value. The purpose of this switching was to eliminate any error due to the zero of the induction in the specimen. This zero cannot be attained easily since the remanent magnetization depends on the nature of each specimen.

The signal due to the magnetization of the specimen, n volts, was obtained by subtracting the signal due to an imperfect bucking of the search coils from the total signal read on the recorder.

In Eq. (1) n and n_0 are determined by simple reading, $\Delta\phi_{\text{SLFS}}$ is known and N is known. Only the area of the specimen, A_{spec} , has to be determined for each magnetic measurement. The B_s determinations were converted to a percentage of martensite by assuming B_s is proportional to the amount of magnetic phase.

Thus, if x is the amount of martensite, we have

$$x/100 = B_s/B_0$$

B_0 is the saturated induction of a completely martensitic specimen. The value B_0 varies with composition and must be calculated theoretically for each alloy.³⁰

D. Optical Microscopy and Electron Microscopy Techniques

Optical microscopy of strain induced martensite in the two alloy series revealed that in low S.F.E. alloys martensite crystals were extremely fine and could not be resolved at 1000X. In order to compare the size of

the martensite crystals with the S.F.E. it was necessary to scan large areas of the specimens and photograph representative areas. While transmission and replica studies provide sufficient resolution, the scanning electron microscope allowed large areas to be scanned at low magnification such that representative areas could be selected and studied at higher magnifications. Scanning electron microscope studies were used to study the transformation products in austenites with no prior deformation at elevated temperature. Specimens were polished and etched to ensure maximum surface relief. The specimens were then lightly (200\AA) shadowed with platinum; the shadowing technique resulted in improved contrast in the scanning microscope. The specimens were studied carefully in an optical microscope and typical areas of α martensite selected for study. Magnifications of $12,000\times$ were necessary to resolve the finest martensite crystals.

Optical microscope techniques were used to follow the nucleation and growth characteristics of the strain induced martensite. Tensile specimens initially 0.050 inches in thickness were ground to a thickness of 0.040 inches in a jig. Completely flat, uniform specimens resulted and the surface of these specimens was polished to a scratch free finish. The specimens were then intermitently strained in tension and the polished surface was studied after fixed amounts of strain. The surface was studied under oblique lighting in the optical microscope. A dark field effect resulted and surface upheavals were clearly visible at relatively low magnification ($400\times$). The polished surface was marked with a grid of fine scribe lines such that after each interval of strain, specific areas could be re-identified and micrographs taken. The specimens were finally repolished and etched in order to positively distinguish between slip lines and upheavals caused by transformation to martensite.

E. X-ray Techniques

An x-ray diffractometer was used to determine the relative volume fractions of phases in the partially transformed alloys after tensile straining. The technique was used to check the magnetic measurement of the amount of transformation to α martensite and to detect the presence of any ϵ phase in the Fe-Ni-Cr alloys. In addition a back reflection technique was used to study rolling textures in deformed austenitic alloys.

Back reflection photographs were used to study preferred orientation in deformed sheet specimens. Monochromatic chromium K_{α} radiation was used to examine polycrystalline sheet specimens after a 25% deformation at 450°C. Specimens of the high S.F.E. alloy Fe-35Ni and the low S.F.E. Fe-12Ni-22Cr were polished and etched to remove the surface polishing layer and mounted in the x-ray camera. Back reflection pinhole photographs were taken revealing a marked preferred orientation in both specimens. The anticipated textures¹⁰⁻¹¹ in the case of the austenitic alloys with this range of S.F.E.'s were a [100] texture in the case of the low S.F.E. alloy and a mixture of [100] and [111] in the case of the high S.F.E. alloy. The specimen to film distance and the exposure time used was adjusted to allow study of these reflections.

The x-ray technique to determine relative volume fractions of phases in a multiphase alloy is now well known.^{31,32} It consists of comparing the relative integrated diffraction intensities which are proportional to the volume fractions of the respective phases.

The Norelco X-ray Diffractometer equipped with diffracted beam (200) LiF crystal monochromator was used with CuK_α radiation. This monochromatization techniques eliminated a lot of the x-ray fluorescence background, which made possible the use of CuK_α radiation.

The relative integrated intensities of peaks corresponding to the $(10.1)_\epsilon$, $(200)_\gamma$, and $(200)_\alpha$ were compared to calculate volume percents of ϵ , γ and α . The patterns were obtained from the flat polished surface of the gage sections of the tensile specimens. These peaks were sufficiently separated that interference was highly unlikely. For each peak, the relative integrated intensity, I, is

$$I = \left(\frac{I_o e^4}{m^2 C^4} \frac{\lambda^3 A}{32\pi r} \right) \frac{1}{v} [|F|^2 \times P \times LP] \frac{e^{-2M}}{2\mu}$$

constant = K

where the first two terms equal a constant, K, independent of kind and amount of diffracting substances, and

v = volume of unit cell

F = structure factor

P = multiplicity factor

LP = Lorentz polarization factor = $\frac{1 + \cos^2 2\theta \cos^2 2\theta_m}{\sin\theta \sin 2\theta}$

θ = Bragg angle of each line

θ_m = Bragg angle for monochromator; for (200 -LiF, $\theta_m = 22^\circ 34'$
for CuK_α .

e^{-2M} = temperature factor

$1/2\mu$ = Absorption factor for flat specimens

Letting,

$$R = \frac{1}{v} [|F|^2 \times P \times LP] e^{-2M}$$

then in the three phase material here,

$$I_{\alpha} = \frac{K R_{\alpha} C_{\alpha}}{2\mu_m}$$

$$I_{\gamma} = \frac{K R_{\gamma} C_{\gamma}}{2\mu_m}$$

$$I_{\epsilon} = \frac{K R_{\epsilon} C_{\epsilon}}{2\mu_m}$$

where μ_m = linear absorption coefficient of mixture

C_i = volume fraction of i^{th} phase.

The equations above together with the fact that

$$C_{\alpha} + C_{\gamma} + C_{\epsilon} = 1.0$$

will yield the C_i 's. Factors for the calculation of R_i are shown in Table VIII.

III. EXPERIMENTAL RESULTS

While the program of study was not designed to optimize thermomechanical treatments of the alloys it was anticipated that if S.F.E. was an important parameter in the strain induced transformation some interesting tensile data might result at cryogenic temperatures. Since excellent combinations of strength and ductility were obtained, tensile data is presented together with transformation data in considerable detail. Due to the volume of data presented, this section is designed to present the data in a concise manner with a minimum of comment in order to facilitate referral. A full discussion of the data is presented in the next section of the thesis. Where possible an attempt has been made to separate the large volume of tensile data from data gathered in studies of the phase transformations occurring during straining.

A. Series I CARBONLESS ALLOYS

Fully annealed austenitic alloys were deformed by varying amounts between 0% and 80% at 450°C. The response to this prior deformation in terms of tensile characteristics and in terms of subsequent strain induced transformation was studied by tensile testing specimens at test temperatures of RT, -72°C and -196°C. The tensile characteristics and the amount of martensite formed during testing were followed in each case. The results for the carbonless alloys are shown in Figs. 3 through 6 and are tabulated in Tables 1 through 3.

1. Tensile Strength Data

The yield strength of all alloys fell within the range of 25,000 to 50,000 psi at 0% deformation to 75,000 to 100,000 psi at 80% deformation when tested at RT. The increase in yield strengths when tensile tests were conducted at -196°C was small as can be seen in Figs. 3 through 6.

Little difference was observed in yield strength values between the four alloys.

2. Ductility

Marked differences were observed in the ductilities of the four alloys as represented by elongation data. The elongations obtained with alloys of low S.F.E. appeared higher. Elongations tended to increase with decreasing test temperature with all four alloys but elongations in the case of the lower S.F.E. alloys (Fe - 15 Ni - 15 Cr and Fe - 12 Ni - 22 Cr) tended to be higher and fell off less with increasing prior deformation.

In all Series I alloys transformation of austenite to martensite during straining at cryogenic temperatures was associated with improved values of uniform elongation. This effect is most marked in a given alloy at a given test temperature in that the elongation data for specimens with increasing prior deformation remains approximately constant.

In the case of the Fe- 35 Ni, Fe - 15 Ni - 15 Cr alloys the transformation occurring is $\gamma \rightarrow \alpha'$ martensite, while in the case of the lower S.F.E. alloy Fe - 12 Ni - 22 Cr the sequence of transformation considered is $\gamma \rightarrow \epsilon \rightarrow \alpha$. Between 5-10% of ϵ was detected by x-ray metallographic techniques in all Fe - 12 Ni - 22 Cr tensile specimens tested at cryogenic temperatures where transformation to α martensite had occurred. The ϵ hcp phase was not detected in any of the other alloys tested in Series I. While the ϵ phase contributes the mechanical properties by work hardening²¹ the strain induced α -phase formation will remain the main cause for the strengthening of austenite in the Fe - 12 Ni - 22 Cr alloy.

Both yield and ultimate strength levels in this series of alloys were low. The increase in yield strength between alloys with a 0% and 80% prior deformation is small. The bcc martensite phase, stronger than the

parent austenite is effective in strengthening the parent austenite and preventing premature failure by necking.

The fact that TRIP does enhance uniform elongation in this alloy series is confirmed by the fact that in all cases where martensite was not formed during testing elongations declined with prior deformation.

3. Phase Transformation

It is significant that no difference is observed in the total amount of martensite formed during tensile testing in the alloy series with widely differing S.F.E.'s. In the Fe- 35 Ni alloy although the overall tensile elongations are lower, the total amount of martensite produced during testing was as high in all cases as alloys with lower S.F.E. Direct comparison of tests at any one temperature is not valid in any case due to inevitable differences in M_s and M_d temperatures. In the case of the Fe - 23 Ni - 10 Cr alloy it is apparent that M_d in this case is below -196°C and no martensite was produced during tensile testing. In the case of the other alloys in Series I martensite was produced during testing at cryogenic temperatures.

Specimens of all four alloys were examined by x-ray metallographic techniques after testing at cryogenic temperatures. In this manner magnetic measurements for γ and α martensite were checked and any ϵ phase was detected. ϵ was detected in all Fe - 12 Ni - 22 Cr alloys tested below M_d . The amount of ϵ was however small varying between 5-10% in all cases. No ϵ phase was detected in other alloys in Series I.

The final point of interest with this series was that no stabilization effects are observed in the strain induced martensite transformation with this series of alloys.

4. Metallographic Studies

Examples of martensites obtained in Series I alloys are shown in Figs. 7 through 17. Figures 7 through 19 show typical fragmented martensite plates formed in undeformed Fe - 35 Ni alloy strained at -196°C . The plate size is large and individual plates are easily resolved at a magnification of 400X. In Fe - 35 Ni austenite that has been deformed 80% at 450°C prior to tensile straining at -196°C the martensite is "blocky" but individual plates can still be resolved at 1000X, (Fig. 11).

Figures 12 through 15 show the Fe - 15 Ni - 15 Cr alloy after tensile straining at -196°C . In the undeformed austenite the martensite crystals are finer than the Fe - 35 Ni austenite strained under identical conditions. Figure 13 shows typical regions of the austenite where martensite crystals of varying size appear. In the top left corner relatively coarse martensite crystals are observed, while on the right of the micrograph very fine martensite crystals are observed. In austenite that has received a prior deformation of 80% prior to straining at -196°C ultra fine martensite crystal that cannot be resolved at 1000X are formed (Figs. 14 and 15). Figures 16 and 17 show martensite crystals formed during straining at -196°C in the alloy with the lowest S.F.E., Fe - 12 Ni - 22 Cr. In both undeformed austenite and austenite with a prior deformation of 80% at 450°C , straining at -196°C results in very fine martensite that cannot be resolved at a magnification of 1000X.

These data takes on added significance when compared with metallographic studies on carbon containing alloys. In both alloy series the same decrease in martensite size is observed with both increasing prior deformation and with decreasing S.F.E. In referring to the "size" of the martensite observed by metallographic technique reference is made to the general coarseness of the structure rather than the dimensions of individual marten-

site crystals. In the low S.F.E. the structure is so fine that a more quantitative size estimate is not possible from optical micrographs. The relative coarseness of the transformation product within the alloy series is of more interest in the case of this study than fully quantitative size estimates.

5. X-ray studies

X-ray analysis used to determine the relative volume fraction of phases in the alloys of Series I confirmed the magnetic measurements of the volume fractions of γ and α martensite in partially transformed specimens and revealed the presence of the ϵ phase in Fe - 12 Ni - 22 Cr specimens tested below R.T.

A comparison of X-ray data and magnetic data showed an excellent one-to-one correspondance in the relative volume fractions of α martensite and austenite in specimens with no prior deformation. Prior deformation introduces preferred orientation into the specimens resulting in some error in the X-ray determinations but good agreement was still maintained between X-ray, optical and magnetic determinations of the amount of transformation to martensite that had occurred in a given specimen.

X-ray analysis also indicated the presence of the ϵ phase in partially transformed Fe - 12 Ni - 22 Cr austenite. The ϵ phase was not detected in any other alloy in Series I. The ϵ - hcp phase was observed in Fe - 12 Ni - 22 Cr alloys after testing at -72°C and -196 C . No ϵ was detected after R.T. testing. The relative volume fractions of the three phases after testing at cryogenic temperatures was calculated from the integrated intensities of the $(200)_{\gamma}$, $(10.1)_{\epsilon}$ and $(200)_{\alpha}$ peaks. A typical series of diffractometer peaks is shown in Fig. 18 for an alloy with no prior deformation tested at -72°C ($(200)_{\alpha}$ peak not shown). Alloys tested at -72°C showed

approximately 10% of the ϵ phase, while in alloys tested at -196°C there was approximately 5% of the ϵ phase. At these two test temperatures approximately 45% and 60% transformation to martensite had occurred indicating that the amount of ϵ phase was diminishing with increased transformation to martensite.

Back reflection photographs of as deformed sheet specimens of the Fe - 35 Ni and Fe - 12 Ni - 22 Cr alloys showed a marked variation in deformation texture developed in the two austenitic alloys. Figure 19 shows the $(200)_{\gamma}$ reflection for both alloys after a 25% deformation at 450°C . The marked difference in texture is apparent from examination and comparison of these two Debye rings. In the Fe - 12 Ni - 22 Cr a very marked [100] texture has developed even after only a relatively light 25% deformation. It can be seen that the diffracted intensity is very high within a 30° angle of the rolling direction while the intensity of poles outside this region is low. Thus although there is considerable scatter of the [100] direction in that arcs of intensity are gathered around the rolling direction one can conclude that the normals to the (100) type planes are definitely aligned in the rolling direction giving a marked [100] texture.

In the case of the Fe-35Ni alloy a marked texture was also observed. The sheet texture in this case however had less symmetry than that of the previous alloy and thus could only be adequately described by a full pole figure determination. It is sufficient to say that the texture has less symmetry than the simple cube texture developed in the low S.F.E. alloy.

B. Series II CARBON CONTAINING ALLOYS

A series of carbon containing alloys with similar S.F.E. variations to the carbonless series was run for comparison purposes. In this way the results of this study could be related to the more practical field of alloy

design and in particular to the field of TRIP steels. In carbon containing alloys a direct correlation between uniform elongation data and transformation to martensite during tensile testing was anticipated. While this was in no way a development program and no optimization procedures were pursued, it was anticipated that if S.F.E. was an important factor in TRIP type alloys then some promising data would result. This proved to be the case. In the case of carbon containing alloys several factors of interest were emphasized. Of interest in the field of alloy design was

- (a) correlating elongation data with phase transformation data
- (b) response to prior deformation and the variation thereof with S.F.E.
- (c) direct comparisons obtained with carbonless alloys.

Of equal importance was more basic information obtained on the strain induced martensite transformation and response to prior deformation of the alloys

- (a) variation in the rate of transformation to martensite with S.F.E. in deformed austenites.
- (b) identification of the manner in which S.F.E. affects the response to prior deformation or subsequent transformation mechanisms.

Thus while a regular variation in S.F.E. was obtained within each alloy series, there are also other variations such as composition, and deformation textures. These factors will be considered together with the variation in S.F.E.'s within the alloy series in the following section of the thesis after the presentation of experimental data.

In this section the tensile and magnetic data will be summarized. These data will then be discussed in more detail together with more definitive studies that were carried out on these materials in Section C.

Tensile and magnetic data for these alloys is fully tabulated in Tables 4 through 6 and is plotted in Figs. 20 through 22.

1. Tensile strength data

The two alloys with the lower S.F.E., Fe - 12 Cr - 12 Ni - 4 Mo - 0.30 C and Fe - 15.5 Cr - 8 Ni - 4 Mo - 0.32 C responded more favorably to prior deformation at 450°C than the Fe - 25 Ni - 4 Mo - 0.28 C alloy. The low S.F.E. alloys exhibited a very rapid increase in yield stress with increasing prior deformation. This favorable response to prior deformation at 450°C in alloys with low S.F.E. was attributed in part to the presence of Cr in the case of the two Cr containing alloys. In the Fe - 25 Ni - 4 Mo 0.28 C alloy, molybdenum is added in sufficient quantity to tie up carbon as molybdenum carbides, which are precipitated in the form of fine carbides during deformation at 450°C.³⁴ Chromium is also a strong carbide former. The presence of two strong carbide formers means that chromium carbide Cr₂₃C₆ (usual composition for low and medium carbon steels) will be present as well as molybdenum carbides Mo₂C and MoC. The composition of the chromium carbide as compared with molybdenum carbides means that relatively more carbide will be present and due to the increased alloy content a finer dispersion of carbide is likely. This finer dispersion of carbides would account for the more rapid work hardening rate and increase yield strengths due to the increased frequency of dislocation barriers.³⁵ Dislocations pile up and multiply around these barriers during deformation.

2. Ductility and Phase Transformations

In the case of TRIP type steels ductility as represented by elongation must be considered in conjunction with any phase transformation occurring during tensile straining. Certain important generalizations are immediately apparent from comparing Figs. 20 through 22.

1. Elongations in the undeformed condition are generally good but tend to increase with decreasing S.F.E.

2. When no martensite is formed during tensile straining elongation values fall off rapidly with increasing prior deformation in the case of all alloys. In the case of all alloys with an 80% prior deformation, elongations recorded for room temperature tests were of the order of 5%. All alloys failed in a ductile fashion however with high reduction in area indicating potential ductility.
3. In all alloys when tested below M_d , no stabilization effect was observed for the strain induced transformation. This is in strict contradiction to the thermally induced martensite transformation.
4. When martensite was produced during tensile straining, ductilities as represented by elongation data improved.
5. The increase in elongation was markedly greater for alloys with a low S.F.E. than the high S.F.E. alloy.
6. The total amount of martensite produced during tensile straining was not affected by S.F.E. If anything, the total amount of transformation was greater in the alloy with a high S.F.E. This is significant in that it can be concluded that it is not the amount of martensite induced that is important to promoting uniform elongation but either:
 - (a) When the transformation is induced (at what stage of the tensile test) or what form the transformation takes (i.e. Luders band etc) or
 - (b) the form, size and distribution of the martensite.

The availability of martensite nuclei will have a profound effect on both of these factors particularly the latter. As in the carbonless alloys, the variation of S.F.E. within the alloy series will have a marked effect on preferred orientation developed during the deformation of the alloys.

Orientation effects will affect the number of slip systems available and the stress distribution in the alloy which will undoubtedly affect the austenite-martensite transformation. These effects will be considered more fully in the discussion of the experimental data.

While it was considered that the comparative aspects of the study yielded the most important information, it was noted that the data obtained from the carbon containing alloys with lower stacking fault energy is extremely promising. It proved quite difficult to obtain alloys with exactly corresponding M_s and M_d temperatures. Thus while the Fe - 12 Cr - 12 Ni - 4 Mo - 0.30 C alloy showed optimum TRIP characteristic when tested at -196°C . The other two alloys in Series II showed optimum transformation rates at -72°C . Because of this only general comparisons could be made.

However, the Fe - 12 Cr - 12 Ni - 4 Mo - 0.30 C alloy when deformed 57% and 80% at 450°C gave yield strengths of 280,000 psi and 309,000 psi with elongations of 46.8% and 31.0% respectively. These figures represent an excellent combination of strength and ductility for cryogenic temperatures.

The Fe-15.5Cr-8Ni-4Mo-0.32C alloy when deformed 80% at 450°C gave a yield strength of 265,000 psi with an elongation 31.0% when tested at -72°C which also represents excellent mechanical properties at this temperature.

Series II(a)

As stated previously all of the alloys in Series I and II had been designed such that no transformation to martensite would occur during R.T. testing. This was to enable direct comparison of tensile characteristics both with and without transformation occurring during testing. The Fe-25Ni-4Mo-0.28C alloy exhibited its optimum strength - ductility combinations at -72°C . The composition of this alloy was adjusted to transfer this optimum performance to room temperature. An Fe-24Ni-4Mo-0.25C alloy was selected for this study and the results of room temperature testing of this alloy are shown in Fig. 23.

It can be seen that the yield strength was somewhat lower at lower deformations (compared to Fe-25Ni-4Mo-0.29C alloy) but not appreciably so. The rate of transformation to martensite during tensile straining was low (M_d was only slightly above R.T.) but the martensite formed was effective in producing high uniform elongations. A specimen with a 20% prior deformation had a yield strength of 91,500 psi with an elongation of nearly 80%.

It was observed in the case of all the carbon steels tested that when the TRIP mechanism was operative the optimum conditions for enhanced elongations appeared to be in alloys deformed between 15% and 30%. Prior deformations up to 30% resulted in improved elongations in all cases.

The data for the Fe-24Ni-4Mo-0.25C alloy indicated that by adjusting the composition of all alloys in Series II good strength ductility combinations could be obtained at R.T.

3. Metallographic studies

A detailed metallographic study of the strain induced martensite formed during tensile testing of carbon containing alloys is shown in Figs. 24 through 30.

The micrographs show that in the alloy with the lowest S.F.E., the Fe-8Ni-15.5Cr-4Mo-0.32C (S.F.E. 7-10 ergs cm^{-2}) the martensite crystal size is much finer than in the case of the high S.F.E. alloy Fe-25Ni-4Mo-0.28C (S.F.E. 50 ergs cm^{-2}). These alloys are shown in Figs. 29 and 30 and Figs. 24 and 25 respectively.

In the high S.F.E. alloy the martensite is relatively coarse and at a magnification of 1000X appears "blocky" in nature. In the low S.F.E. alloy the martensite is very fine and in all cases individual plates are not resolved at 1000X. The intermediate case is represented by the Fe-12Ni-12Cr-4Mo-0.030C alloy (S.F.E. 12-17 ergs cm^{-2}). In this latter

case when the austenite had undergone low prior deformation at 450°C (0% and 15%) the martensite formed on subsequent testing appears partially as coarse "blocky" martensite but after higher degrees of prior deformation the martensite becomes very fine again and is unresolvable into individual plates at 1000X. Micrographs of this alloy are shown in Figs. 26 through 28.

Thus the coarseness of strain induced martensite in metastable austenites decreases with decreasing S.F.E. and with increasing prior deformation of austenite. Further the decrease in coarseness with decreasing S.F.E. is observed in both carbon containing and carbonless alloys.

C. The Strain Induced Martensite Transformation

The data gathered in studies discussed previously showed the amount of martensite formed when a given alloy was strained past its yield point. Magnetic measurements checked by optical and x-ray metallographic techniques were used to determine the amount of martensite formed in these alloys prior to failure in all cases except the Fe-35Ni alloy. The latter alloy is ferromagnetic when austenitized and in this case x-ray and optical estimates of the amount of martensite were obtained. Metallographic data showed that the size of the strain induced martensite crystals decreased with decreasing stacking fault energy.

In order to obtain quantitative data on the kinetics of the strain induced transformation, the transformation in carbon containing alloys was studied in more detail. In the Fe-12Ni-12Cr-4Mo-0.30C alloy, optimum conditions for transformation induced plasticity were observed at -196°C at LN₂ temperature. Since LN₂ is a non-conductor, it was possible to attach the permeameter around a tensile specimen such that the gauge length of the specimen was suspended freely in the search coil. Then

permeameter and specimen were immersed in LN_2 and a continuous record of the transformation was recorded during straining of the specimen to failure. A continuous record of the transformation was obtained for alloys deformed between 0 and 80% prior to testing. The engineering stress-strain curves together with the record of transformation occurring during straining is shown in Fig. 31. At small prior deformations a straight line curve was approached as the proportion of martensite formed increased uniformly with strain. With higher prior deformations a non linear curve was obtained. While it was not possible to obtain continuous records of transformation at -72°C , a number of spot checks on carbon containing alloys that were tested in a discontinuous fashion indicated that a similar series of curves would have been observed in all cases.

While data on the total amount of martensite per unit strain formed during straining was computed, before conclusions could be drawn about the strain induced transformation further information was needed on the kinetics of the transformation or how the transformation proceeded with strain. Also, since the ultra fine martensite in the low S.F.E. alloy could not be resolved optically, additional studies were necessary to make an estimate of the relative size of the martensite crystals formed.

Tensile specimens of carbon containing alloys in the undeformed condition were ground flat and the surface polished to a scratch free finish. The specimens were strained discontinuously and the surface studied at fixed intervals of the strain. The surface of the tensile specimen was studied under oblique lighting and surface upheavals caused by transformation to martensite were clearly visible. Initially two types of deformation processes had been distinguished and identified. These two types will be called Type A and Type B and were important in that the onset of the martensite transformation was also effected.

Type A

This type of deformation was observed in austenites that had undergone prior deformation of 55% and 80% at 450°C. A Luders type' band of high local deformation forms on yielding with a high degree of transformation within the band (30-60% transformation within the deformation band). Initially no transformation occurs outside this narrow deformation band. The band then propogates along the length of the specimen and a period of low work hardening rate is observed in the stress strain curve. After the deformation band has traversed the specimen and if fracture does not occur the work hardening rate increases and further transformation to martensite occurs along the gauge length.

Type B

This type of deformation was observed in austenites with low amounts (0%, 15%, and 25%) of prior deformation. In this case no marked yield point is observed on the stress strain curve. After the material yields martensite begins to form uniformly along the entire gauge length and the amount increases with strain.

Due to the two types of deformation observed in specimens with varying degrees of prior deformation, specimens of undeformed austenite were selected for further study since the amount of transformation to martensite increased uniformly with increasing strain after the onset of transformation occurred on yielding.

The polished surfaces of tensile specimens of all three alloys in the fully annealed austenitic condition were studied under oblique lighting. After a discontinuous strain of approximately 20% the specimens were repolished and etched to distinguish between strain markings and surface upheavals due to transformation to martensite.

Figures 32 thru 34 show specific areas of the polished surface of tensile specimens of the Fe-25Ni-4Mo-0.28C, Fe-12Ni-12Cr-4Mo-0.30C and Fe-8Ni-15.5Cr-4Mo-0.32C alloy respectively (after varying degrees of tensile straining). In the first alloy the surface disruptions caused by martensite can be clearly distinguished and may be compared with an optical micrograph of the same specimen after a 16% tensile strain after repolishing and etching. In the second two alloys, surface disruptions were harder to detect. Due to the very fine transformation products in the two low S.F.E. alloys the disruption of the polished surface caused by transformations was very difficult to distinguish from surface strain markings even after the specimens were repolished and etched since it proved impossible to identify specific areas after repolishing.

This data is discussed more fully in the following section.

IV DISCUSSION

There is a large body of data in the literature on martensitic transformation in both carbon containing³⁵⁻³⁸ and carbonless³⁹⁻⁴² alloys. The thermally induced transformation and the strain induced transformation have both been studied in some detail. The majority of these studies have tended to compare data for the transformation in widely differing alloy systems and arrived at rather broad generalizations. In recent years detailed studies of the morphology of martensite in a number of systems has revealed that orientation relationships and the habit plane of martensite crystals and parent austenite can vary with composition of the alloy under investigation. In the study presented here a carbonless series of alloys was compared with a comparable carbon containing series. The carbonless series of alloys was based on the Fe-Cr-Ni system which offers the opportunity to obtain a regular variation in S.F.E. while keeping the M_s temperature of the alloys constant. In the equivalent carbon containing series molybdenum was added to ensure a strong carbide former was present in sufficient quantity to tie up all the carbon in the alloy (nominally 0.3%) even in the absence of chromium. The data revealed that a number of transformation characteristics varied consistently with S.F.E. in both series.

Comparison studies were important in providing a basis for broader generalizations on the transformations characteristics of these alloys but emphasis was also placed on carbon containing alloys where the data found direct application to TRIP steel.

The initial discussion in this section will center on the characteristics of the martensite transformation in the two alloy series. Basic characteristics of the transformation in the two alloy systems will be

discussed and in the following sections an attempt will be made to correlate these characteristics with tensile data.

A. The Strain Induced Martensite Transformation

A martensitic transformation is one in which the growth of the product crystals takes place by a systematic coordinated movement of many atoms of parent crystals. The distance moved by any one atom is a fraction of a lattice spacing. The chemical composition of the parent and the product is the same but since there is a change in lattice, the shape and volume of the martensite crystal is different. To accommodate this change in shape and volume the parent lattice is subjected to a high degree of accommodation strain.

An understanding of the kinetics of martensitic reactions depend on a quantitative understanding of the rate of nucleation and growth characteristics. Martensite nuclei or embryos have not been observed directly thus conclusions about the transformation must be drawn by observation of the transformation once the martensite crystals have grown to finite dimensions and by observation of the size and distribution of the final product. A tabulated summary of data for the transformation characteristics in the two alloy series is shown in the two tables following. Transformation characteristics in the two alloy series are not shown together since the transformation is basically different in carbonless and carbon containing alloys.

The onset of transformation in each case coincided with yielding. In the majority of tests the yielding of austenite initiated the strain-induced transformation to martensite however in a number of tests where the stability of austenite was low it was found that the stress-induced formation of martensite could initiate plastic deformation and yielding. The latter

Carbon Containing Alloys

Series II

Alloy Composition		Fe-24Ni-4Mo -0.28C	Fe-12Ni-12Cr -4Mo-0.30C	Fe-8Ni-15.5Cr -4Mo-0.32C
S.F.E		50 ergs/cm ²	15 ergs/cm ²	7-10 ergs/cm ²
Onset of Transformation		On Yielding	On Yielding	On Yielding
Rate of Transformation	Mart/unit strain in undeformed austenite	1.68	0.39	0.46
	Mart/unit strain in austenite with 80% prior deformation	3.35	1.88	1.65
	Effect of prior def. on rate of transf.	marked stimulation	less stimulation	least stimulation
Optical Morphology	Type of martensite and size	ultra fine crystals	very fine crystals	blocky massive martensite
	Effect of prior deformation on size	size decreases	size decreases	size decrease
	Directionality	growth in preferred directions	growth in preferred directions	non-direction
Kinetics of Transformation (in undeformed austenite).	Progress of transformation with increasing strain	Growth of existing crystals together with nucleation of new crystals	Transf. proceeds by formation of large number of fine crystals	Transf. proceeds by formation of a large number of fine crystals

Carbonless Alloys
(Series I)

Alloy Composition		Fe-35Ni	Fe-15Ni-15Cr	Fe-12Ni-22Cr
S.F.E.		50 ergs/cm ²	17 ergs/cm ²	10 ergs/cm ²
Onset of Transformation		On Yielding	On Yielding	On Yielding
Rate of Trans-formation	Mart/unit strain in undeformed austenite	2.04	1.39	1.24
	Mart/unit strain in austenite with 80% prior deformation	1.80	1.30	1.44
	Effect of prior def. on rate of trans-formation	none	none	none
Optical Morphology	Type of martensite and size	long fragmented plates	fine crystals	ultra fine crystals
	Effect of prior deformation on size	size decreases	size decreases	size decreases

case causes an inversion of the yield stress temperature relationship and resulted in a decline of the yield strength with test temperature. An example of this is the yield strength of the heavily deformed Fe-25Ni-4Mo-0.28C alloy. The onset of transformation thus depended on the inherent strength of the austenite and on the stability of the austenite in both series of alloys.

Prior deformation of austenite at elevated temperature introduces marked changes in the substructure of the austenite deformation textures dependent on the S.F.E. and in the case of carbon containing alloys changes in the composition and stability of the austenite matrix. In this respect therefore, more basic data on the transformation can be drawn from a study of the transformation in fully annealed austenite.

1. Transformation in Austenite with No Prior Deformation

In undeformed austenite the rate of transformation per unit strain after yielding depended upon the relative stability of the alloy at the given test temperature. Thus the temperature interval between the M_d temperature of the alloy and the test temperature determined the rate of transformation regardless of the S.F.E.

The morphology of the martensite produced during straining however varied in consistent fashion within both series of alloys. In both series of alloys the size of the martensite crystals observed declined with decreasing S.F.E.

In the carbonless alloy with the highest S.F.E. a coarse plate like martensite was observed while the alloys with lower S.F.E. exhibited a much finer transformation product. Speich and Swann⁴³ have observed

that in Fe-Ni alloys the martensite formed in alloys containing greater than 25% nickel tended to be plate like in shape, while, in alloys containing decreasing nickel content, the martensite appeared in the form of "blocky" crystals and plate like martensite was not observed. The change in martensite morphology was associated with the increase in the amount of transformation twinning with increasing Ni content in the thermally induced martensite. Kelly and Nutting¹⁹ have postulated that twinning in martensite is favored by austenites of high S.F.E. (Ni increases the S.F.E. of austenite). This effect of S.F.E. is opposite to that found for mechanical twinning in f.c.c. metals where low S.F.E. favors deformation by twinning.⁴⁴

This suggests that the effect of solutes on the M_s temperature is more important than their effect on S.F.E. Patterson and Wayman⁴⁵ studying the thermally induced transformation in Fe-Ni alloys also observed that martensite crystals became more irregular and fragmented as the Ni content decreased. This was associated with a two stage transformation mechanism, the first stage involving twinning, the second involving slip shear with the same elements as the twinning elements observed in the same plate.

The studies referenced above were related to the thermally induced martensite transformation and while no similar studies have been conducted on the strain induced transformation the data is of interest when considering the morphology of the martensites observed in the high Ni alloys of Series I and II. Reference is made in this study to the optical appearance of the martensite observed. While observations are made on the coarseness of the transformation products it must be born in mind that the optical studies do not reveal the internal structure of the martensite. Thus the massive "blocky" type martensite observed in Fe-Ni alloys up to about 28% nickel consists of groups of dislocated laths⁴⁶ and as discussed above the plate

like martensite observed in the Fe-35Ni alloy is internally twinned. In this study while the morphology of the martensite undoubtedly varied within each alloy series the detailed morphology and internal structure of the martensite was not determined.

Consider first the alloys in Series I. In the Fe-35Ni alloy with no prior deformation (Figs. 7 thru 9) martensite was coarse but plate like. The plates were heavily fragmented but individual plates could be easily resolved at 400X. In the undeformed Fe-15Cr-15Ni alloy (Figs. 12 and 13) plate like martensite could not be resolved. The overall size of the martensite crystals was much finer but there were areas where both coarse and fine martensite was observed (Fig. 13). In the undeformed Fe-22Cr-12Ni alloy the martensite crystals were uniformly very fine; individual crystals could not be resolved at 1000X.

In considering the variation in the coarseness with S.F.E. within the series variations other than S.F.E. must be considered. The change in composition can result in differences in this series of alloys, which may explain the difference in behavior between low and high S.F.E. alloys. The ϵ -hcp phase was positively identified by X-ray analysis in the Fe-12Ni-22Cr alloy after testing at cryogenic temperatures and a large body of evidence has been referenced previously to suggest that the hcp structure acts as an intermediate phase in the $\gamma \rightarrow \alpha$ transformation. While the ϵ phase was not detected in the Fe-15Ni-15Cr alloy the Fe-Ni-Cr alloys will still have a greater stacking fault probability than the Fe-35Ni alloy. Kelly and Nutting¹⁹ have proposed a mechanism based on the possibility of stacking faults as nuclei for martensite and thus there is a strong possibility that the variation in coarseness of martensite in the alloy series can be attributed to these effects. The ϵ phase may restrict the growth of α martensite and the variation in stacking fault

probability may affect the availability of favorable nucleation sites.

A similar variation in the coarseness of martensite was observed in the case of carbon containing austenites. Martensite crystals formed during the straining of undeformed austenite decreased in size with decreasing S.F.E. of the alloy. The Fe-25Ni-4Mo-0.128C alloy exhibited coarse "blocky" martensite crystals (Fig. 24). The Fe-12Cr-12Ni-4Mo-0.30C alloy (Figs 26 and 27) represented the intermediate case where some coarse martensite was observed together with very fine martensite crystals which could not be resolved at 1000X. The alloy with the lowest S.F.E., the Fe-15.5Cr-8Ni-4Mo-0.3 alloy transformed to ultra fine martensite (Fig. 29 and 30) that again could not be resolved at 1000X. The ultra fine martensite crystals formed in the undeformed parent austenite in the latter two alloys was resolved at 6,000X for the Fe-12Cr-12Ni-4Mo-0.30C alloy and 12,000X for the Fe-15.5Cr-8Ni-4Mo-0.3 alloy with the scanning electron microscope (Figs. 35 and 36 and 37 and 38 respectively). The martensite formed in the latter alloy with the lowest S.F.E. was considerably finer and a qualitative estimate was made concluding that the average crystal size in the Fe-15.5 Cr-8Ni-4Mo-0.32C alloy was 1/2 of the crystal size in the Fe-12Cr-12Ni-4Mo-0.30C alloy. In both the carbon containing and carbonless series of alloys the grain size of all alloys within a given series was comparable. Since the austenites were undeformed prior to transformation there were limited barriers to the growth of the martensite crystals and the wide variation of crystal size must be attributed to the availability of favorable nucleation sites. Again as with Series I the stacking fault probability varies within the series and this could affect the supply of nucleation sites.

In order to study the course of transformation with increasing strain, specimens of undeformed carbon containing alloys were polished and then strained discontinuously. After each interval of strain, the polished

surface of the specimens were studied under oblique lighting to detect surface upheavals. After strain of approximately 20% the specimens were repolished and etched in order that the appearance of the etched martensite could be correlated with surface disruption observed on the polished surfaces.

The tests were conducted on undeformed austenite since continuous monitoring of the transformation occurring during straining indicated that, after yielding transformation commences and continues uniformly with increasing strain (Fig. 31). In the case of the Fe-25Ni-4Mo-0.28C alloy a positive distinction between martensite, slip lines and deformation twins was possible by repolishing and etching techniques. However in the case of the low S.F.E. alloys since considerable repolishing was necessary to ensure satisfactory micrographs the areas studied during discontinuous straining could not be reidentified after polishing and the similarity of the upheavals caused by the fine transformation products could not be positively distinguished from surface strain markings. The comparative aspects of the study were thus limited but the tests are reported here to indicate the potential of the technique in distinguishing between the growth of existing martensite and the nucleation of new crystals during the course of straining.

Figure 32(a), (b) (c) and (d) show the polished surface of an Fe-25Ni-4Mo-0.28C specimen after strains of 2, 4, 8 and 16% respectively. Figure 32(e) shows the surface of the specimen after a 16% strain, after the surface has been repolished and etched. Martensite areas can be clearly observed and correlated with surface upheavals observed on the polished surface.

After a 2% strain large martensite crystals are clearly visible (arrow, Fig. 32(a)). The transformation proceeds with increasing strain by the

nucleation of new plates usually although not exclusively in the area of existing plates (arrow, Fig. 32(b)). Some growth of existing plates is observed (arrow Fig. 30(c)) but the main increase in transformation is due to the appearance of new plates. All the martensite crystals were comparatively large and easily resolvable at 400X. Figure 32(e) showing etched martensite again shows the tendency for an autocatalytic effect of one martensite plate tending to nucleate another in the close vicinity. This results in a tendency for several clusters of martensite crystals to form. After 16% strain the plate like nature of martensite is evident. As the deformation proceeds in the alloy a high degree of transformation occurs and the plate like nature of the martensite is not easily distinguished (Fig. 24).

In the case of the second two carbon containing alloys in Series II the fine nature of the martensite crystals resulted in a situation where the slight surface disruption caused by the transformation appeared very similar in size and appearance to surface strain markings. Figures 33(a) (b), (c) and (d) show surface markings on a polished surface after 2, 4 8 and 20% strains. Figure 33(e) shows the same surface after a 20% strain and after repolishing and etching. The etched surface shows the martensite to be very fine and very finely separated bands of martensite form. These bands are generally although not invariably bi-directional forming cross-hatched patterns. The martensite crystals form imperfect lines crossing at a variable angle but the variation is relatively small varying around a mean of approximately 110° . Maskimova and Nikonorva⁴⁷ have suggested that the criterion governing the arrangement of strain induced martensite plates is that of maximum relief of applied stress. This is best achieved when the deformation produced by each martensite plate has at least a large

component in the direction of stress. This leads to production of martensite plates meeting at an obtuse angle.¹⁹

While some surface markings can be definitely identified as slip lines such as the coarse widely separated lines at the bottom of this series of figures, it is difficult to draw positive conclusions due to the ambiguity between slip lines and martensite upheavals. Figure 34(a),(b),(c) and (d) show similar surface markings observed on the polished surface of an Fe-8Ni-15.5Cr-4Mo-0.32C specimen after varying degrees of strain. Figure 34(e) show the corresponding etched surface. Again the fine nature of the martensite makes a positive identification of slip lines and upheavals due to transformation almost impossible.

In the case of the alloys with low S.F.E. observation of the transformation was limited to a study of the final product. The final transformation product was extremely fine martensite crystals with a size difference of approximately 2x between the alloys with a S.F.E. of approximately 15 ergs/cm² and 8 ergs/cm² respectively.

2. Transformation in Alloys with Prior Deformation

The deformation of annealed austenite at elevated temperature (450°C) results in a number of changes in the substructure which can vary with S.F.E. and will in turn affect subsequent transformation of austenite to ϵ and α martensite.

1. The variation in S.F.E. within a given alloy series will result in different dislocation substructures.³

2. After deformation at elevated temperature the deformation texture observed in the austenitic alloys shows a marked variation with S.F.E. In low S.F.E. alloys a sharp [100] texture develops. In high S.F.E. alloys a less symmetrical texture is observed.

3. In carbon containing alloys deformation at elevated temperature results in the precipitation of carbides in the austenite matrix. The amount and type of precipitates will be dependent on the composition of the austenite. The depletion of solutes from solid solution as carbide precipitates will result in changes in S.F.E. and changes in the M_s and M_d temperatures of the alloys.

To determine the effect of prior deformation on both carbon containing and carbonless alloys the curves shown in Fig. 41 and 42 were computed. The rate of transformation to martensite per unit strain in undeformed austenite for each alloy was taken as a baseline. This rate of transformation was subtracted from the rate of transformation per unit strain in austenite that has received prior deformation at 450°C . The resultant figure represents the increase in the rate of transformation during tensile straining at cryogenic temperatures due to prior deformation and is plotted against the amount of prior deformation at 450°C .

Figure 41 shows that the rate of transformation is unchanged by prior deformation in carbonless alloys. The dislocation substructure resulting from deformation of the austenite hinders the growth of martensite resulting in mechanical stabilization of the austenite and refining the size of martensite crystals. The preferred orientation effects however particularly in the case of low S.F.E. alloys where the normals to the (100) planes tend to align along the rolling direction (and the tensile axis) might be expected to stimulate transformation. In this orientation more slip systems are active and the resultant increase in dislocation interactions could account for a stimulation of transformation. In carbonless alloys while the rate of transformation is not changed by prior deformation the resultant α martensite is considerable finer. The amount of ϵ phase detected

in the Fe-12Ni-22Cr alloy was unaffected by the amount of prior deformation. Carbon containing alloys show a marked increase in transformation rate with increasing prior deformation. Figure 42 shows an increasing transformation rate with increasing prior deformation in all four carbon containing alloys tested. This effect is caused by chemical changes in the austenitic matrix occurring during deformation at 450°C. With the precipitation of carbides during deformation of austenite, alloying elements are removed from solid solutions. The first consequence of this is that the M_s and M_d temperatures are raised locally. After nucleation of martensite in this adjusted matrix the nucleus must propagate through an austenite which has a high density of dislocations and carbide precipitates. Both would be expected to retard the growth of martensite. Thus the increased rate of transformation (due to change in M_s and M_d) and the refinement of transformation products observed after prior deformation can be rationalized on these grounds. Deformation textures formed during the rolling operation at 450°C can also play a role in aiding transformation as with the carbonless alloys. Dillamore and co-workers^{11,12} have studied deformation textures in pure metals with a range of S.F.E.'s between 10-200 ergs/cm². The texture developed depends on the ease of cross-slip in the system. If cross slip can occur easily (high S.F.E.) the fcc metal will adopt a [111] texture. In alloys with a low S.F.E. a [100] texture is observed. In the range of S.F.E.'s considered in the two alloy series studied in this work, the low S.F.E. alloys would be expected to show a marked [100] texture while the high S.F.E. alloys (50 ergs/cm²) would be expected to show a mixed [111] and [100] texture. The marked [100] texture was detected in Fe-Ni-Cr alloys with low S.F.E. and while the exact texture in high S.F.E. alloys was not determined a marked preferred orientation of

[100] and [111] type poles was observed. Rolling textures of this type where [100] poles tend to align with the rolling direction will tend to increase dislocation interaction. If the martensite embryo is considered as a stress embryo (strain is important in that it results in stress peaks above the average stress level in the lattice) increased interaction and stress concentrations at pile-ups can result in a stimulation of transformation.

B. Tensile Characteristics

The concept of transformation induced plasticity (TRIP) involves the utilization of a phase transformation, in this case the austenite-martensite transformation, to prevent premature necking and failure of the parent austenite. The composition of the steel can be adjusted such that after thermo-mechanical treatment and at a given test temperature the austenite martensite transformation will begin in regions of high local strain where necking is occurring. The necked region is strengthened by the harder and stronger martensite phase and subsequent deformation is forced into areas adjacent to the necked region. Necking is arrested and uniform elongation along the gauge length is promoted.

In the case of carbonless alloys with low S.F.E. a three phase situation exists. The austenite transforms during tensile straining at cryogenic temperatures to ϵ and α martensite. Strengthening of the parent austenite is seen as an increased resistance to dislocation motion and both the ϵ and α phase can act as obstacles. While the ϵ phase can thus act to strengthen the austenite work by Mangonon²¹ indicates that the dominant strengthening phase is the α martensite phase. The b.c.c. martensite was effective in strengthening the parent austenite.

Thus while prime interest was centered on carbon containing alloys in terms of the ultra high strength and high ductility exhibited during cryogenic tensile testing, the carbonless alloys also exhibited good TRIP characteristics.

1. Carbonless Alloys

The yield strengths of undeformed carbonless alloys were all below 50,000 psi at R.T. The effect of decreasing test temperature on the yield stress of the austenite depended on two factors. The yield strength of austenite increases with decreasing test temperature, however, in addition the stability of the austenite with respect to transformation to martensite also decreases with temperature. When the stability of the austenite is low, stress induced transformation to martensite can initiate yielding at a relatively low stress level. The yield stress of undeformed austenite (solid lines) and austenites deformed 80% at 450°C prior to testing are shown in Fig. 43. The behavior of the undeformed austenites will be considered first. In the case of the Fe-23Ni-10Cr alloy the yield strength increases uniformly with decreasing test temperature. No transformation to α martensite or the ϵ phase was detected after cryogenic tensile tests. The alloy shows a consistent increase in yield strength with decreasing test temperature. The Fe-35Ni alloy also shows a consistent increase of yield strength with temperature indicating a relatively high stability of austenite. Transformation to martensite during tensile straining occurred only at the lowest test temperature, -196°C.

In the case of the Fe-15Ni-15Cr and Fe-12Ni-22Cr alloys the stability of both alloys below R.T. is comparatively low. The Fe-15Ni-15Cr alloy transformed to α martensite during straining at both -72°C and -196°C but no ϵ phase was observed. Transformation to the ϵ and α martensite occurred at both -72°C and -196°C during tensile straining of the Fe-12Ni-22Cr alloy. The yield strength of the Fe-15Ni-15Cr alloy increases only slightly

with decreasing test temperature and the yield strength of the Fe-12Ni-22Cr alloy remains constant. This indicates that in these alloys at cryogenic test temperatures, stress induced transformation of $\gamma \rightarrow \alpha$ and $\gamma \rightarrow (\epsilon, \alpha)$ respectively occurs at a relatively low stress level and initiates yielding. Thus the normal modulus dependence of yield strength with temperature is not observed.

The yield strengths of the austenitic alloys after an 80% deformation at 450°C are also shown in Fig. 43. The yield strength of the Fe-35Ni alloy shows a relatively small increase in yield strength due to work hardening at 450°C. The larger increase in yield strength of the other three alloys indicates that these alloys contain some small proportions of carbon. While the iron used in the alloys contained less than 0.005% by weight of carbon the chromium used was not of ultra high purity and the high work hardening rate in the Cr containing alloys indicates the precipitation of carbides during deformation at 450°C.

Strain induced martensite was effective in all cases in preventing premature failure during tensile straining by strengthening the austenite and increasing the work hardening rate. The martensite produced during tensile straining was stronger than the parent austenite. The tensile curves in all cases were smooth with no marked yield point and no marked Luders strain. The formation of martensite was reflected primarily in the work hardening rate observed and secondarily was reflected in the amount of uniform elongation obtained. Figure 44 shows the yield strength and ultimate tensile strengths of Fe-35Ni austenites with varying degrees of prior deformation at two different test temperatures. The larger spread

between the U.T.S. and yield curves reflects the increase work hardening rate and the uniform elongation data recorded at the lower test temperature (-196°C) were double the elongations recorded at -72°C . The improvement in ductility was most marked in heavily deformed austenite. Prior deformation increases the yield strength of the austenite and work hardening by dislocation mechanisms is not sufficient to prevent premature necking and failure. Thus in the case of the Fe-23Ni-10Cr alloy where only minimal quantities of martensite were formed during straining at -196°C elongation decreased rapidly with increasing prior deformation.

A limited amount of transformation was recorded for the Fe-15Ni-15Cr alloy during straining at -72°C but the rate of transformation was not high enough to prevent a marked decrease in elongation with increasing prior deformation. However, at the lower test temperature (-196°C) the stability of the austenite is reduced and the rate of transformation in the alloy was sufficient to result in high uniform elongations even in heavily deformed austenite.

The Fe-12Ni-22Cr alloy is the least stable of the carbonless alloys tested. At a test temperature of -72°C the transformation rate $\gamma \rightarrow (\epsilon, \alpha)$ is sufficient to increase the work hardening rate over that achieved during room temperature straining and improved ductility of deformed austenite results. Figure 43 shows the U.T.S. and yield strength data for this alloy plotted against the amount of prior deformation at the three different test temperatures. The increased work hardening rate attributed to transformation is seen as a widening spread between the curves at R.T. and at -72°C . At a test temperature of -196°C the alloy is even less stable and the rate of transformation is thus increased. This increased transformation rate is reflected largely in the work hardening rate but is not reflected by increased elongation data. It was observed in both carbon-

less and carbon containing alloys that when optimum elongation data was obtained the transformation rate and therefore the work hardening rate was relatively low. There is thus an optimum transformation rate (or austenite stability) for maximum elongation. Further reduction of austenite stability (lowering of test temperature) results in increased transformation rates which give rise to a more rapid work hardening rate but not in higher elongation values.

This can be seen clearly in the case of the curves of Fig. 45 for the Fe-12Ni-22Cr alloy. Yield strengths are similar at all test temperatures. Increased transformation with decreasing test temperature results in high ultimate strength levels at -196°C . Elongation data for the cryogenic tests are however, essentially similar. The work hardening rate of specimens tested at -72°C was sufficient to prevent early necking. At -196°C the increased work hardening rate at -196°C produced a rapid rise in the stress in the sample until the rate of hardening was not sufficient to prevent necking and failure at the higher stress levels reached.

2. Carbon Containing Alloys.

The yield strengths of fully annealed austenitic alloys and alloys deformed 80% at 450°C are plotted against test temperature in Fig. 46. The yield strength of the undeformed alloys increases with decreasing test temperature. The yield strength of the heavily deformed Fe-12Cr-12Ni-4Mo-0.30C and Fe-15.5Cr-8Ni-4Mo-0.32C alloys also increased with decreasing test temperature but the yield strength of the deformed Fe-25-Ni-4Mo-0.28C alloy decreased with decreasing temperature. The latter alloy is the least stable of the three alloys in Series II and as the test temperature decreased stress induced transformation to martensite initiated yielding at a relatively low stress levels. Prior deformation at elevated temperatures above M_d reduces the stability of all the austenitic

alloy in Series II by chemical means. During processing alloy carbides are precipitates and the resulting depletion of alloying elements in the austenitic matrix reduces the stability of the matrix. In the Fe-25Ni-4Mo-0.28C alloy prior deformation reduces the stability of the alloy to a point where the initiation of transformation by elastic stress causes plastic deformation and an apparent inversion of yield strength relation to test temperature.

The response to prior deformation in this alloy series is shown in Fig 47; the room temperature yield strengths for the three alloys are plotted against the amount of prior deformation at 450°C. At low deformation the yield strengths are similar. At higher deformations the response to prior deformation was superior in alloys with a low S.F.E.

This was attributed mainly to the presence of high percentages of chromium in the low S.F.E. alloys. During deformation at 450°C carbides are precipitates in the austenitic matrix as a result of vacancy enhanced diffusion, the vacancies being generated during plastic deformation.⁴⁹ The dispersion of carbides is controlled by the amounts of deformation, the concentration of carbide forming elements, and the diffusivity of the carbide forming solute. All alloys in the carbon containing series contained sufficient molybdenum to tie up carbon as carbides Mo_2C and MoC . For large deformations the diffusivity of Mo and Cr vary by an order of magnitude with molybdenum being greater than chromium. However, the presence of large quantities of chromium in addition to molybdenum will undoubtedly increase the amount of carbide precipitation and ensure a good dispersion of precipitates. In addition the slightly higher concentration of carbon in these alloys will also aid carbide dispersion. Thus a fine dispersion of small precipitates is anticipated in these Cr containing

alloys. This precipitation during deformation results in high dislocation densities after deformation since dislocations are pinned at these precipitates and multiply rapidly. Thus the higher yield strengths in low S.F.E. alloys are attributed to the larger proportions of Cr and hence the enhanced availability of carbide forming elements.

Ductility as represented by elongation was excellent in all cases in the undeformed condition at all test temperatures. However, elongation tended to be greater in alloys with the lower S.F.E. as was true in the case of the carbonless alloy series. When no transformation occurred during tensile testing elongations declined with increasing prior deformation. In the RT tests where no transformation occurred all alloys that had been deformed 80% at 450°C prior to testing exhibited elongation of the order of 5%.

Transformation to martensite during tensile straining was reflected primarily in the work hardening rate during straining, and secondarily, in elongation data in deformation austenites. The criteria for the onset of necking is

$$\frac{d\delta}{d\epsilon} = \delta$$

where δ and ϵ are the true stress and true strain levels respectively. In deformed austenite therefore where the stress levels are above 200,000 psi, the work hardening rate $d\delta/d\epsilon$ must be high in order to prevent premature necking and failure.

In the Fe-25Ni-4Mo-0.29C alloy room temperature ductility of deformed austenite as represented by elongation data was low. This alloy was the least stable of the three alloys in Series II however, and during testing

at -72°C , considerable transformation to martensite occurred during testing. The rapid rate of transformation indicated that the M_d of this alloy was close to R.T. The transformation to martensite during testing resulted in increased work hardening rates and improved elongation data in both deformed and undeformed austenite. At a test temperature of -196°C the stability of austenite was further reduced resulting in an increase in the work hardening rate during straining. Figure 48 shows the stress-strain curves for the alloy with an 80% prior deformation for tensile tests at -72°C and -196°C . The increase in the work hardening rate at the lower test temperature is evident. At the test temperature of -196°C yielding was initiated by the onset of transformation at a stress of 143,000 psi, the stress level rose to an ultimate of over 300,000 psi at which point the austenite was almost completely transformed.

Optimum strength-ductility ratios for this alloy were thus obtained at -72°C . The full series of stress-strain curves for the alloy at this test temperature are shown in Fig. 49.

At lower deformation levels the onset of transformation occurs uniformly along the gauge length of the specimen and the stress-strain curves are smooth and regular. After larger amounts of prior deformation a marked two stage stress-strain curve is observed. These two different types of curve correspond to the two different processes of deformation referred to under the experimental results section as Type A and Type B (p. 27). In the case of this alloy in heavily deformed austenite yielding was caused by the onset of transformation. There was then a period of very low strain hardening in the curve similar to a Luders strain. As the material yielded a local area of high strain or a neck began to form and was then arrested due to rapid work hardening caused by the relatively high

degree of transformation taking place in this area. No transformation occurs outside this deformation band which then traverses the specimen during the period of Luders strain. The high degree of local strain and the negligible increase in stress during this period of Luders strain indicate that strain plays an important part in the transformation during the passage of the Luders band. Following the period of Luders strain there was a period of rapid strain hardening. The stress increased rapidly with increasing strain and it was assumed that the martensite was again stress induced. The two stages of the stress-strain curve were observed in highly deformed alloys only where a high degree of localized strain occurs after yielding at a relatively high stress level. In undeformed alloys the transformation commenced as yielding occurred and the transformation progressed uniformly along the gauge length of the specimen with increasing strain.

Data for the Fe-12Cr-12Ni-4Mo-0.30C alloy at R.T. indicate that undeformed austenite has good inherent ductility. However, at R.T. this ductility declines rapidly with increasing prior deformation. This alloy had the highest stability (lowest M_d temperature) in Series II and at $+72^\circ\text{C}$ no transformation occurred during testing and again elongation values declined rapidly to below 10% with increasing prior deformation. At a test temperature of -196°C however the stability of the austenite was reduced to the level where a considerable degree of transformation occurred during straining. The tests were conducted in a non-conducting liquid nitrogen bath and it was possible to continuously monitor transformation occurring in the specimens by attaching the permeameter, specimen in position, and immersing the whole apparatus in LN_2 while testing the specimen on an Instron tensile tester. The stress strain curves for this alloy and curves showing the transformation occurring during testing at -196°C are shown in Fig. 31.

A similar pattern is seen in the nature of the curves as in the alloy discussed previously. With low prior deformation a smooth curve is obtained and the transformation occurring during straining proceeds almost linearly with strain. At high prior deformations (55% and 80%) a two stage stress-strain curve and transformation curve are obtained. A Luders band traverses the specimen and large quantities (30-50% in this case) of the martensite form within the band. Since high degrees of strain are associated with the transformation some martensite will be induced ahead of the band initially as the band traverses the specimen and thus causes the parabolic nature of the transformation curve in this case. After the period of Luders type strain a critical stress is reached in the specimen, the rate of transformation increases as does the work hardening rate and a steep rise in the stress-strain curve is observed. The stress-strain curves at this temperature indicate conditions are optimum for good ductility as represented by elongation data. Excellent combinations of strength and ductility are obtained (Table VI). Strength ductility ratios of 182,000 yield with 66% elongation, 280,700 yield with 47% elongation, and 309,700 with 31% elongation show excellent promise for cryogenic temperature applications.

The final alloy in Series II, Fe-15.5Cr-8Ni-4Mo-0.32C was of intermediate stability between the first two alloys. Transformation to martensite occurred during testing at -72°C although the rate of transformation was considerably lower than that observed in the Fe-25Ni-4Mo-0.28 alloy at that test temperature. The stress-strain curves for this alloy at a test temperature of -72°C are shown in Fig. 50. The curves are similar to those shown in Fig. 31, for the Fe-12Cr-12Ni-4Mo-0.30C alloy except for the fact that the Luders strain in specimens with high degrees of prior deformation is longer and the specimens failed directly the Luders strain

was complete. During testing at -196°C the alloy showed less stability and the work hardening rate was increased over that observed at -72°C due to the increased transformation rate but elongations decline slightly although not as drastically as during testing at R.T.

Overall the stability of austenite appeared to decline less rapidly with test temperature in alloys of low S.F.E. The M_d of Fe-25Ni-4Mo-0.28C alloy appeared very close to R.T. and at a test temperature of -72°C the transformation rate was very rapid. The composition of this alloy was changed very slightly to Fe-24Ni-4Mo-0.25C. Data for the R.T. testing of this additional alloy is shown in Table VII. The undeformed austenitic alloy still did not transform during R.T. testing, however prior deformation at 450°C reduced the stability of the alloy sufficiently such that transformation at a very slow rate occurred during the testing of all specimens of this alloy with prior deformation. The yield strength of the Fe-24Ni-4Mo-0.25C alloy was slightly lower than that of the Fe-25Ni-4Mo-0.28C alloy at R.T. and the transformation rate was very slow. This slow transformation rate was ideal for optimizing elongation in this high S.F.E. alloy. The R.T. stress-strain curves for this alloy are shown in Fig. 51. In the alloy with 20% prior deformation at 450°C a R.T. elongation of nearly 80% was recorded. Elongations declined with increasing prior deformation but the alloy with an 80% prior deformation still retained excellent ductility.

V. SUMMARY AND CONCLUSIONS

In a study of this nature where an extensive amount of data was gathered it often facilitates full comprehension to list conclusions in a concise form rather than in the form of a more open discussion. Therefore, conclusions and summarial discussion are presented below under the same headings as in the preceding section.

A. The Strain Induced Martensite Transformation

1. The coarseness of strain induced martensite formed in austenite by straining below M_D decreases with decreasing S.F.E. Massive blocks (carbon containing) or large fragmented plates (carbonless) formed in high S.F.E. alloys while α martensite formed in low S.F.E. alloys was very fine.
2. In the carbonless series of alloys the ϵ -hcp phase was detected in the Fe-12Ni-22Cr alloy after tensile straining below M_D . It was assumed that in this low S.F.E. alloy the ϵ phase acted as an intermediate phase in the austenite - α martensite transformation.
3. Dislocation substructures in deformed austenitic alloys decrease the size of martensite crystals compared with martensite crystals formed in fully annealed austenite,⁴⁸ by limiting the growth of the crystals. While the overall size of the martensite was refined in deformed alloys as compared with undeformed alloys, the rate of transformation was either unaffected (carbonless alloys) or stimulated (carbon containing). This indicates that prior deformation also affects the nucleation rate in austenite (see Conclusion 4).
4. No mechanical stabilization effects were observed in either series of alloys. The rate of transformation per unit strain was unaffected by prior deformation in carbonless alloys (Fig. 41). The unchanged transformation rate together with the refinement in size of the martensite

indicated an increased rate of nucleation. In carbon containing alloys prior deformation enhanced the rate of transformation (Fig. 42). The increase transformation rate is attributed to the lowering of austenite stability due to precipitation of alloy carbides during deformation.

5. It was not possible to correlate the difference in the optical morphology of the martensite directly with the variation in S.F.E. within the two alloy series, particularly in deformed austenites. Within a given alloy series dislocation substructures varied with S.F.E., varying deformation textures were introduced during deformation, precipitation reactions varied with composition in deformed carbon-containing alloys and in Fe-Ni-Cr alloys in the low S.F.E. alloy the sequence of transformation was $\gamma \rightarrow \tau \rightarrow \alpha'$ compared with $\gamma \rightarrow \alpha'$ in the high S.F.E. alloys.

6. The rate of transformation in any given alloy is determined by the difference between the M_D temperature of the alloy and the test temperature under consideration. While this positive correlation could be made concerning the rate of transformation, the size and distribution of martensite could not be correlated directly to S.F.E. Only tentative correlations between the indirect effects of the changing S.F.E. (mentioned in 5) and the nature of transformation products were attempted.

B. Carbonless Alloys

1. The yield strength of the carbonless alloys at cryogenic temperatures was strongly effected by the stability of austenite. In some cases where a minimal increase in yield strength with decreasing test temperature was observed, the stress induced transformation to martensite at cryogenic temperature initiated yielding at a relatively low stress level.

2. Ductility as represented by elongation tended to be higher in alloys with low S.F.E.

3. Martensite formed during tensile straining at cryogenic temperatures was effective in increasing the work hardening rate of tensile specimens preventing premature necking and increasing uniform elongation.

4. In the Fe-12Ni-22Cr alloy while the ϵ phase undoubtedly contributed to the strengthening of austenite, the strain induced α phase was considered the main cause of strengthening.

5. The average size of the strain induced martensite crystals tended to decrease with decreasing S.F.E. The finer martensite resulted in a refined structure and appeared more effective in producing excellent TRIP characteristics.

6. Optimum ductility in terms of high uniform elongation data was obtained when a relatively slow rate of transformation to α martensite was observed during tensile straining. (See conclusion for carbon containing alloys).

C. Alloys Containing Carbon (Nominally 0.3% C)

1. Alloys with a low S.F.E exhibited a greater increase in yield strength with increased prior deformation at 450°C. This was attributed partially to the high percentages of the strong carbide former Cr in these alloys rather than differences in S.F.E. Yield strengths in excess of 320,000 psi and 270,000 psi were reached for the Fe-12Cr-Ni-4Mo-0.30C and the Fe-15.5Cr-8Ni-4Mo-0.32C carbon alloys respectively after an 80% deformation at 450°C. After a similar prior deformation the yield strength of the Fe-25Ni-4Mo-0.20C alloy was below 200,000 psi at all test temperatures.

2. The yield strength of the two low S.F.E. austenitic alloys increased with decreasing test temperature. The yield strength of the Fe-25Ni-4Mo-0.28C alloy showed a slight decrease with decreasing test temperatures. This inversion of the yield strength temperature relation was attributed

to stress induced transformation to martensite initiating yielding at a relatively low stress level when the stability of the alloy was low.

3. Ductility as represented by elongation was excellent in all cases in the undeformed condition at all test temperatures. However, elongation tended to be greater in alloys with the lower S.F.E. as was true in the case of the carbonless alloy series.

4. When no transformation occurred during tensile testing elongations declined with increasing prior deformation. In RT tests where no transformation occurred all alloys that had been deformed 80% at 450°C prior to testing exhibited elongation of the order of the 5%.

5. In the Fe-24Ni-4Mo-0.28C alloy, the Fe-12Cr-12Ni-4Mo-0.30C alloy and the Fe-15.5Cr-8Ni-4Mo-0.32C alloy the M_d temperatures were such that the strain induced martensite transformation was induced at -72°C, -196°C and -72°C respectively. In these alloys at these test temperatures the martensite transformation was effective in producing greatly enhanced uniform elongations in deformed alloys. Elongations tended to increase with prior deformation and reached a maximum after 15-30% prior deformation. After reaching a maximum elongations tend to decline at a uniform slow rate with increase prior deformation.

6. The amount of martensite produced during tensile straining was not the important factor in optimizing elongation data. Maximum elongations were obtained when the transformation rate and thus the work hardening rate during tensile straining was relatively low. Figure 52 shows a plot of elongation data vs transformation for all carbon containing alloys for all tests in which more than 10% martensite was formed during straining. It can be seen that low transformation rates producing work hardening rates only slightly higher than the inherent work hardening rates of the parent austenite result in optimum elongation data.

7. As with the carbonless alloys, prior deformation resulted in no stabilization of the strain induced martensite transformation. In fact the rate of transformation was stimulated by prior deformation (Fig. 42).

8. Uniform elongations induced by the strain induced transformation were consistently greater in alloys with lower S.F.E. This was attributed to the finer distribution of transformation products.

9. The fracture characteristics of all three carbon containing alloys in Series II were similar. Figs. 53 through 55 show scanning electron microscope micrographs taken of the fracture surfaces of the three alloys. In all cases an area of large dimples (low energy fracture in austenite) was separated from an area of smaller dimples (fracture in martensite) by a stretched region or a transition region between the two fracture areas.

ACKNOWLEDGEMENTS

The author wishes to express his grateful appreciation to Professor V. F. Zackay, E. Parker and G. Thomas for their encouragement and support throughout the course of this investigation.

Special thanks is extended to Mr. John Holthuis whose assistance and expertise were invaluable in achieving close control of processing parameters.

This work was performed under the auspices of the United States Atomic Energy Commission through the Inorganic Materials Research Division of the Lawrence Radiation Laboratory.

REFERENCES

1. Zackay, V. F., Parker, E. E., Fahr, D., and Busch, R., Trans. ASM 252, 60 (1967).
2. Dunning, J., M. S. Thesis, University of California, Berkeley, 12/1966.
3. Breedis, J. F., Acta Met. 13, 230 (1965).
4. Cohen, M., Trans AIME, 212, 171 (1958).
5. Cohen, M., Machlin, E., Paranjpe, V., Thermodynamics in Phys Metallurgy p. 242, Amer. Soc. Met., Cleveland, Ohio (1945).
6. Swann, P. R., Corrosion, 1963, vol. 19, No. 3, p. 102.
7. Fawley, R., Quader, M. and Dodd, R., Trans. of Met. Soc. of AIME Vol. 242, p. 771 (1968).
8. Smallman, R. E. and Green, D., Acta Met., 12, 145 (1964).
9. Dillamore, I. L., and Roberts, W., Acta Met., 12, 281 (1964).
10. Dillamore, I. L. et al., Acta Met., 12, 155 (1964).
11. Dillamore I. L., et. al., Phil. Mag., 9, 517 (1964).
12. Dillamore, I. L., and Smallman, R. E., Phil. Mag. 12, 191, (1965).
13. Reed, R. P., Acta Met. 10, 865, (1962).
14. Breedis, J. F., and Robertson, W. D., Acta Met., 10, 1077 (1962).
15. Lagneborg, R., Acta Met., 12, 823 (1964).
16. Venables, J. A., Phil. Mag., 7, 35 (1962).
17. Dash, J., and Otte, H. M., Acta Met., 11, 1165 (1963).
18. Breedis, J. F., Trans. Met. Soc. AIME, 230, 1583 (1964).
19. Kelly, P. M. and Nutting, J., Journal Iron and Steel Inst., 197, 199, (1961)
20. Kelly, P.M., Acta Met., 13, 635 (1965).
21. Mangonon, P. L., Ph.D. Thesis, University of Cal., Berkeley, Aug (1968).
22. Cina, B., Acta Met., 6, 748 (1958).
23. Reed, R. P., and Guntner, C. J., Trans. Met. Soc. AIME, 230, 1713 (1964)

24. Gunter, C. J. and Reed, R., Trans ASM 55, 399, (1962).
25. Nutting, J. and Dulieu, D., Iron and Steel Institute Report No. 86 p. 140, Iron and Steel Institute, London, (1964).
26. Douglass, D., Thomas, G. and Roset, W., Corrosion, Vol. 20, p. 15 (1964).
27. Hirsch, P. B., et al., Electron Microscopy of Thin Crystals, p. 429-32 Butterworth and Co., (1965).
28. Andrews, K. W., Journal of Iron and Steel Institute, p. 721, July (1965).
29. Schneider, H., Foundry Trade J., 108 562-563, (1960).
30. Angle, T., J.I.S.I., p. 165, May (1964).
31. Cullity, B. D., Elements of X-ray Diffraction, (Addison-Wesley, Notre Dame), (1956).
32. Taylor, A., X-ray Metallography, (John Wiley, New York), (1961).
33. Hall, J. A., M.S. Thesis, p. 3, University of Calif., Berkeley, June 1968.
34. Thomas, G., Schwartz, D. and Gerberich, W., High Strength Materials, V.F. Zackay, Ed., John Wiley and Sons, N.Y. p. 284, (1965).
35. Das Gupta, S. and Lement, B., Trans. AIME, p. 727, Sept. (1951).
36. Dash, J., and Otte, H., Acta Met., p. 1169 11, (1963).
37. Fiedler, H. C., et al., Trans. ASM, 47, 267 (1955).
38. Bolling, G. and Richman, R., Acta Met., 678, V. 15, (1967).
39. Kulin, S. and Speich, G., Journal of Metals , 258, 3, (1952).
40. Machlin, E., and Cohen, M., Journal of Metals, 489, May (1952).
41. Reed, R.P., Acta Met., 1287, 15, (1967).
42. Cohen, M. and Pati, S., Acta Met., 189, 17 (1969).
43. Speich, G. and Swann, P., J. Iron and Steel Inst., 203, 480 (1965).
44. Johari, O., and Thomas, G., Acta Met., 12, 1153 (1964).
45. Patterson, R. and Waymen, C., Acta Met., 14, 347 (1966).
46. Das, S. and Thomas, G., Trans. AIME (in press).

47. Makaimova, O. and Nikonorova, A., Prob. Metalloved Fiz. Metal, 4, 123, (1965).
48. Zackay, V. F., and Parker, E. R., High Strength Materials, V. F. Zackay Ed. (John Wiley, N.Y) p. 130 (1965).

TABLE I. Series I Room Temperature Tests

Alloy Composition	Prior Def. at 450°C %	Yield Strength (p.s.i)	UTS (p.s.i)	Elonga. %	Martensite Formed During Testing %
Fe-35Ni	0	48,160	59,710	25.1	1.0
	15	56,020	63,490	10.1	1.6
	25	59,200	66,840	8.5	1.8
	55	72,600	78,380	5.0	2.0
	80	78,740	81,740	8.1	1.7
Fe-23Ni-10Cr	0	21,780	57,720	34.1	2.7
	25	73,690	82,770	7.6	1.7
	55	93,980	101,580	5.3	1.5
	80	115,780	123,280	4.5	1.5
Fe-15Ni-15Cr	0	31,420	67,040	37.3	1.5
	15	60,810	70,830	22.0	2.2
	25	74,030	78,680	13.2	2.1
	55	93,980	100,940	5.7	1.0
	80	109,490	116,230	8.5	1.0
Fe-12Ni-22Cr	0	29,210	73,900	62.0	2.2
	10	72,060	88,200	45.1	2.0
	25	81,150	92,870	35.9	1.9
	45	91,350	98,250	21.0	1.8
	80	101,200	108,940	20.6	1.8

TABLE II Series I Dry Ice

Alloy Composition	Prior Def. At 450 C %	Yield Strength (p.s.i.)	UTS (p.s.i.)	Elonga. %	Martensite Formed During Testing %
Fe-35Ni	0	59,560	73,640	16.9	2.3
	15	66,950	76,520	14.5	2.1
	25	72,800	84,610	15.2	1.7
	55	82,110	91,090	12.6	1.7
	80	89,130	97,240	12.4	2.1
Fe-23Ni-10Cr	0	36,600	70,500	36.1	1.2
	25	91,360	96,290	10.8	1.0
	55	112,540	119,250	5.8	1.0
	80	135,640	141,210	6.6	2.0
Fe-15Ni-15Cr	0	35,510	87,260	58.6	13.8
	15	64,920	98,310	44.2	14.6
	25	74,630	105,730	39.6	21.5
	55	97,260	113,180	27.3	8.0
	80	124,420	135,060	18.6	3.0
Fe-12Ni-22Cr	0	28,330	104,500	56.7	53.3
	10	64,918	111,800	47.1	47.9
	25	75,730	117,800	45.7	43.6
	45	86,160	120,000	44.0	41.1
	80	103,120	133,700	37.8	41.5

TABLE III Series I LN₂ Test

Alloy Composition	Prior Def. at 450°C %	Yield Strength (p.s.i.)	UTS (p.s.i.)	Elonga. %	Martensite Formed During Testing %
Fe-35Ni	0	76,200	122,000	28.5	58.0
	15	78,710	117,060	24.9	55.0
	25	81,430	120,780	26.8	60.0
	55	101,390	133,530	27.8	55.0
	80	110,680	136,770	30.6	55.0
Fe-23Ni-10Cr	0	62,140	110,920	56.1	2.3
	25	97,940	127,140	40.1	4.9
	55	133,380	153,480	26.5	4.3
	80	152,010	171,300	15.3	1.5
Fe-15Ni-15Cr	0	47,260	151,670	39.4	54.9
	15	63,030	159,460	41.1	59.1
	25	76,140	163,300	40.6	56.3
	55	100,320	175,100	43.5	56.8
	80	134,400	190,300	43.2	56.1
Fe-12Ni-22Cr	0	33,300	152,000	50.0	62.0
	10	54,450	165,100	55.2	60.5
	25	61,110	165,700	45.0	59.0
	45	82,170	177,410	43.4	58.0
	80	103,880	184,962	37.8	54.7

TABLE IV. Series II Room Temperature Tests Alloys with Carbon

Alloy Composition	Prior Def. at 450°C %	Yield Strength (p.s.i.)	UTS (p.s.i.)	Elonga. %	Martensite Formed During Testing %
Fe-25Ni-4Mo-0.29C	0	50,400	87,460	26.5	1.5
	15	125,300	132,300	7.1	2.0
	25	125,775	132,750	7.0	2.0
	55	157,140	167,700	8.1	5.1
	80	182,500	189,300	4.4	3.2
Fe-12Cr-12Ni-4-Mo-0.30C	0	50,070	102,650	53.0	1.0
	15	127,840	135,750	20.2	1.0
	25	143,100	155,320	12.5	1.0
	55	189,600	204,320	5.1	1.0
	80	222,300	256,300	5.1	1.0
Fe-15.5Cr-8Ni-4Mo-0.32C	0	55,150	112,070	49.5	1.0
	15	100,650	133,000	35.1	1.0
	25	149,200	160,310	19.8	1.0
	55	186,700	195,100	5.8	1.0
	80	236,300	248,200	6.8	1.0

TABLE V Series II Dry Ice Tests (-72 C) Alloys with Carbon

Alloy Composition	Prior Def. at 450 C %	Yield Strength (p.s.i.)	UTS (p.s.i.)	Elonga. %	Martensite Formed During Testing %	
Fe-25Ni-4Mo-0.29C	0	59,163	142,300	43.0	72.0	
	15	127,300	152,100	41.0	79.2	
	25	125,440	191,900	26.5	78.3	
	55	123,300	189,560	25.7	83.0	
	80	161,400	217,543	25.4	85.0	
Fe-12Cr-12Ni-4 Mo-0.30C	0	69,970	130,170	45.3	1.5	
	15	132,810	161,700	28.0	2.0	
	25	129,730	155,510	30.5	2.0	
	55	202,300	215,500	10.0	1.0	
	80	248,300	259,600	7.2	1.0	
Fe-15.5Cr-8Ni-4Mo-0.32C	0	75,600	164,410	48.7	22.5	
	15	136,360	189,700	53.1	34.6	
	25	135,450	192,720	58.1	41.2	
	55	{	225,540	229,040	49.3	41.4
			220,000	240,600	43.2	45.2
	80	{	263,900	263,900	25.5	37.6
265,140			269,050	31.3	51.5	

TABLE VI Series II LN₂ Tests (-196°C) Alloys with Carbon

Alloy Composition	Prior Def. at 450°C %	Yield Strength (psi)	UTS (p.s.i.)	Elonga. %	Martensite Formed During Testing %
Fe-25Ni-4Mo-0.29C	0	88,424	230,340	20.9	85.6
	15	99,700	248,100	14.5	78.1
	25	114,900	268,000	16.6	85.1
	55	130,200	275,850	16.8	100.1
	80	143,800	302,090	19.1	93.4
Fe-12Cr-12Ni-4Mo-0.30C	0	110,850	184,490	44.5	17.3
	15	148,550	236,970	60.5	49.3
	25	182,100	256,700	66.1	61.4
	55	280,700	301,600	46.8	58.7
	80	300,200	303,200	31.0	58.1
Fe-15.5Cr-8Ni-4Mo-0.32C	0	100,000	209,100	43.5	31.5
	15	201,500	268,700	40.2	42.0
	25	218,100	267,400	29.7	51.2
	55	245,500	300,460	26.5	49.6
	80	311,100	329,200	19.7	59.2

TABLE VII. Series II(a) Room Temperature Tests Alloys with Carbon

Alloy Composition	Prior Def. at 450°C %	Yield Strength (p.s.i.)	UTS (p.s.i.)	Elonga. %	Martensite Formed During Testing %
Fe-24Ni-4Mo-0.25C	0	42,300	72,120	39.6	< 1.0
	20	91,540	109,200	79.4	31.5
	35	120,000	138,650	55.5	44.2
	50	144,050	155,700	47.6	51.0
	65	157,140	171,250	39.6	58.9
	80	164,000	175,850	40.6	69.0

TABLES VIII Values of Factors in Calculation of R

$$\text{CuK}_\alpha \lambda = 1.54\text{\AA}$$

Monochromator (200) Lif bent crystal

$$\theta_M \text{ with CuK}_\alpha = 22^\circ 34' = 22.57^\circ$$

Factor	(101) _e	(200) _γ	(200) _{α'}
2θ _B	46.8°	50.8°	65.0°
θ _B	23.4°	25.4°	32.5°
sin θ _B	0.397	0.429	0.537
sin θ _B /λ	0.258	0.278	0.349
f _{FE}	17.7	17.3	15.2
f _{Cr}	16.3	15.8	13.9
f _{Ni}	19.30	18.8	16.6
f* _{alloy}	17.6	17.2	15
F ²	929	4733	912
P	12	6	6
e ^{-2M#}	0.95	0.94	0.92
v	23.2Å ³	46.3Å ³	23.6Å ³
LP	4.27	3.60	2.24
$f^*_{\text{alloy}} = 0.12 f_{\text{Ni}} + 0.22 f_{\text{Cr}} + 0.66 f_{\text{Fe}}$			

FIGURE CAPTIONS

- Fig. 1. Modified phase chart for Fe-Ni-Cr system.
- Fig. 2. Tensile sheet specimen, thickness 0.050 inches.
- Fig. 3. Mechanical properties and transformation data versus percent prior deformation for Fe-35Ni alloy at test temperatures of RT, -72°C and -196°C . Yield strength, ultimate tensile strength, elongation and the percent transformation to martensite are shown plotted against the amount of prior deformation at 450°C .
- Fig. 4. Mechanical properties and transformation data versus percent prior deformation for Fe-23Ni-10Cr alloy at test temperatures of RT, -72°C and -196°C . Yield strength, ultimate tensile strength, elongation and the percent transformation to martensite are shown plotted against the amount of prior deformation at 450°C .
- Fig. 5. Mechanical properties and transformation data versus percent prior deformation for Fe-15Ni-15Cr alloy at test temperatures of RT, -72°C and -196°C . Yield strength, ultimate tensile strength, elongation and the percent transformation to martensite are shown plotted against the amount of prior deformation at 450°C .
- Fig. 6. Mechanical properties and transformation data versus percent prior deformation for Fe-12Ni-22Cr alloy at test temperatures of RT, -72°C and -196°C . Yield strength, ultimate tensile strength, elongation and the percent transformation to martensite are shown plotted against the amount of prior deformation at 450°C .

- Fig. 7. Optical micrograph of Fe-35Ni austenite with 0% prior deformation after tensile testing at -196°C . 400X.
- Fig. 8. Optical micrograph of Fe-35Ni austenite with 0% prior deformation after tensile testing at -196°C , 1000X.
- Fig. 9. Optical micrograph of Fe-35Ni austenite with 0% prior deformation after tensile testing at -196°C , 1000X.
- Fig.10. Optical micrograph of Fe-35Ni austenite with 80% prior deformation after tensile testing at -196°C , 400X.
- Fig.11. Optical micrograph of Fe-35Ni austenite with 80% prior deformation after tensile testing at -196°C , 1000X.
- Fig.12. Optical micrograph of Fe-15Cr-15Ni austenite with 0% prior deformation after tensile testing at -196°C , 400X.
- Fig.13. Optical micrograph of Fe-15Cr-15Ni austenite with 0% prior deformation after tensile testing at -196°C , 1000X.
- Fig.14. Optical micrograph of Fe-15Cr-15Ni austenite with 80% prior deformation after tensile testing at -196°C , 400X.
- Fig.15. Optical micrograph of Fe-15Cr-15Ni austenite with 80% prior deformation after tensile testing at -196°C , 1000X.
- Fig.16. Optical micrograph of Fe-12Ni-22Cr austenite with 0% prior deformation after tensile testing at -72°C , 1000X.
- Fig.17. Optical micrograph of Fe-12Ni-22Cr austenite with 80% prior deformation after tensile testing at -72°C , 1000X.
- Fig.18. X-ray diffractometer trace at RT of Fe-12Ni-22Cr austenite with no prior deformation. The alloy had been tested at -72°C and transformation to ϵ and α martensite was detected.
- Fig.19. Schematic representation of an x-ray back reflection photograph showing the (200) γ reflection obtained from the Fe-35Ni and Fe-12Ni-22Cr alloys after a 25% prior deformation at 450°C .

- Fig.20. Mechanical properties and transformation data versus percent prior deformation at 450°C , for Fe-25Ni-4Mo-0.28C alloy at test temperatures of RT, -72°C and -196°C .
- Fig.21. Mechanical properties and transformation data versus percent prior deformation at 450°C , for Fe-12Cr-12Ni-4Mo-0.30C alloy at test temperatures of RT, -72°C and -196°C .
- Fig.22. Mechanical properties and transformation data versus percent prior deformation at 450°C , for Fe-15.5Cr-8Ni-4Mo-0.32C alloy at test temperatures of RT, -72°C and -196°C .
- Fig.23. Mechanical properties and transformation data versus percent prior deformation at 450°C , for Fe-24Ni-4Mo-0.25C alloy at RT.
- Fig.24. Optical micrograph of Fe-25Ni-4Mo-0.28C alloy with 0% prior deformation after tensile straining at -72°C , 1000 \times .
- Fig.25. Optical micrograph of Fe-25Ni-4Mo-0.28C alloy with 80% prior deformation after tensile straining at -72°C , 1000 \times .
- Fig.26. Optical micrograph of Fe-12Cr-12Ni-4Mo-0.30C alloy with 0% prior deformation after tensile straining at -196°C , 400 \times .
- Fig.27. Optical micrograph of Fe-12Cr-12Ni-4Mo-0.30C alloy with 0% prior deformation after tensile straining at -196°C , 1000 \times .
- Fig.28. Optical micrograph of Fe-12Cr-12Ni-4Mo-0.30C alloy with 80% prior deformation after tensile straining at -196°C , 1000 \times .
- Fig.29. Optical micrograph of Fe-15.5Cr-8Ni-4Mo-0.32C alloy with 0% prior deformation after tensile straining at -72°C , 1000 \times .
- Fig.30. Optical micrograph of Fe-15.5-8Ni-4Mo-0.32C alloy with 80% prior deformation after tensile straining at -72°C , 1000 \times .
- Fig.31. Engineering stress-strain curves and transformation versus strain curves for Fe-12Cr-12Ni-4Mo-0.30C alloy with varying degrees of prior deformation.

- Fig.32. Surface of a polished tensile specimen of undeformed Fe-25Ni-4Mo-0.28C after varying degrees of tensile straining at -72°C , 400X.
- Fig.33. Surface of a polished tensile specimen of undeformed Fe-12Cr-12Ni-4Mo-0.30C after varying degrees of tensile straining at -196°C 400X.
- Fig.34. Surface of a polished tensile specimen of undeformed Fe-15.5Cr-8Ni-4Mo-0.32C after varying degrees of tensile straining at -72°C , 400X.
- Fig.35. Scanning electron micrograph of etched Fe-12Cr-12Ni-4Mo-0.30C alloy after tensile testing at -196°C , 6000X.
- Fig.36. Scanning electron micrograph of etched Fe-12Cr-12Ni-4Mo-0.30C alloy after tensile testing at -196°C , 6000X.
- Fig.37. Scanning electron micrograph of etched Fe-15.5Cr-8Ni-4Mo-0.32C alloy after tensile testing at -72°C , 12,000X.
- Fig.38. Scanning electron micrograph of etched Fe-15.5Cr-8Ni-4Mo-0.32C alloy after tensile testing at -72°C , 12,000X.
- Fig.39. Scanning electron micrograph of etched Fe-25Ni-4Mo-0.28C alloy after tensile testing at -72°C , 6000X.
- Fig.40. Scanning electron micrograph of etched Fe-25Ni-4Mo-0.28C alloy after tensile testing at -72°C , 6000X.
- Fig.41. The increase in the rate of transformation to α' martensite per unit strain versus the amount of prior deformation at 450°C for carbonless alloys.
- Fig.42. The increase in the rate of transformation to α' martensite per unit strain versus the amount of prior deformation at 450°C for carbon containing alloys.

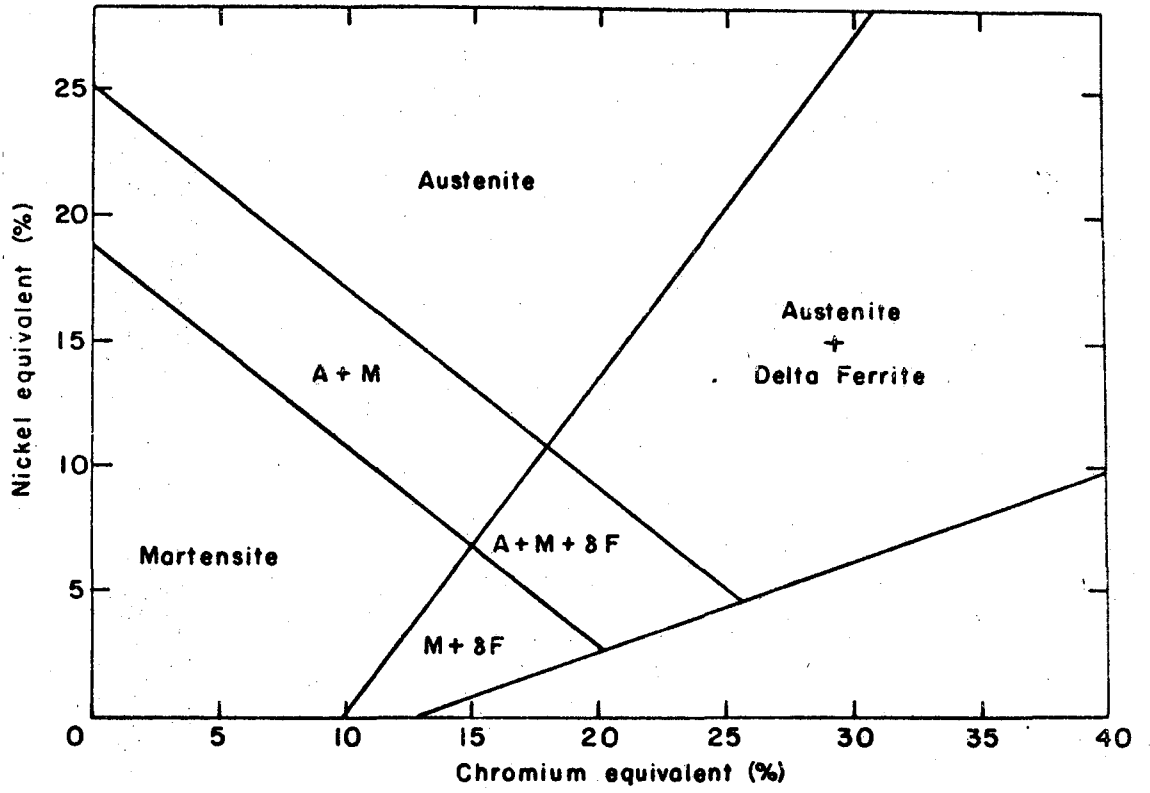
- Fig. 43. The yield strength of carbonless alloys in the undeformed conditions and after an 80% prior deformation at 450°C versus test temperature.
- Fig. 44. The variation of yield strength and ultimate tensile strength with the amount of prior deformation at 450°C for the Fe-35Ni alloy at test temperatures of -72°C and -196°C.
- Fig. 45. The variation of yield strength and ultimate tensile strength with the amount of prior deformation at 450°C for the Fe-12Ni-22Cr alloy at test temperatures of Rt, -72°C and -196°C.
- Fig. 46. The yield strength of carbon containing alloys in the undeformed condition and after an 80% prior deformation at 450°C versus test temperature.
- Fig. 47. The variation of room temperature yield strength with prior deformation at 450°C for carbon containing alloys.
- Fig. 48. Schematic of engineering stress-strain curves for the Fe-25Ni-4Mo-0.28C alloy after an 80% prior deformation at 450°C. Curves for tensile tests at 72°C and -196°C are shown.
- Fig. 49. Engineering stress-strain curves for Fe-25Ni-4Mo-0.28C alloy tested at -72°C after varying degrees of prior deformation at 450°C.
- Fig. 50. Engineering stress-strain curves for Fe-15.5Cr-8Ni-4Mo-0.32C alloy tested at -72°C after varying degrees of prior deformation at 450°C.
- Fig. 51. Engineering stress-strain curves for Fe-24Ni-4Mo-0.25C alloy tested at RT after varying degrees of prior deformation at 450°C.

Fig.52. Plot showing the elongation data for all carbon containing alloys tested versus the rate of transformation to martensite per unit strain during tensile straining.

Fig.53. Fractograph of an undeformed Fe-25Ni-4Mo-0.28C alloy specimens tested at -72°C .

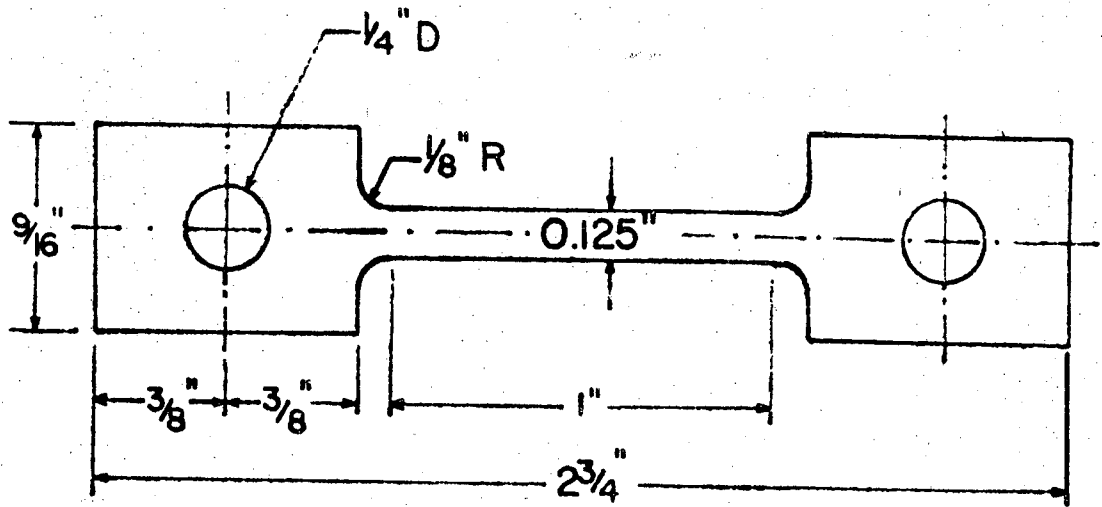
Fig.54. Fractograph of an undeformed Fe-12Ni-12Cr-4Mo-0.20C alloy specimens tested at -196°C .

Fig.55. Fractograph of an undeformed Fe-15.5Cr-8Ni-0.32C alloy specimens tested at -72°C .



XBL 6911-6528

Figure 1

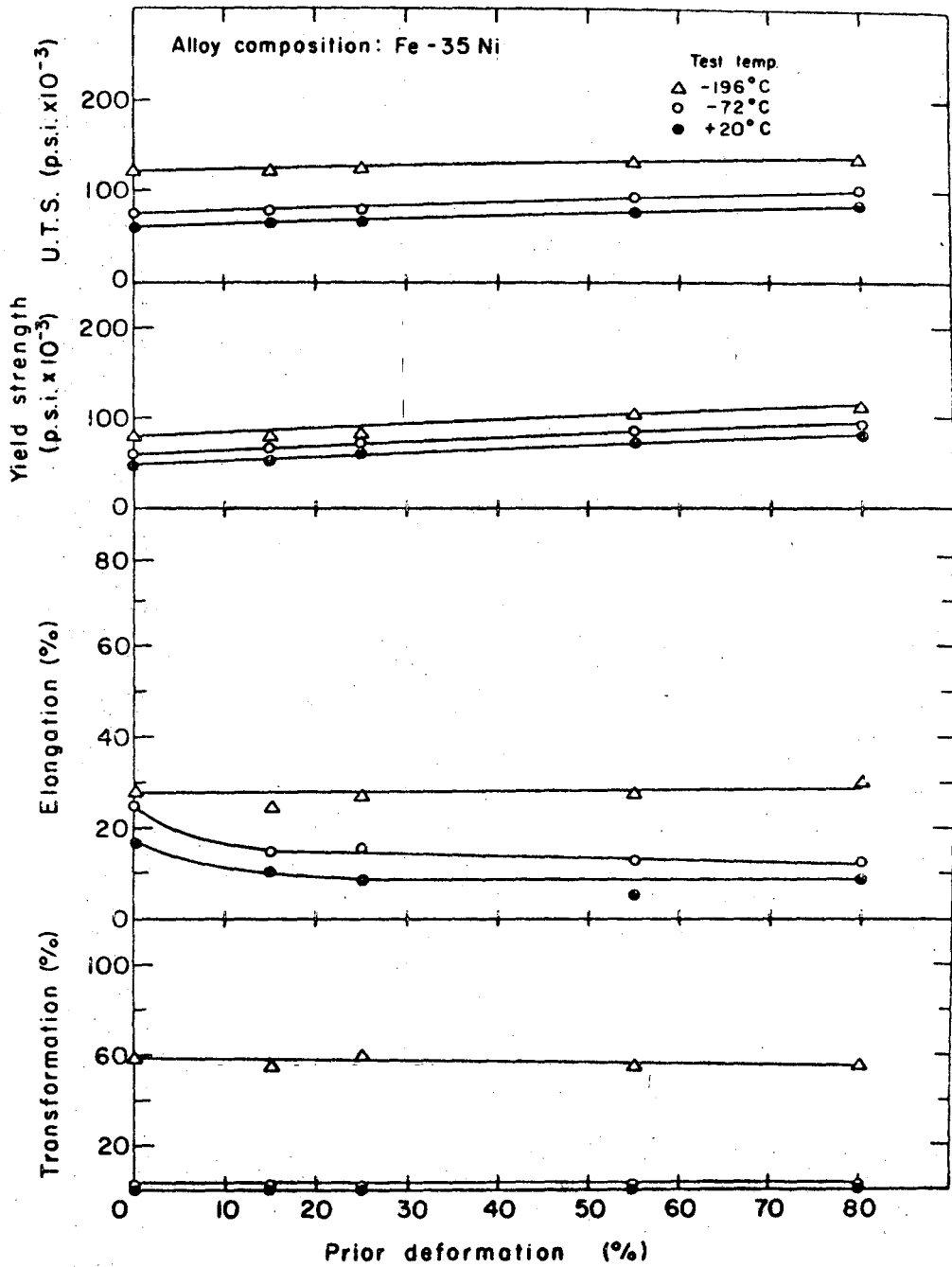


TENSILE SPECIMEN

SCALE: 2:1

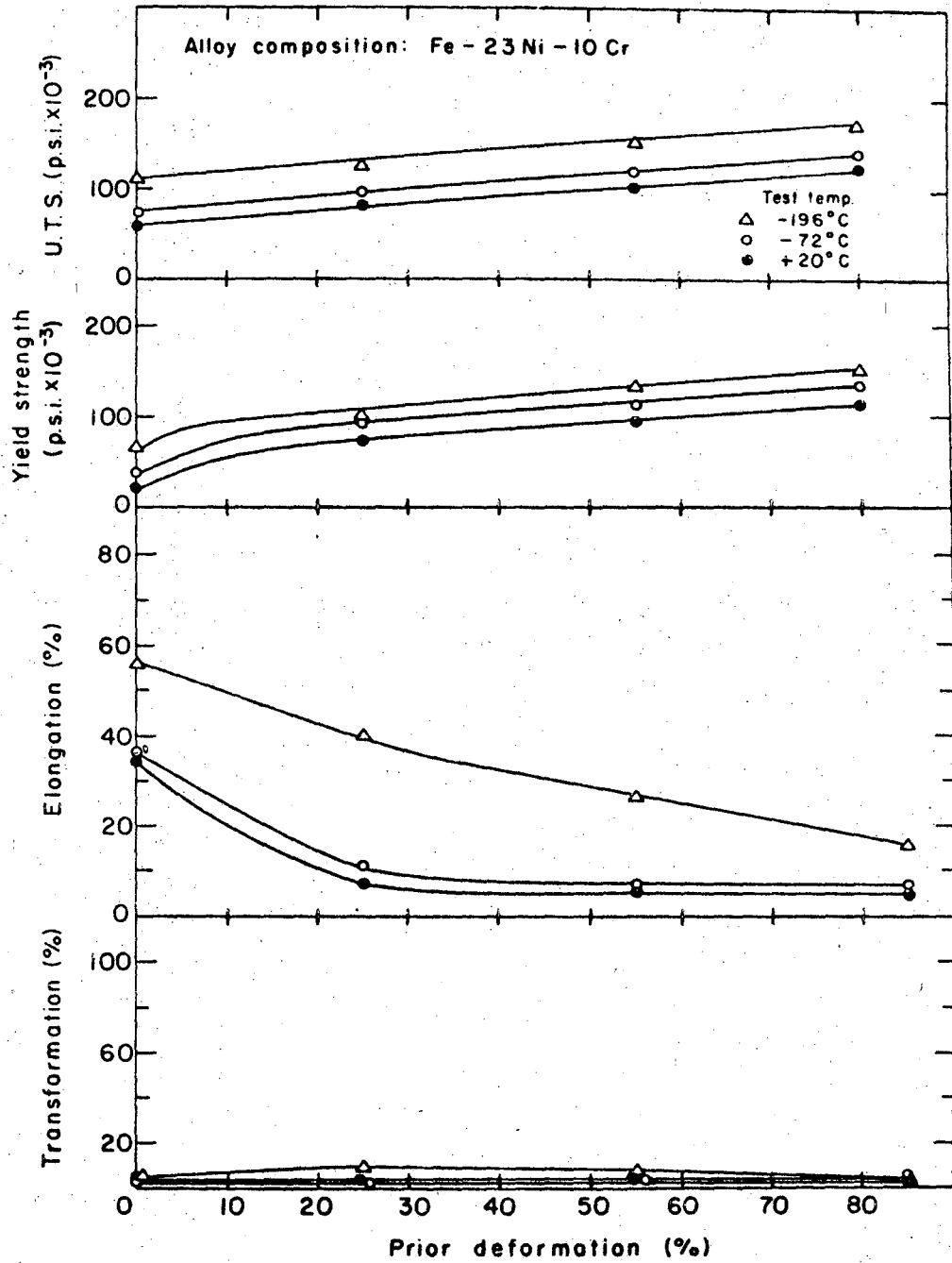
XBL 698-1155

Figure 2



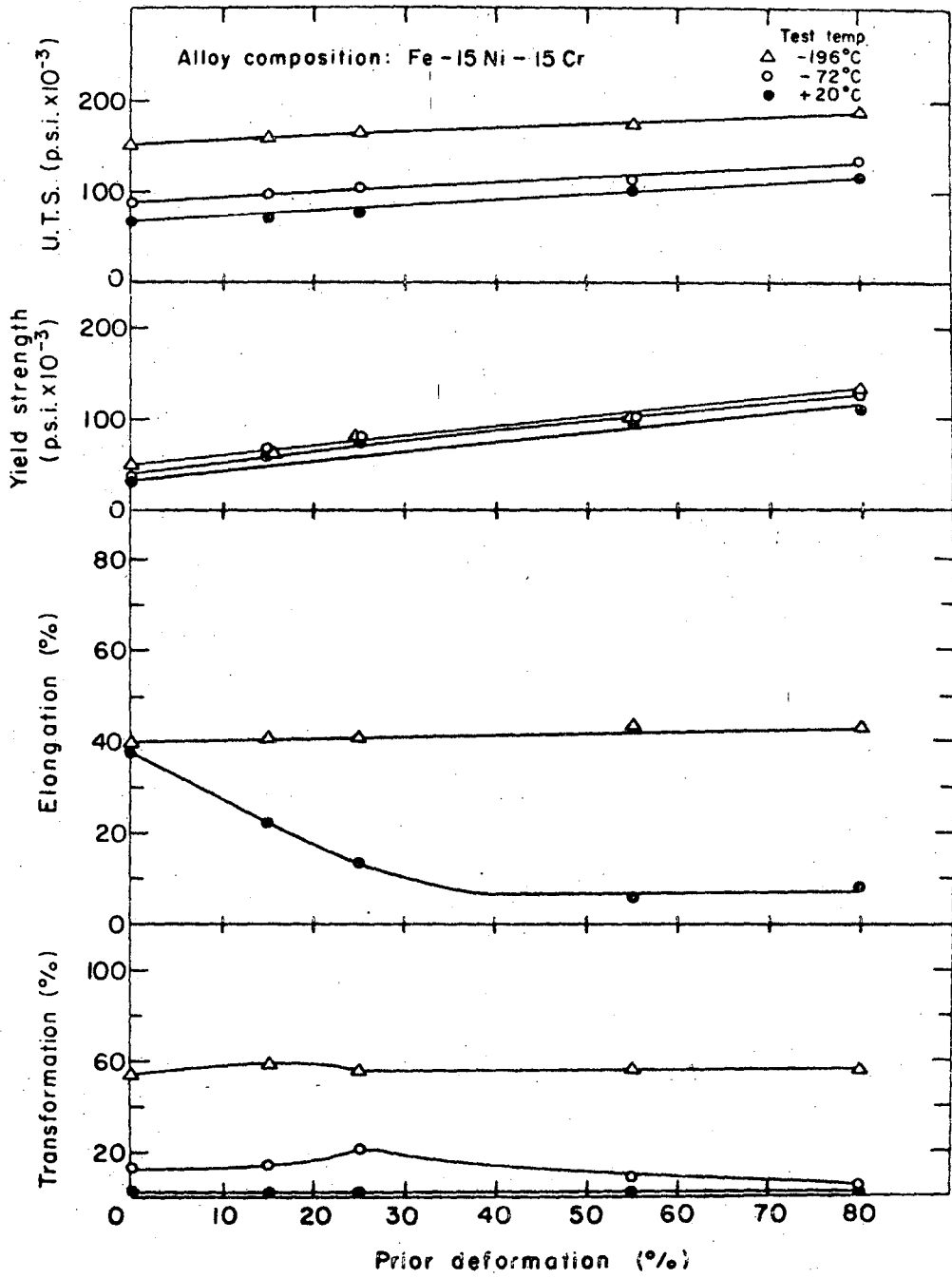
XBL 6911-6526

Figure 3



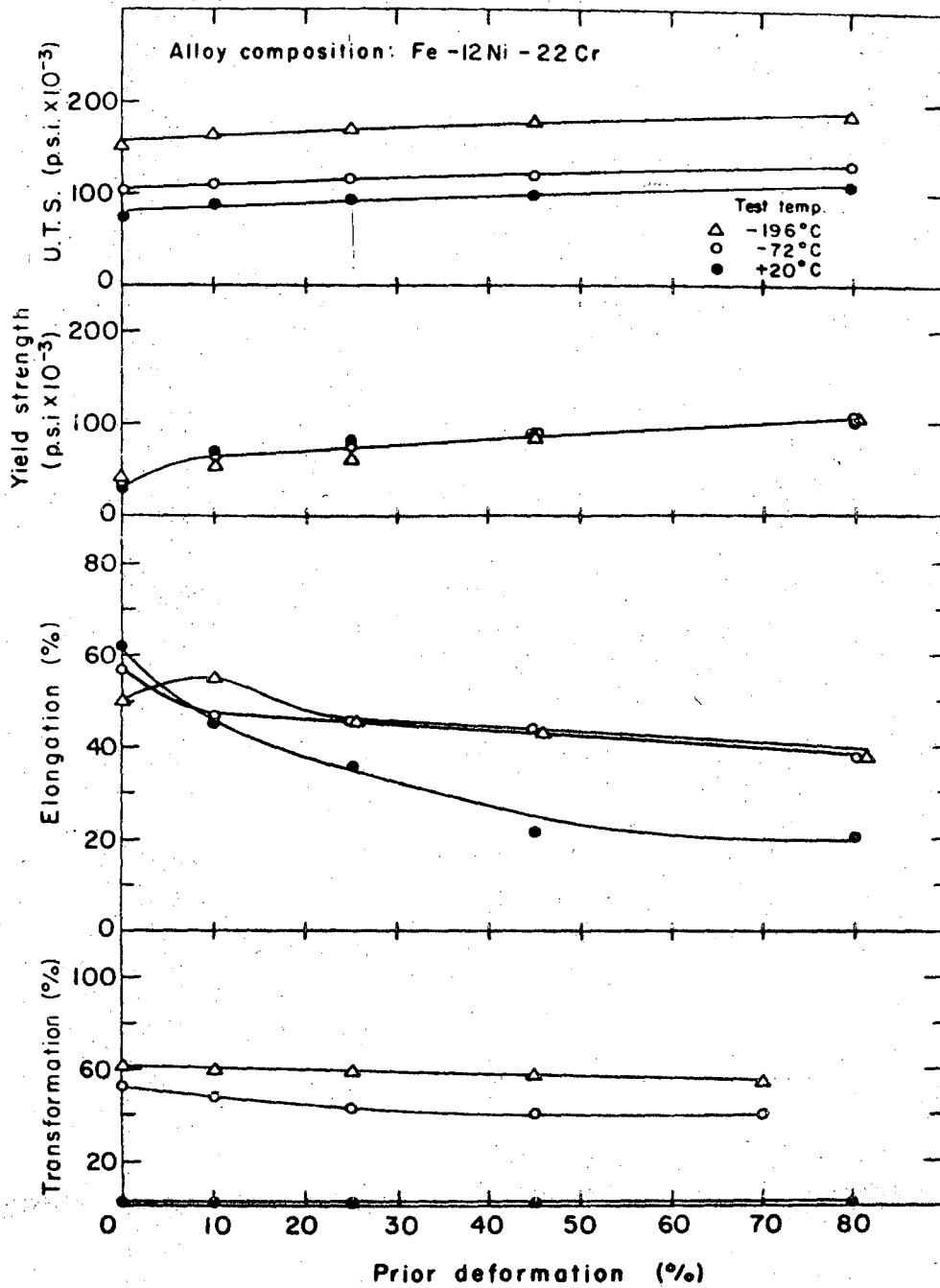
XBL 6911-6522

Figure 4



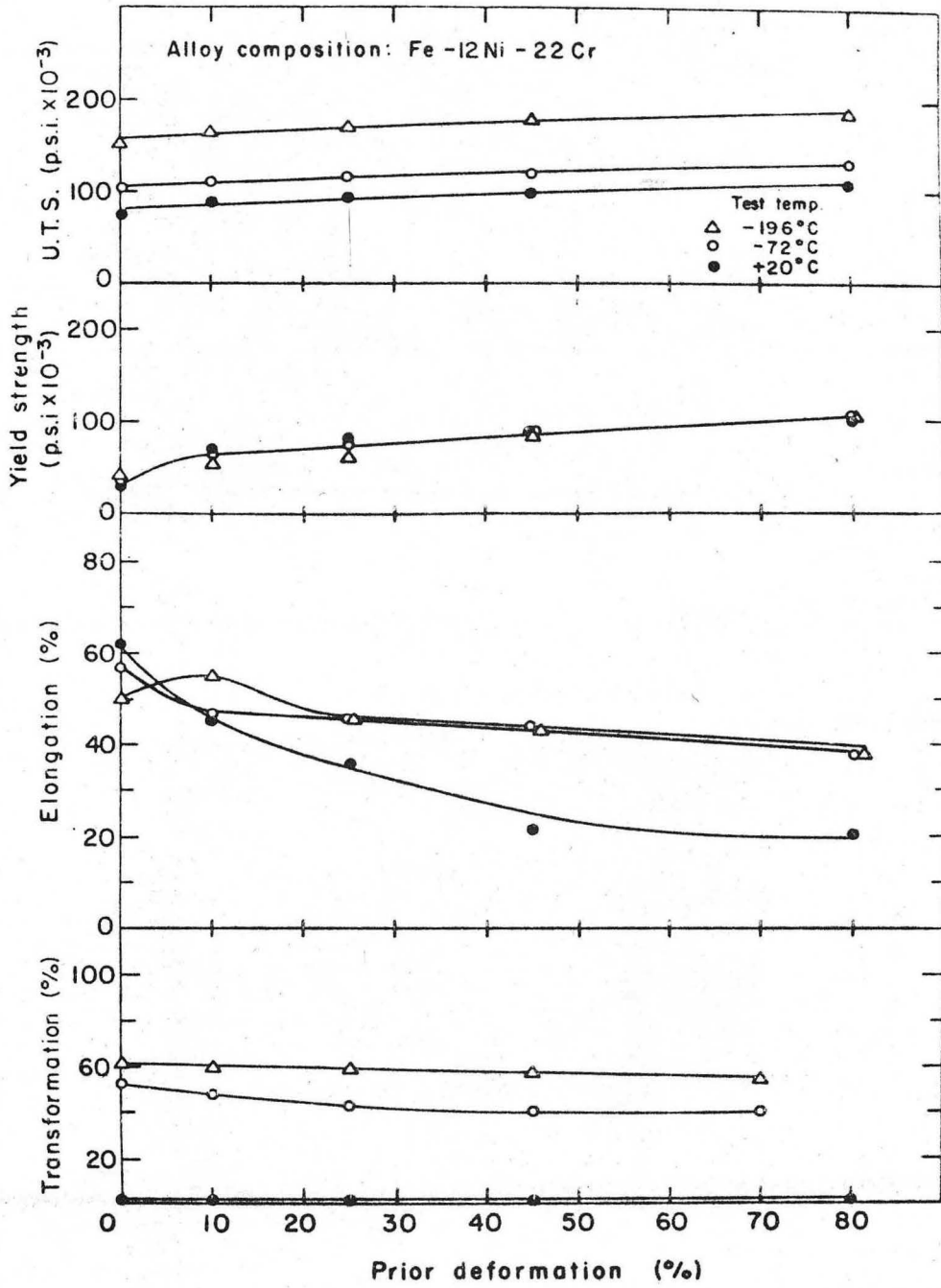
XBL 6911-6523

Figure 5



XBL 6911-6525

Figure 6



XBL 6911-6525

Figure 6

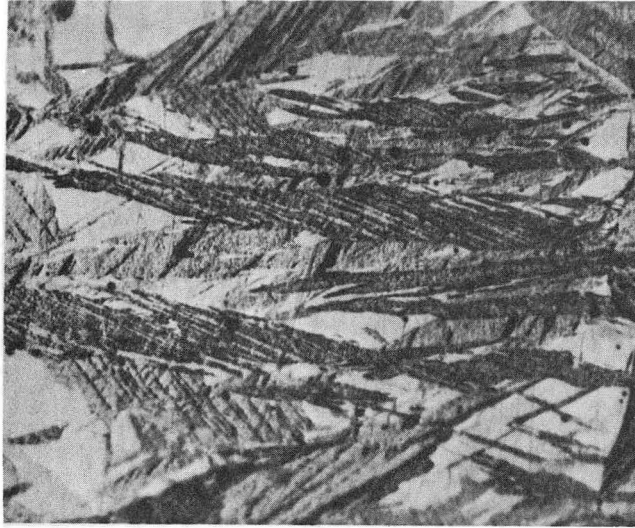
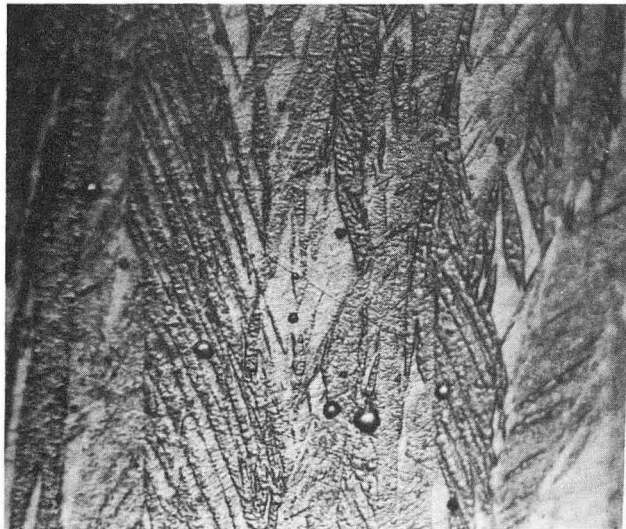


Figure 8



XBB 6911-7427

Figure 7

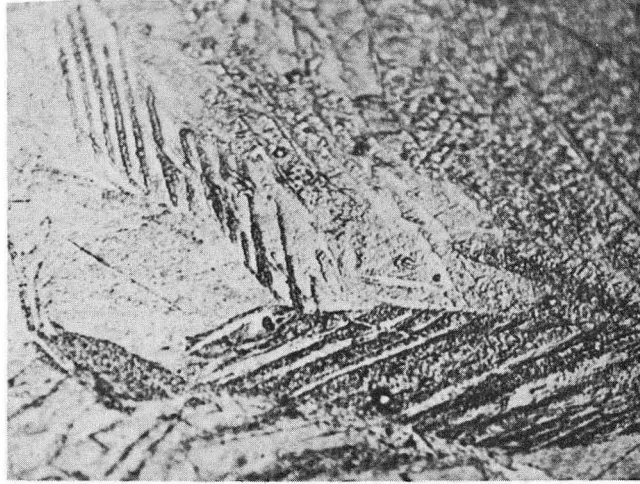
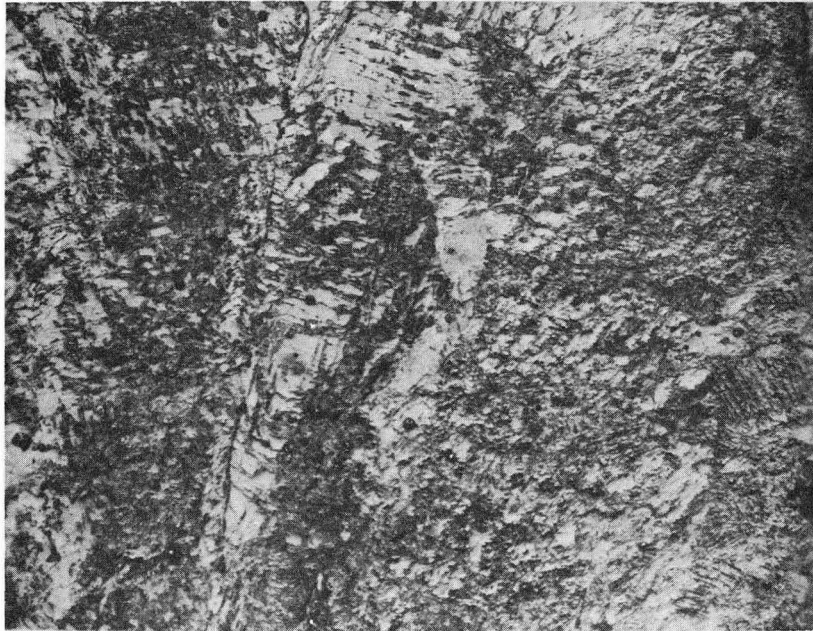


Figure 9



XBB 6911-7428

Figure 10

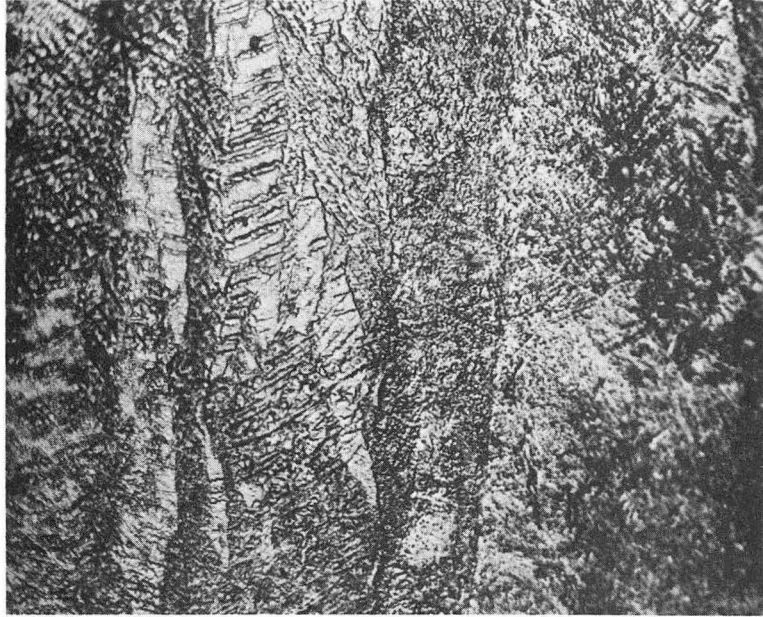


Figure 11

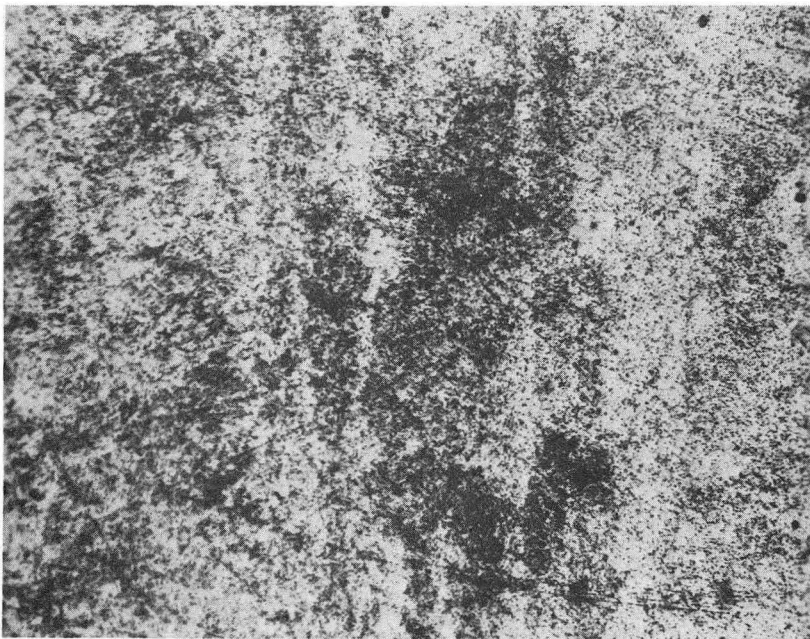


XBB 6911-7429

Figure 12



Figure 13



XBB 6911-7430

Figure 14

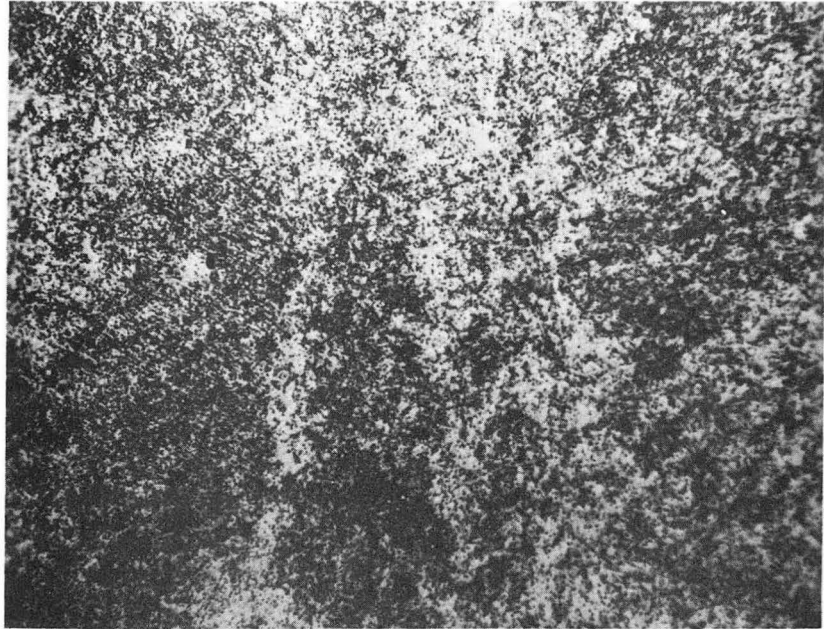
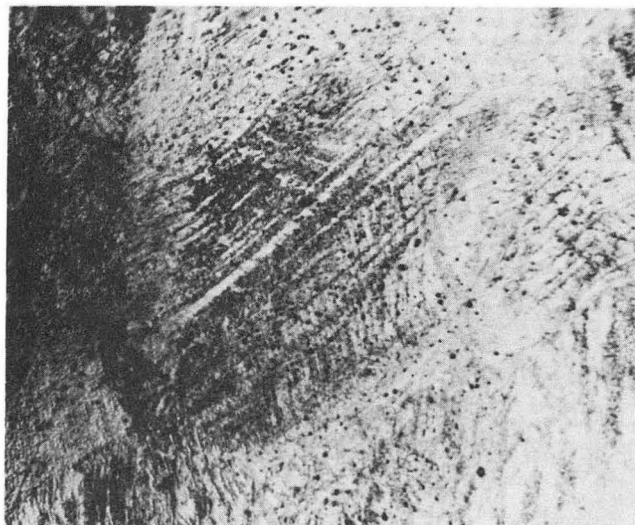


Figure 15



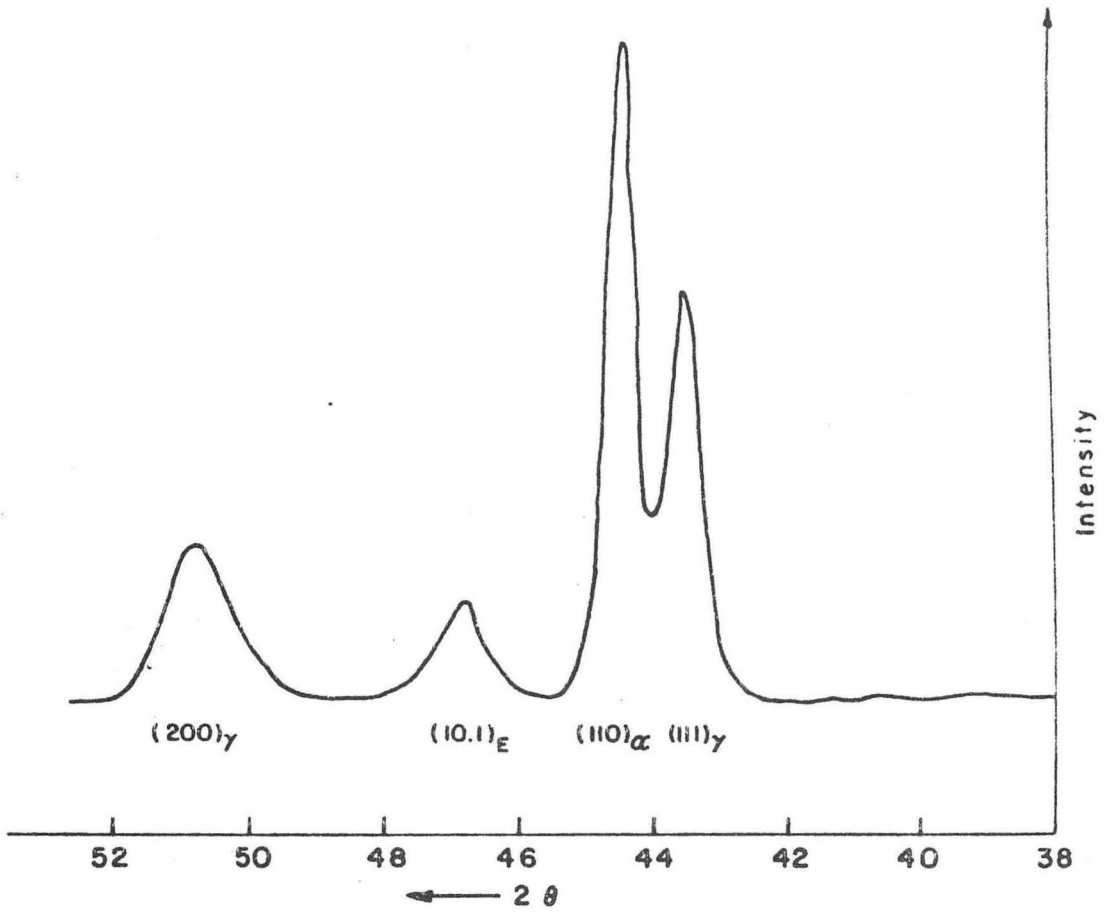
XBB 6911-7431

Figure 16



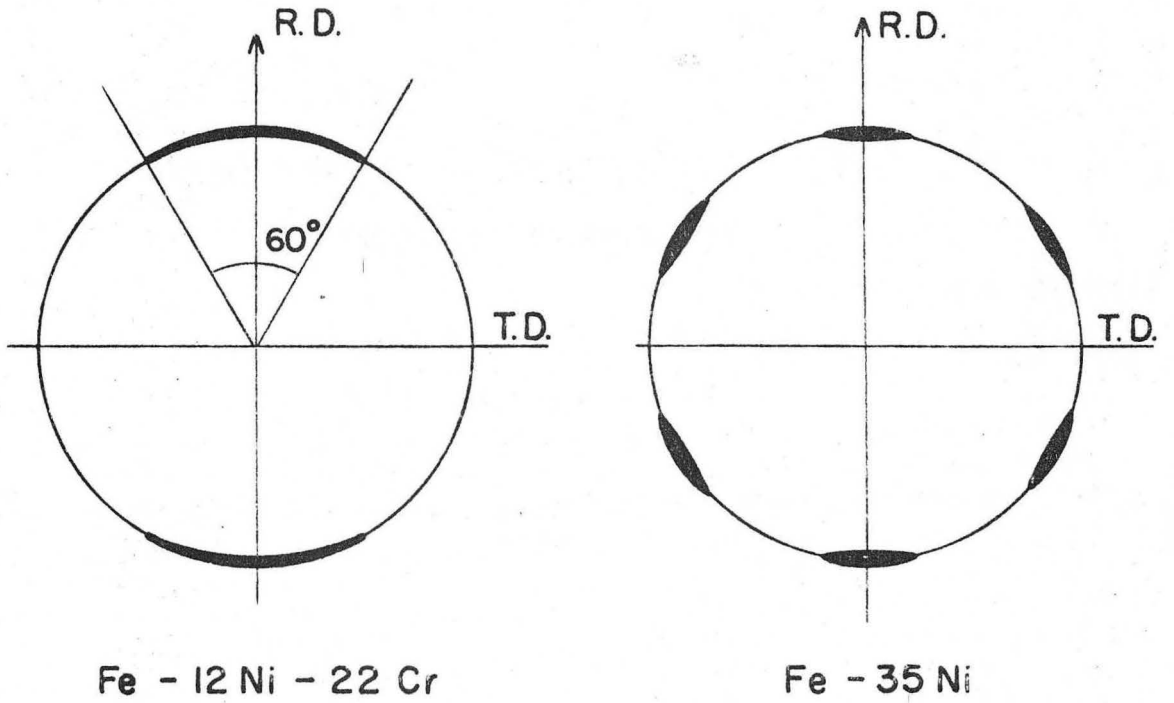
XBB 696-4427

Figure 17



XBL 6911-6527

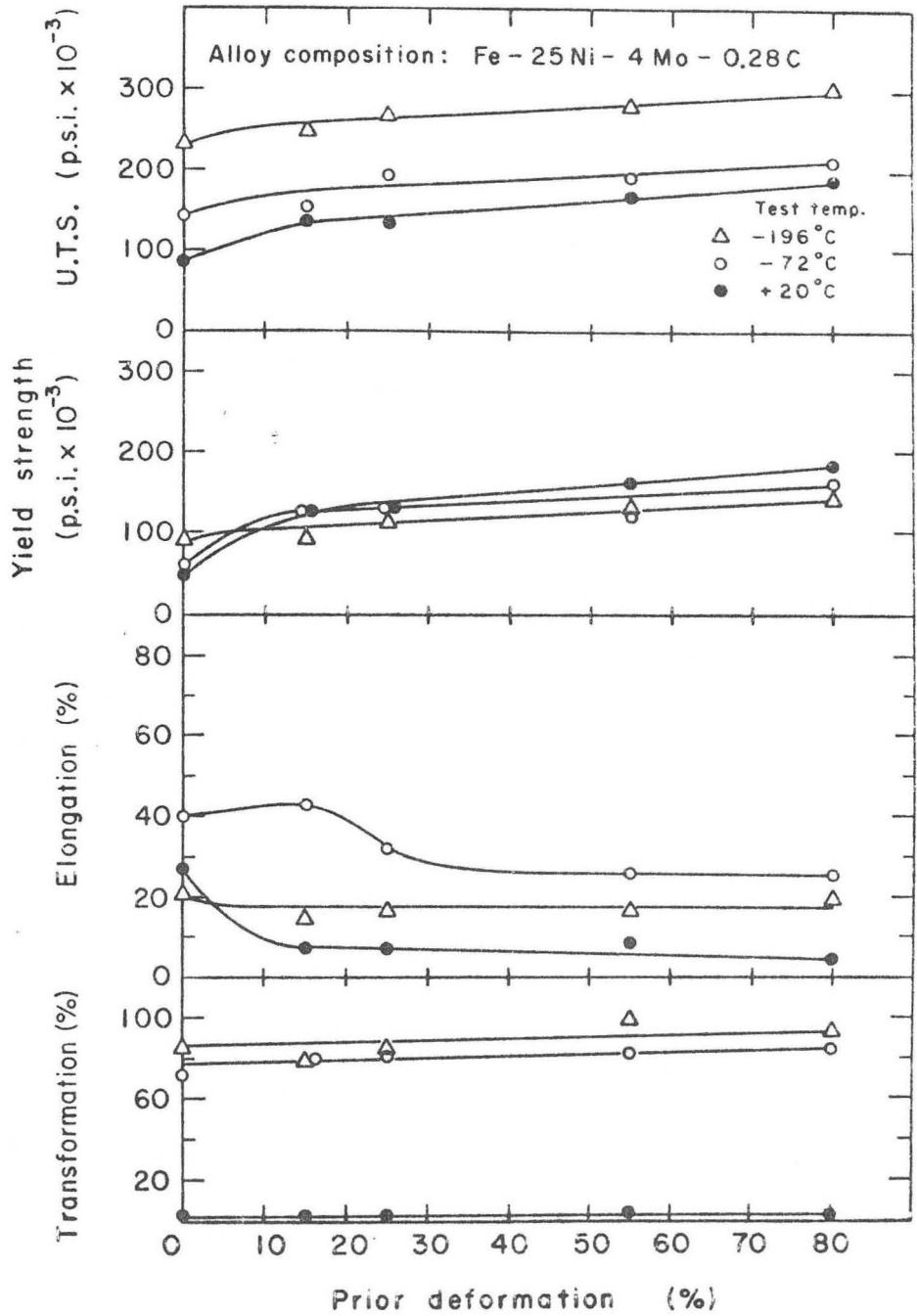
Figure 18



BACKREFLECTION DEBYE RING
(200)_γ Reflection

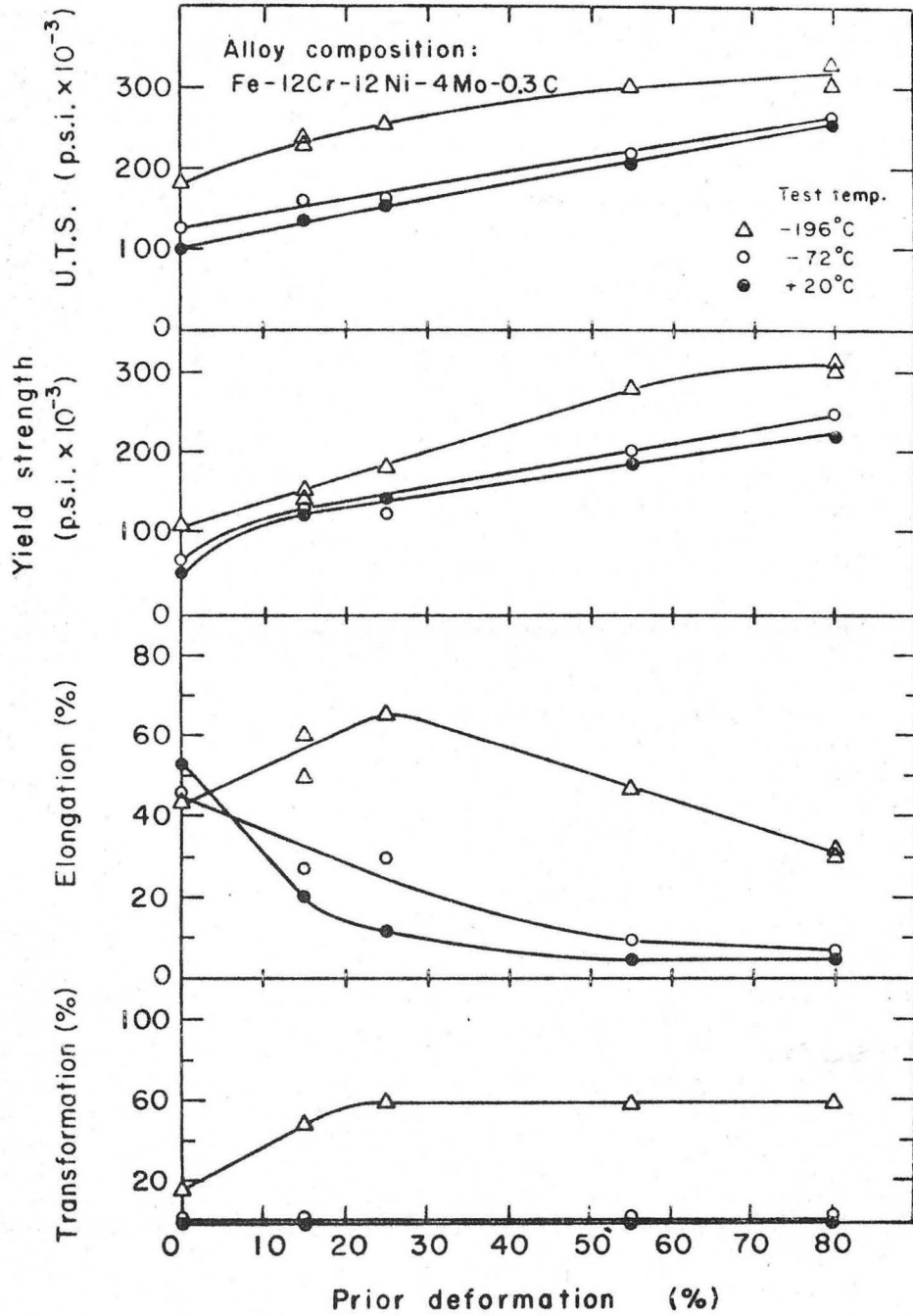
XBL 6911-6518

Figure 19



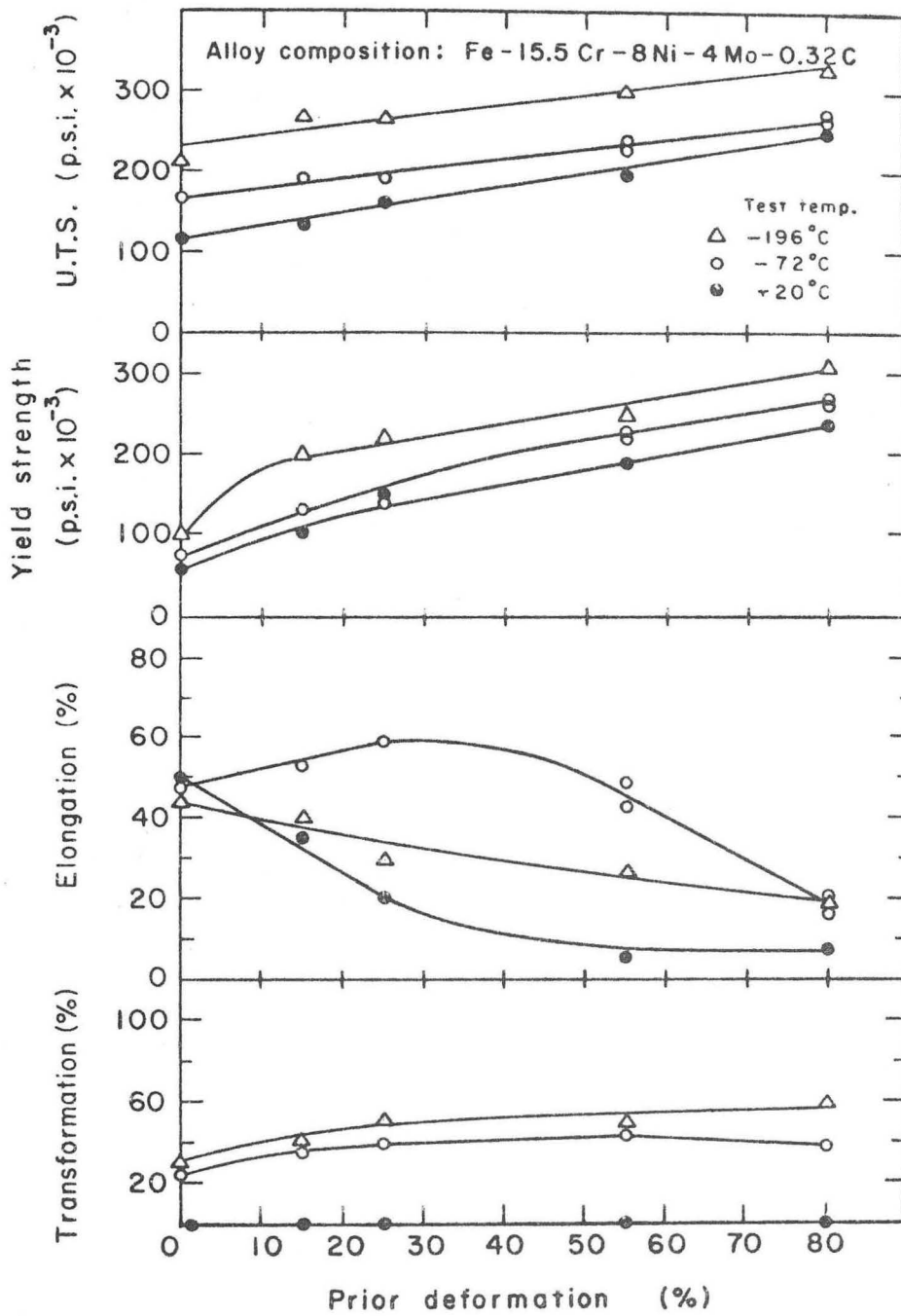
X8L695-2856

Figure 20



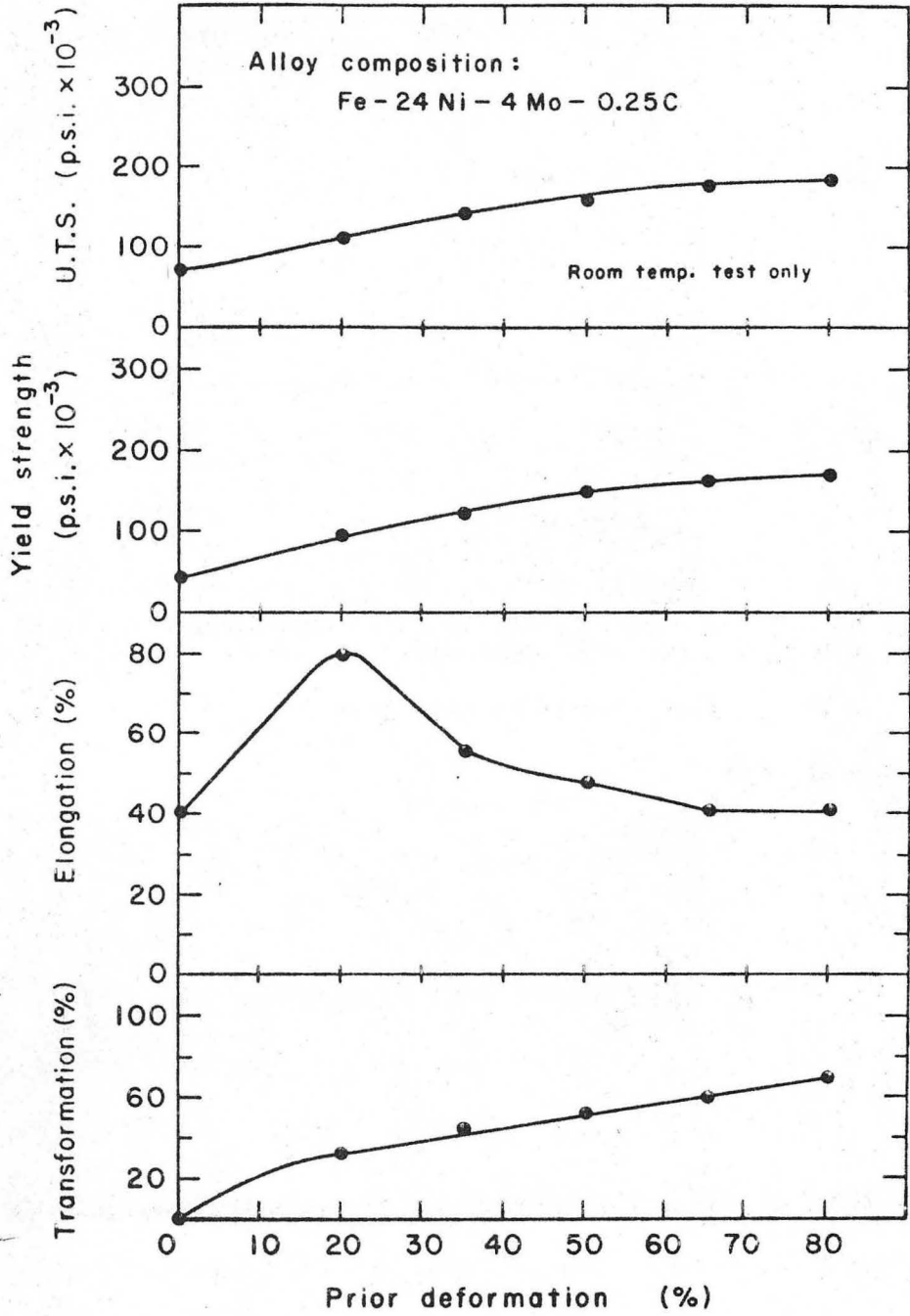
XBL695-2857

Figure 21



XBL 6911-6521

Figure 22



XBL695-2859

Figure 23

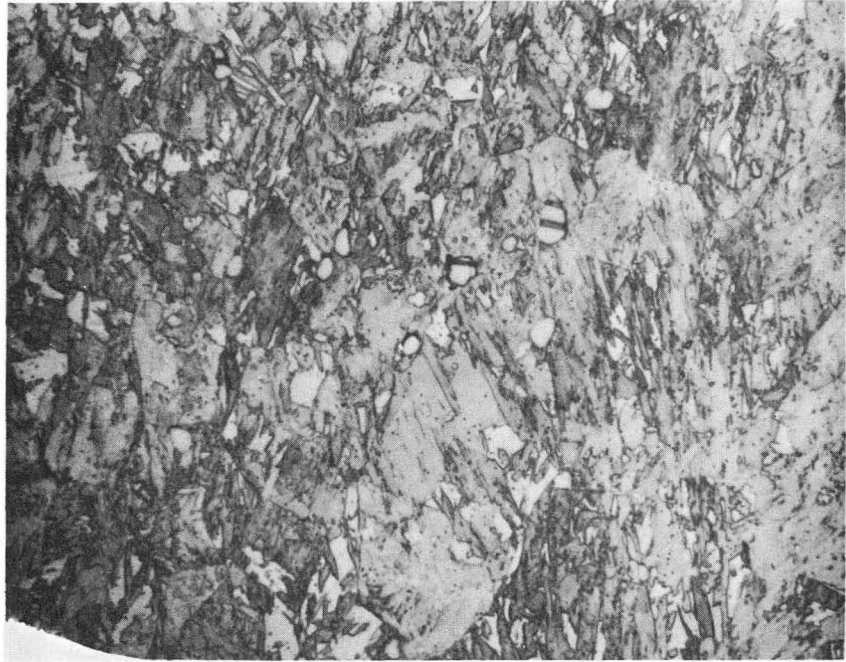


Figure 24

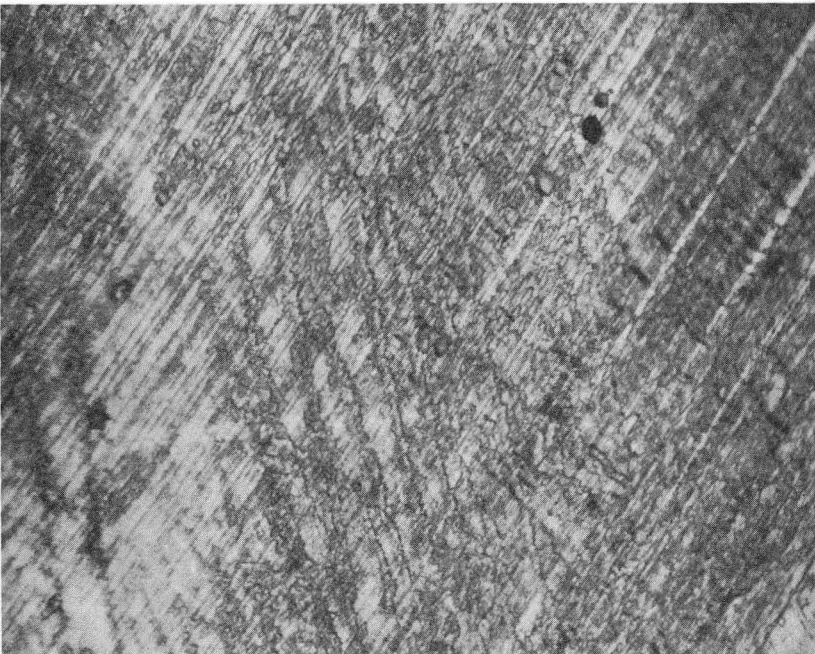


XBB 6911-7432

Figure 25



Figure 26



XBB 6911-7433

Figure 27

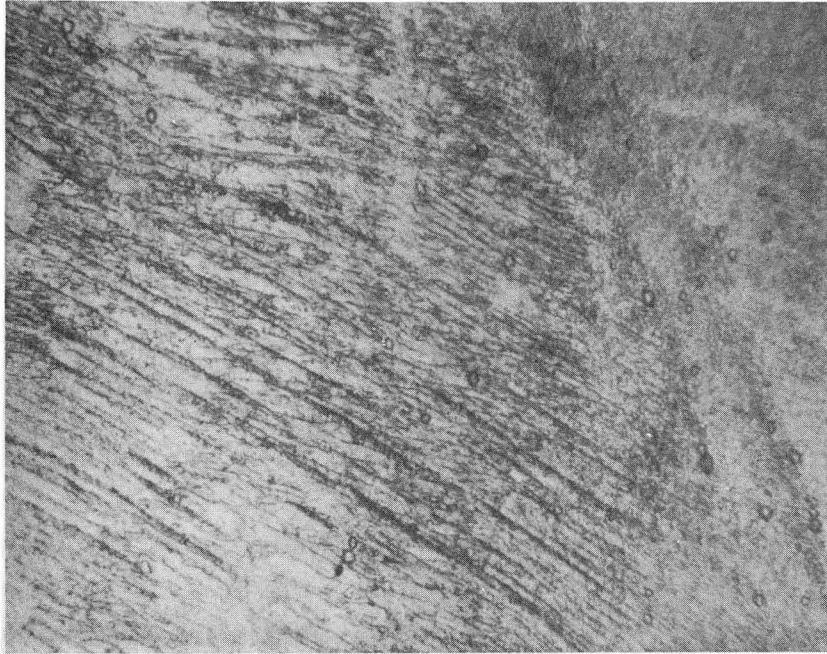


Figure 28



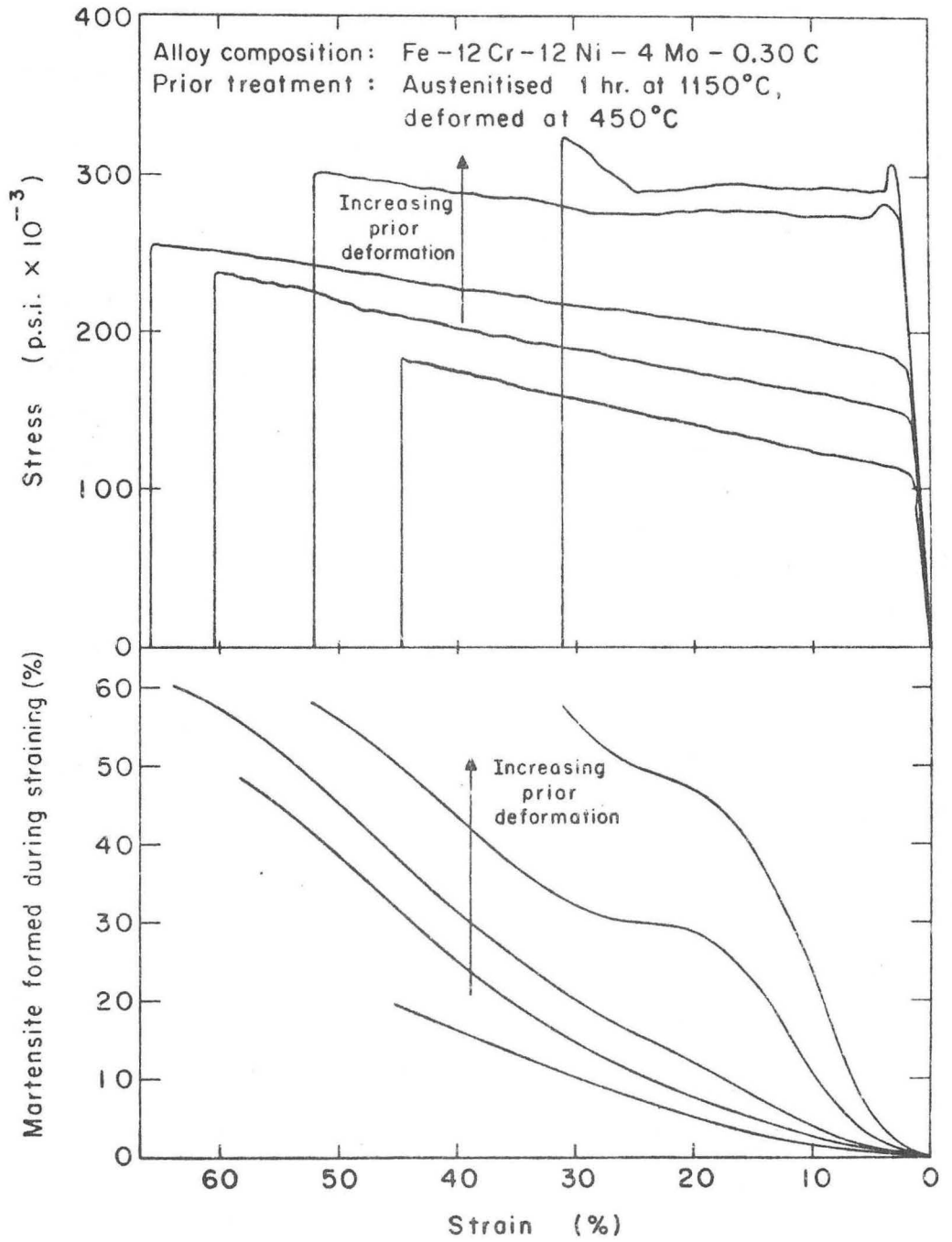
XBB 6911-7434

Figure 29



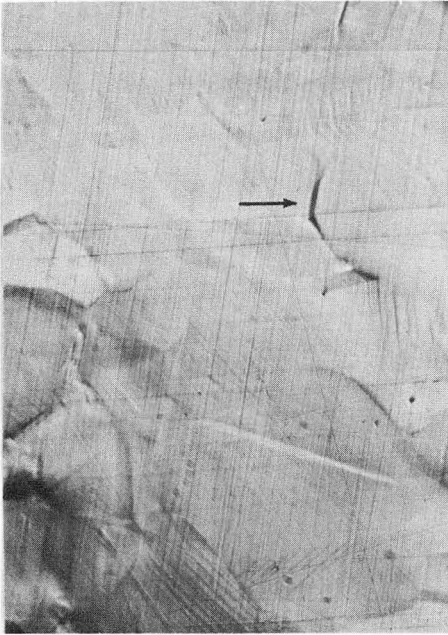
XBB 696-3817

Figure 30



XBL695-2860

Figure 31



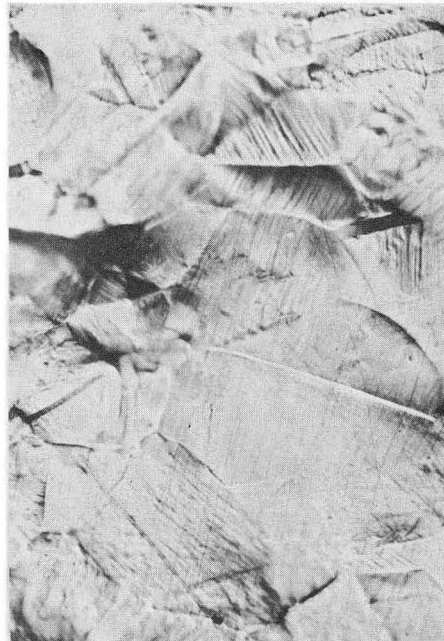
(a)



(b)



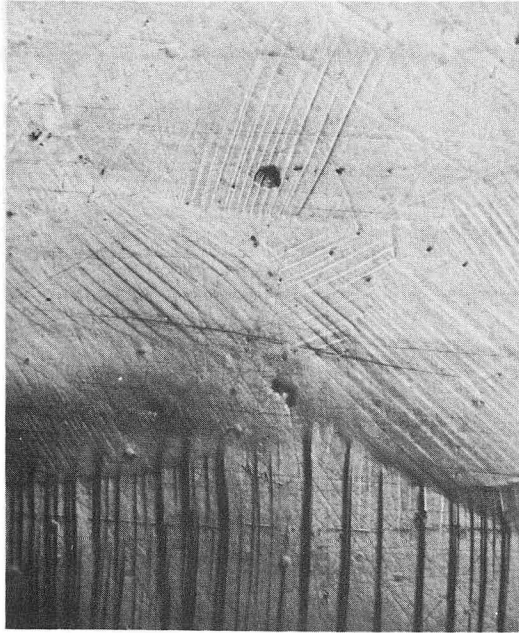
(c)



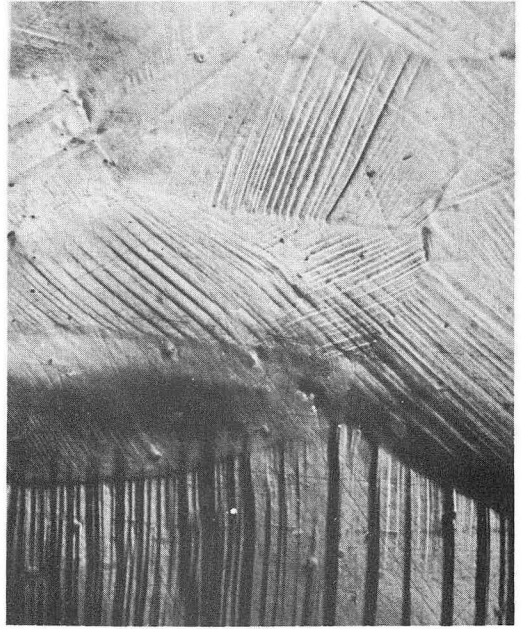
(d)

XBB 6911-7149

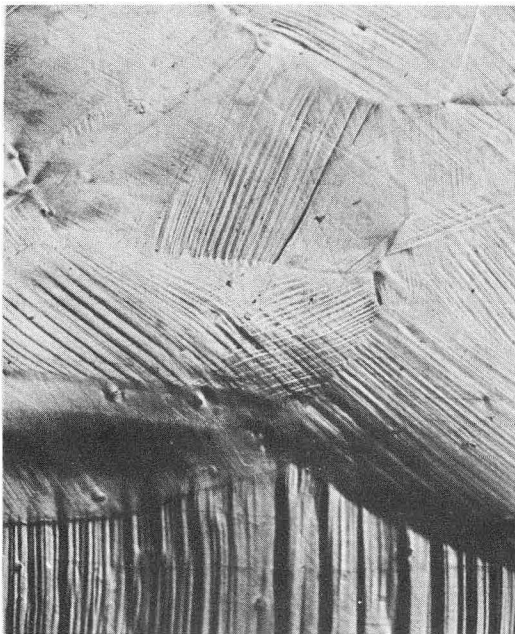
Figure 32



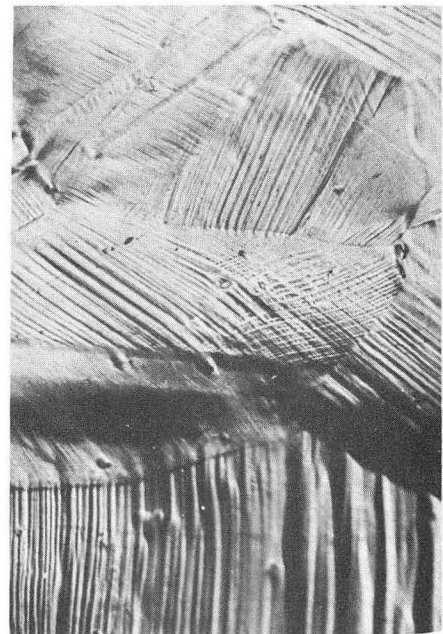
(a)



(b)



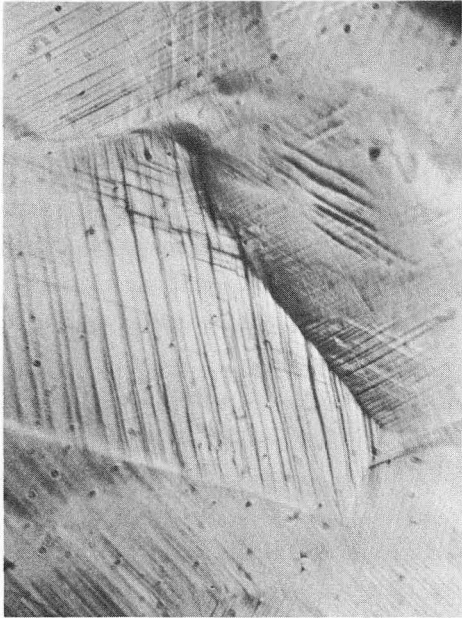
(c)



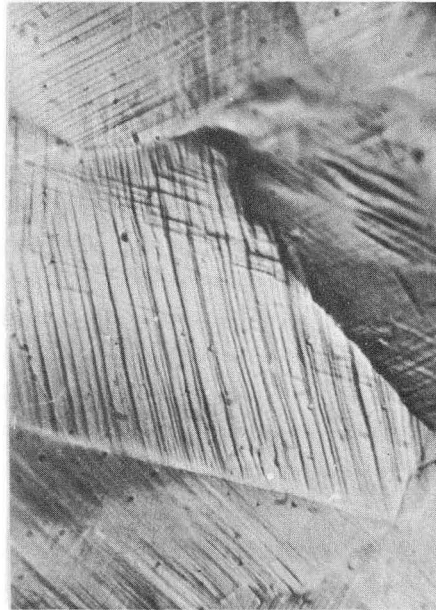
(d)

XBB 6911-7153

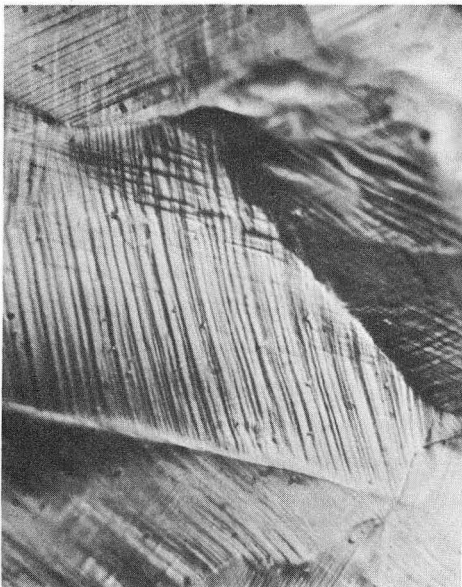
Figure 33



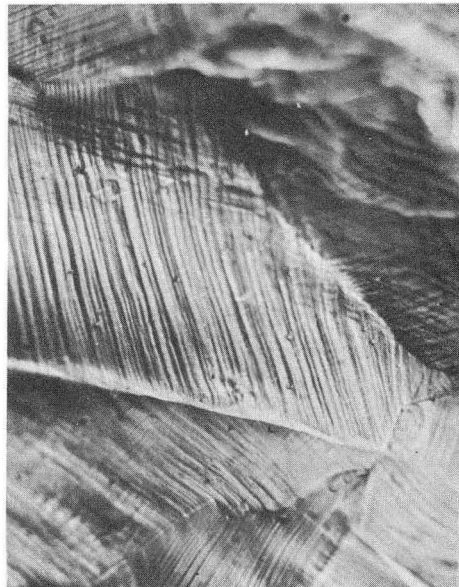
(a)



(b)



(c)



(d)

XBB 6911-7154

Figure 34

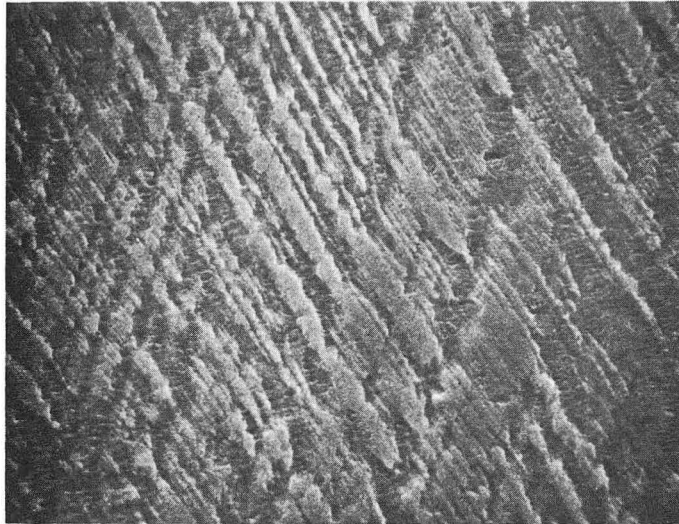
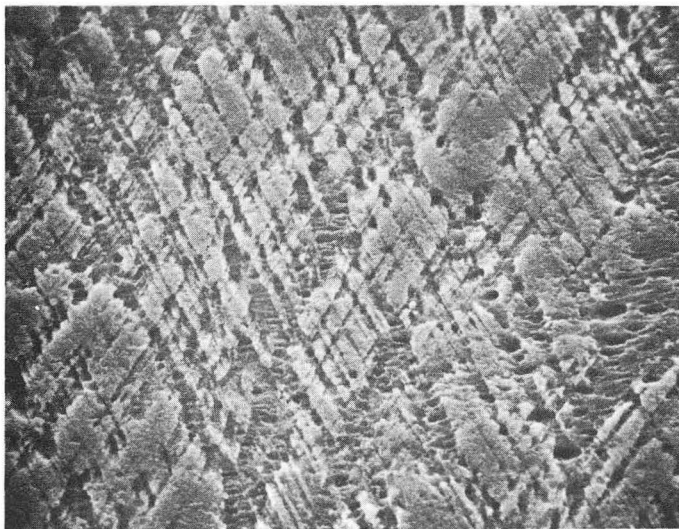


Figure 35



XBB 6911-7435

Figure 36

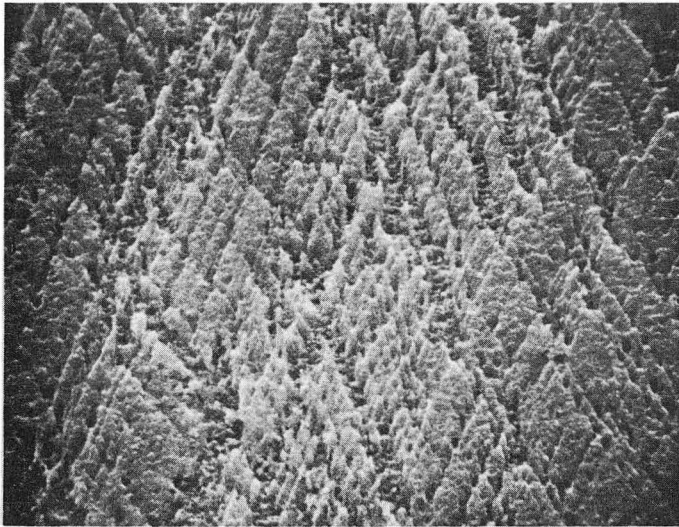
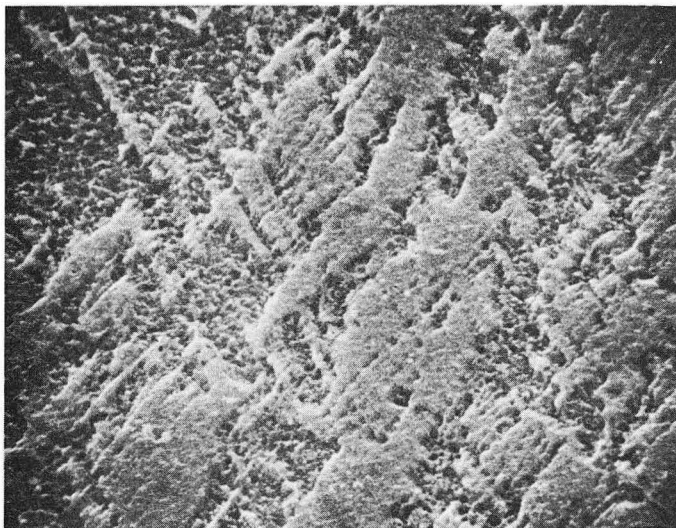


Figure 37



XBB 6911-7436

Figure 38

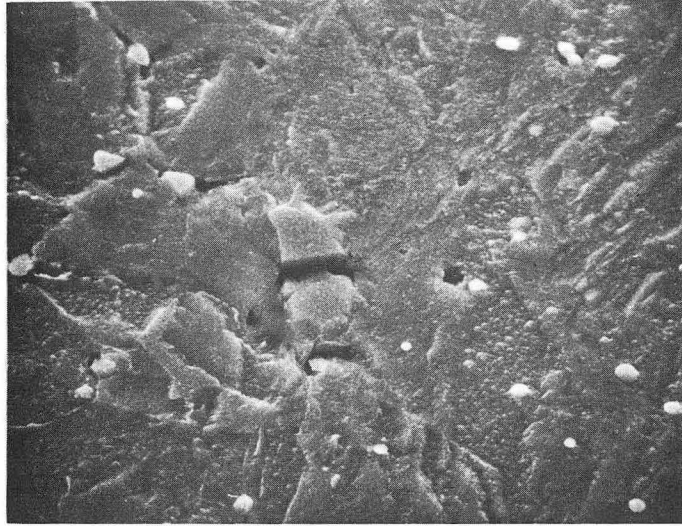
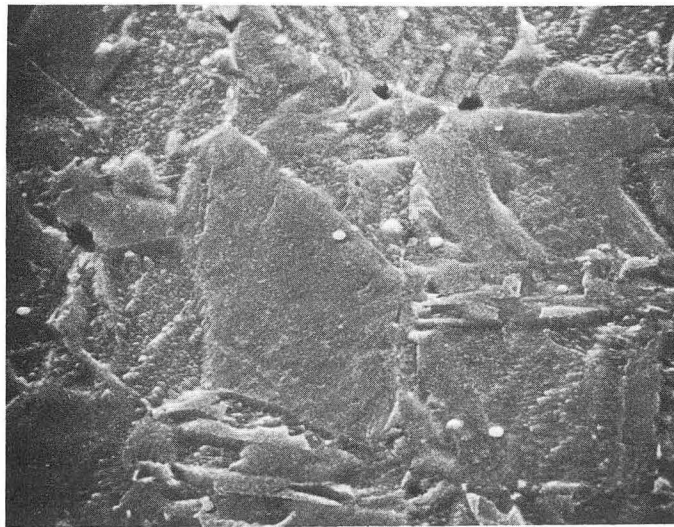
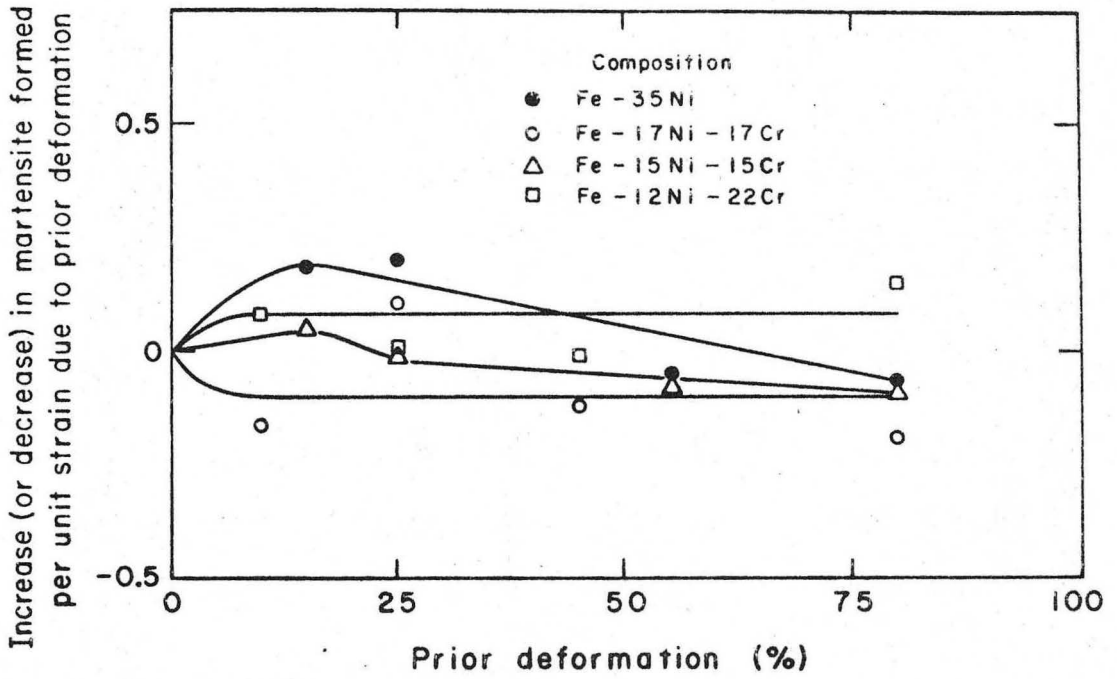


Figure 39



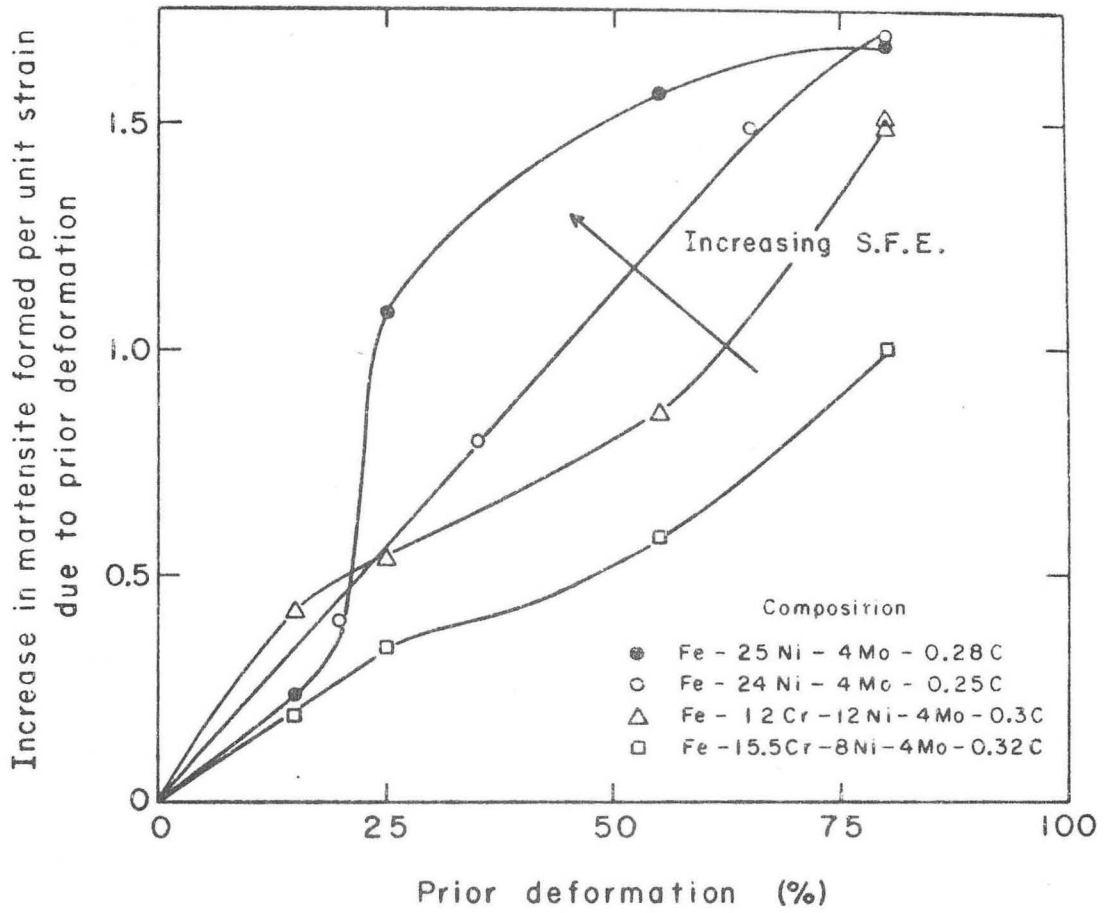
XBB 6911-7437

Figure 40



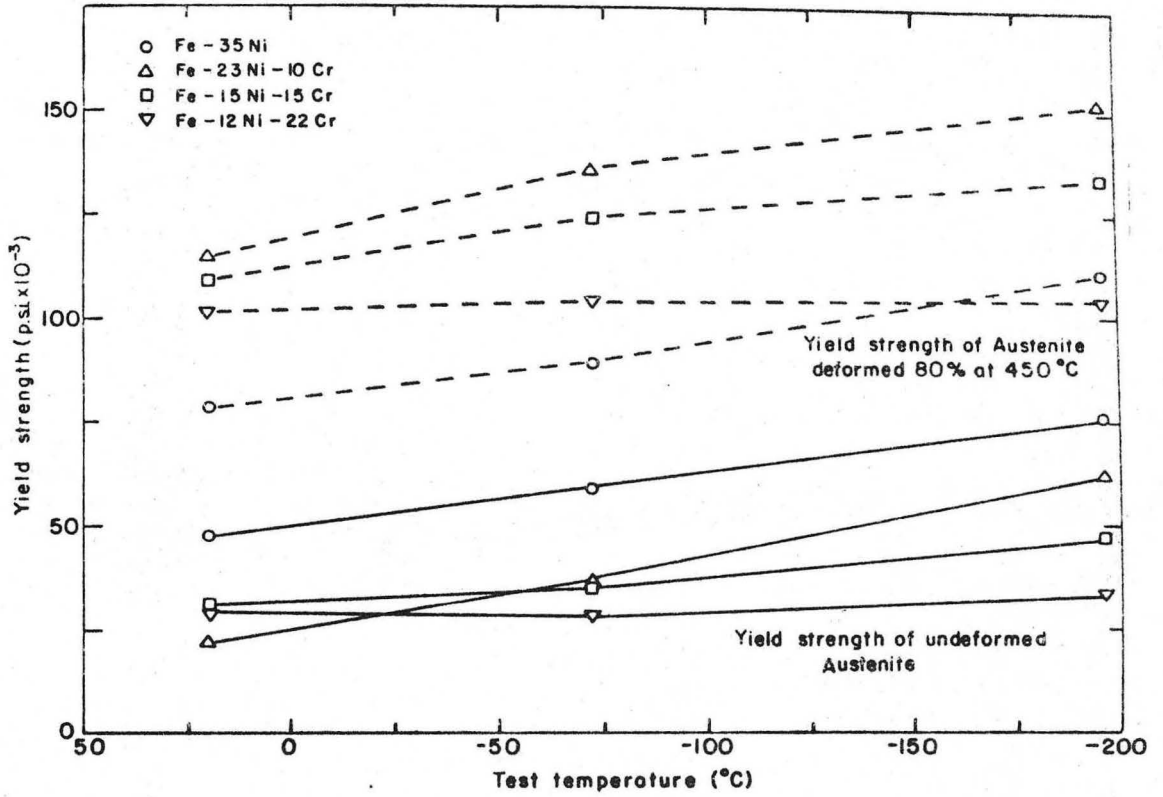
XBL695-2862

Figure 41



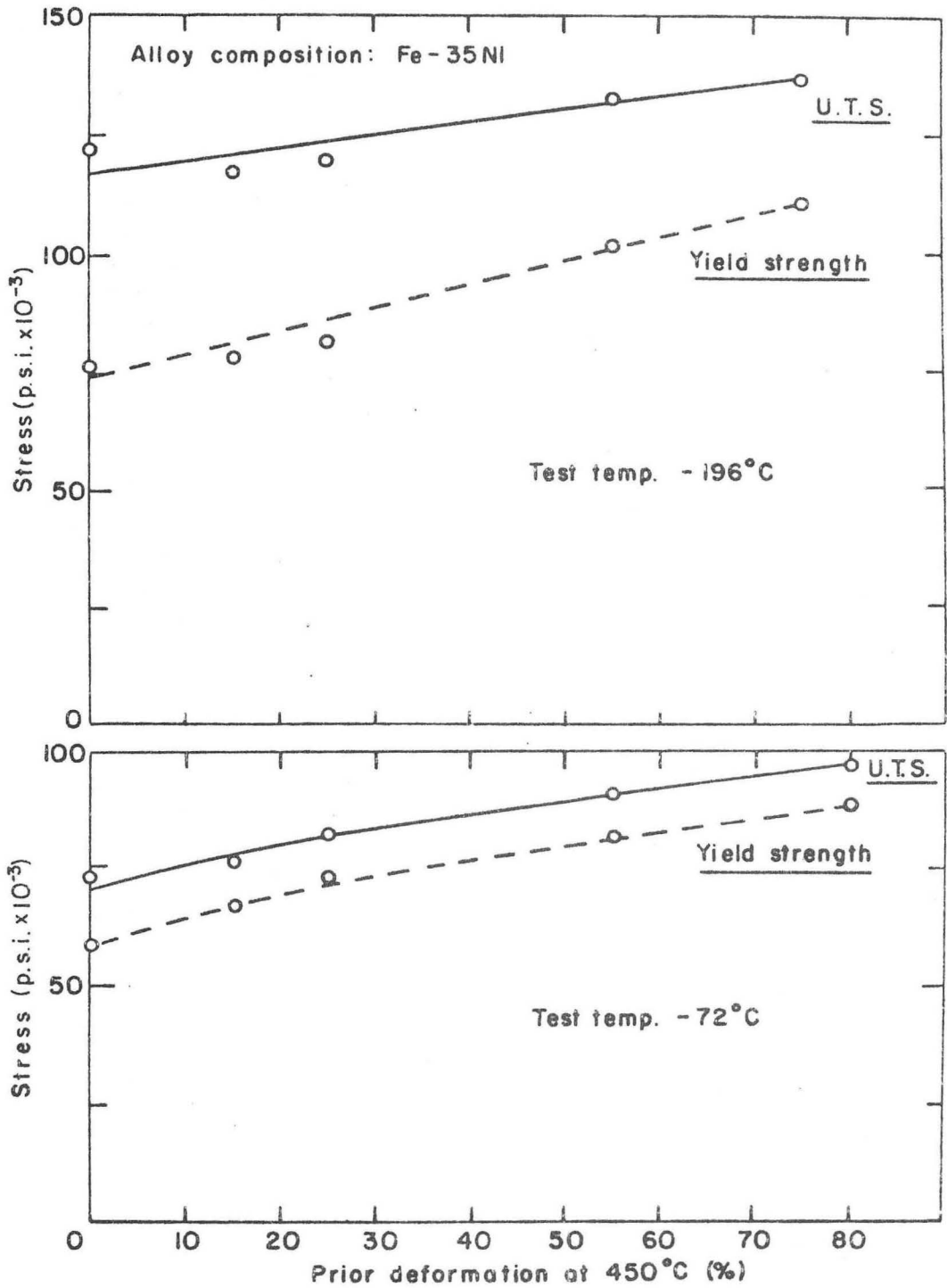
XBL695-2861

Figure 42



XBL 6911-6531

Figure 43



XBL 6911-6520

Figure 44

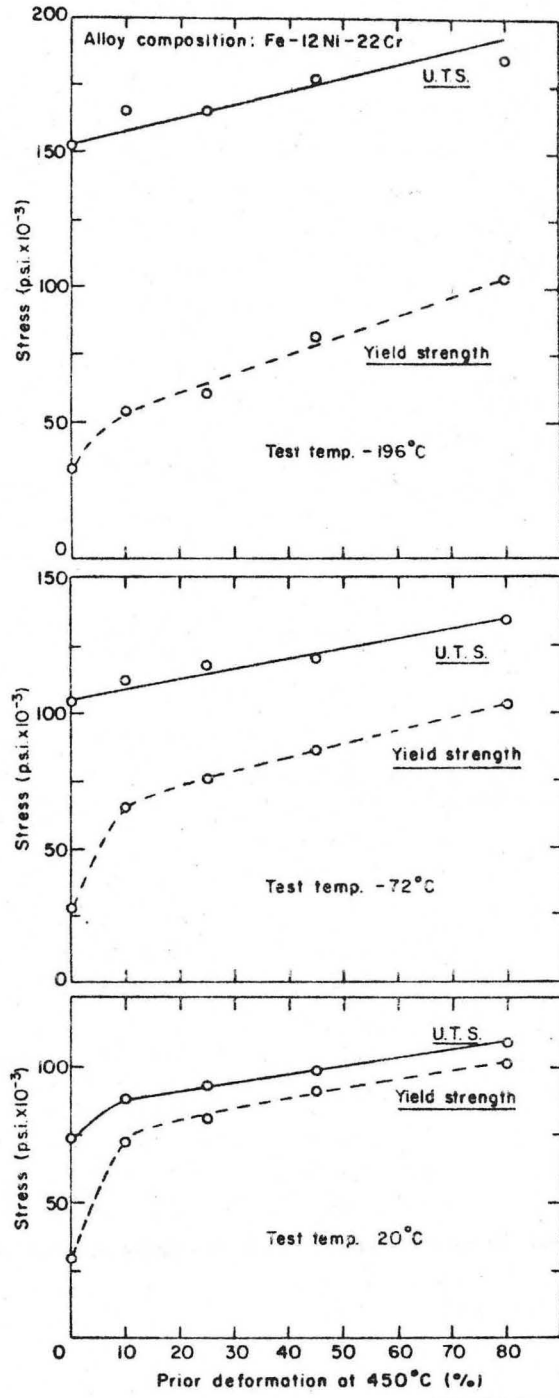
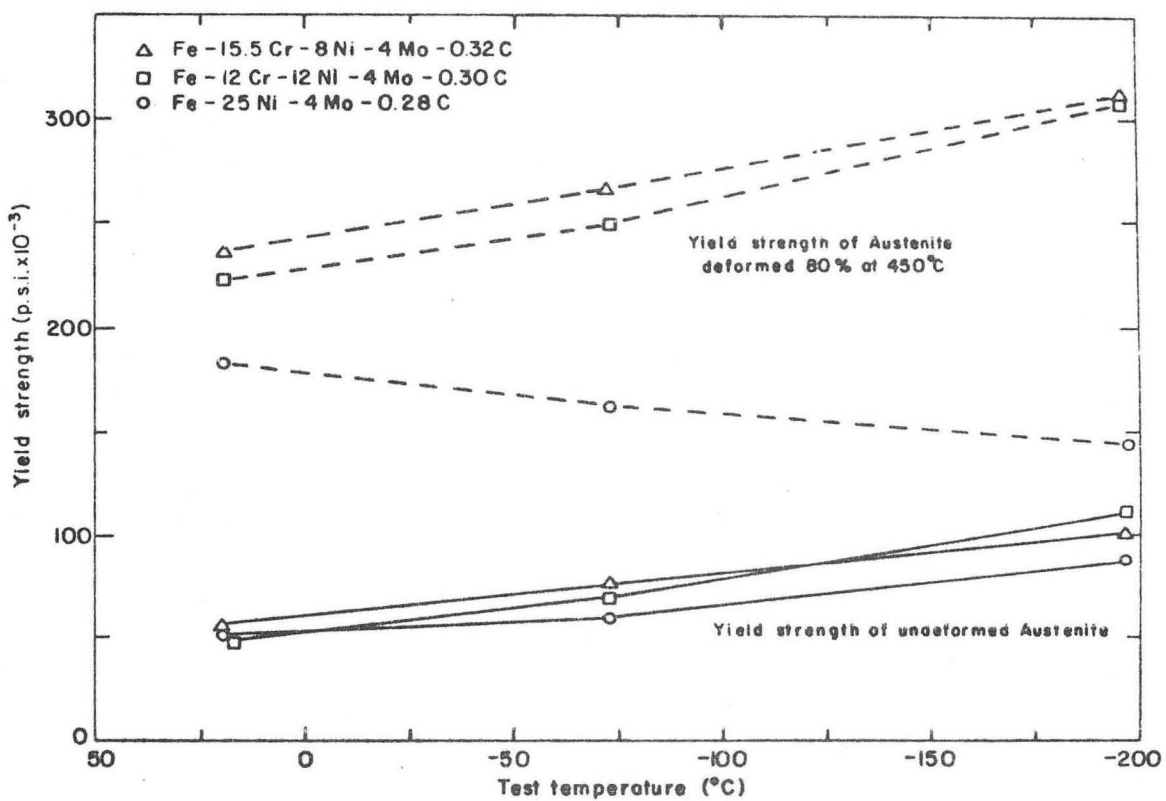
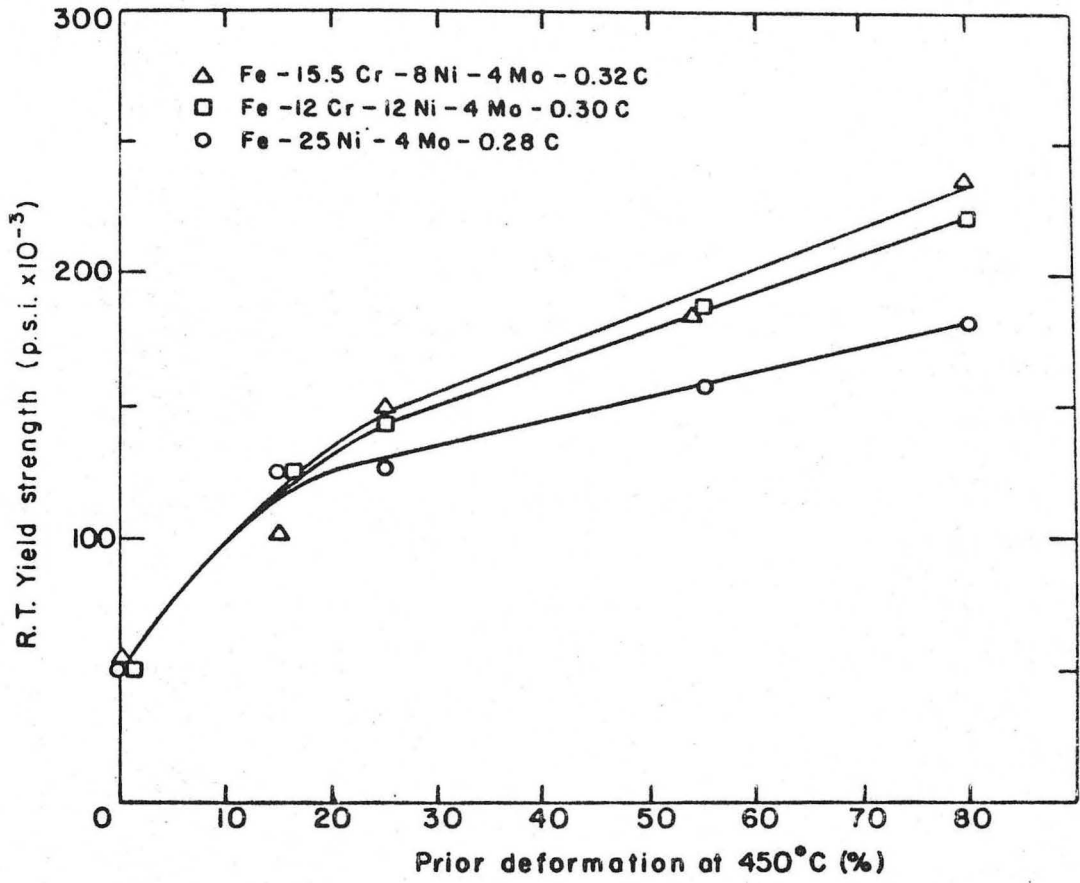


Figure 45



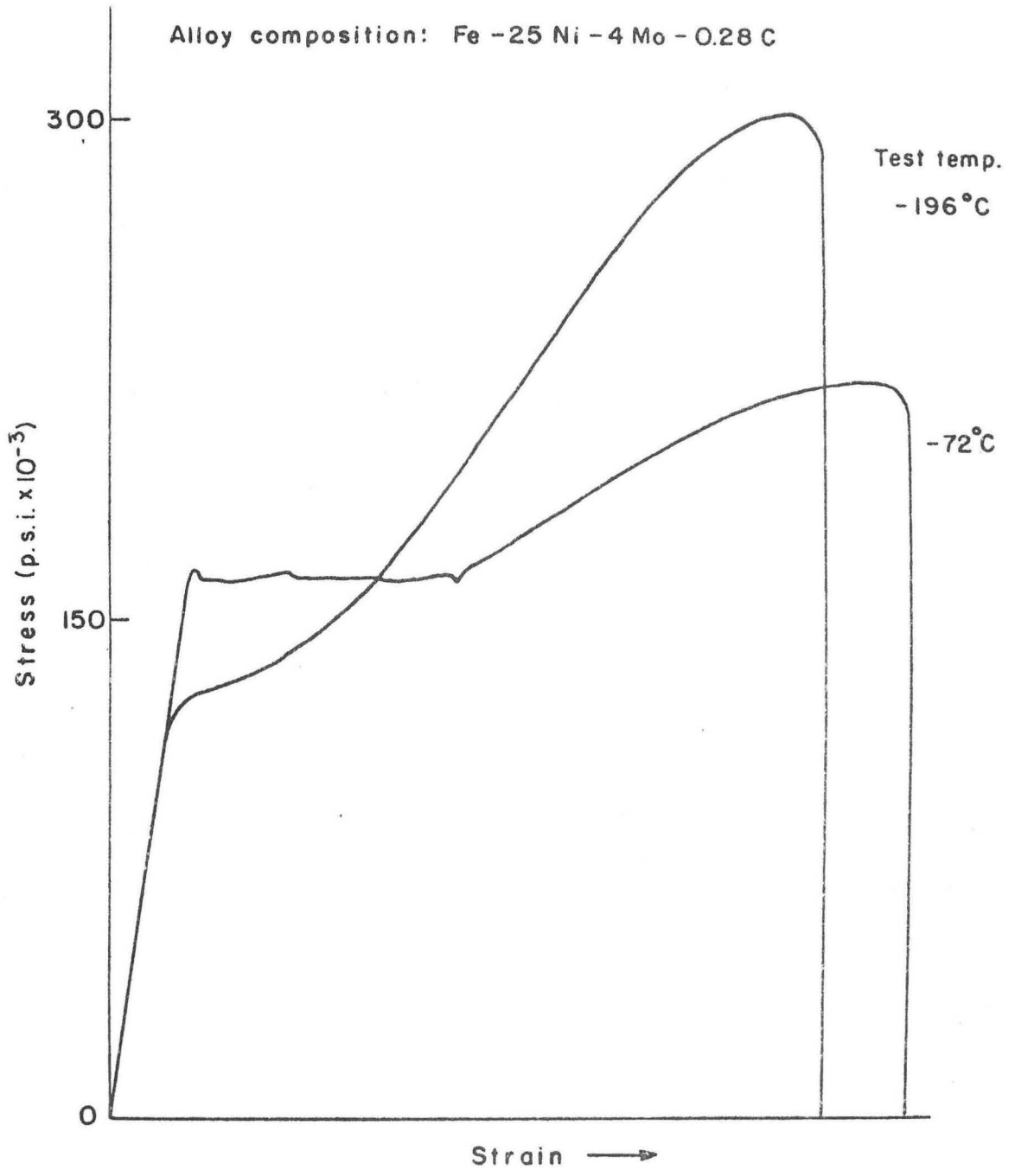
XBL 6911-6529

Figure 46



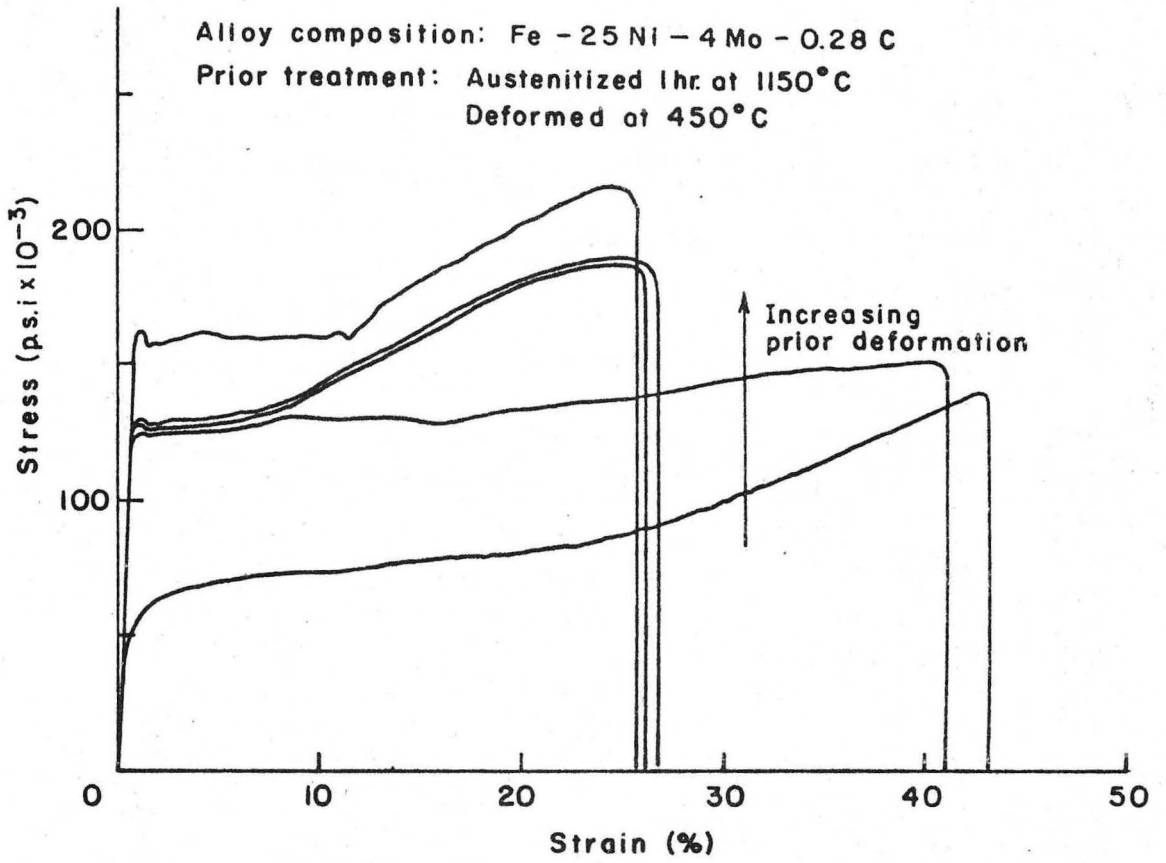
XBL 6911-6530

Figure 47



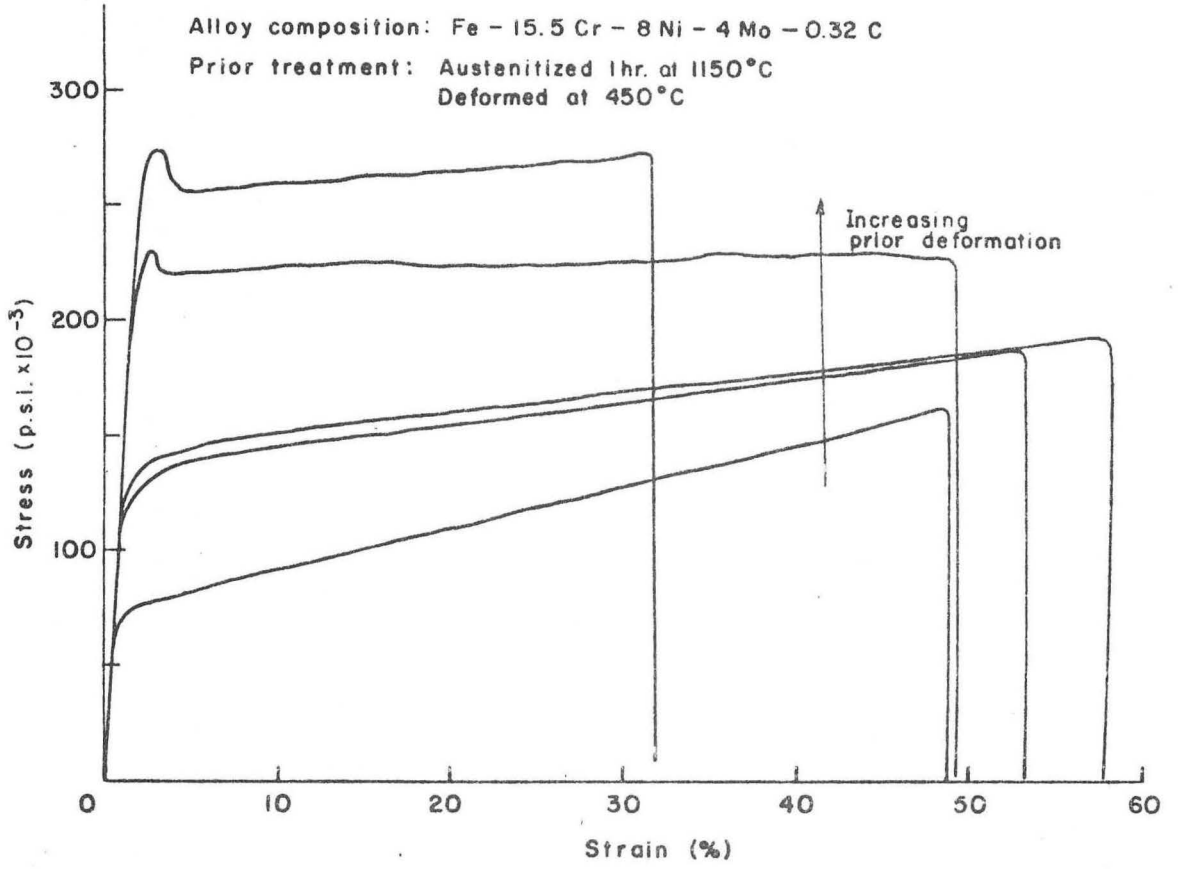
XBL 6911-6519

Figure 48



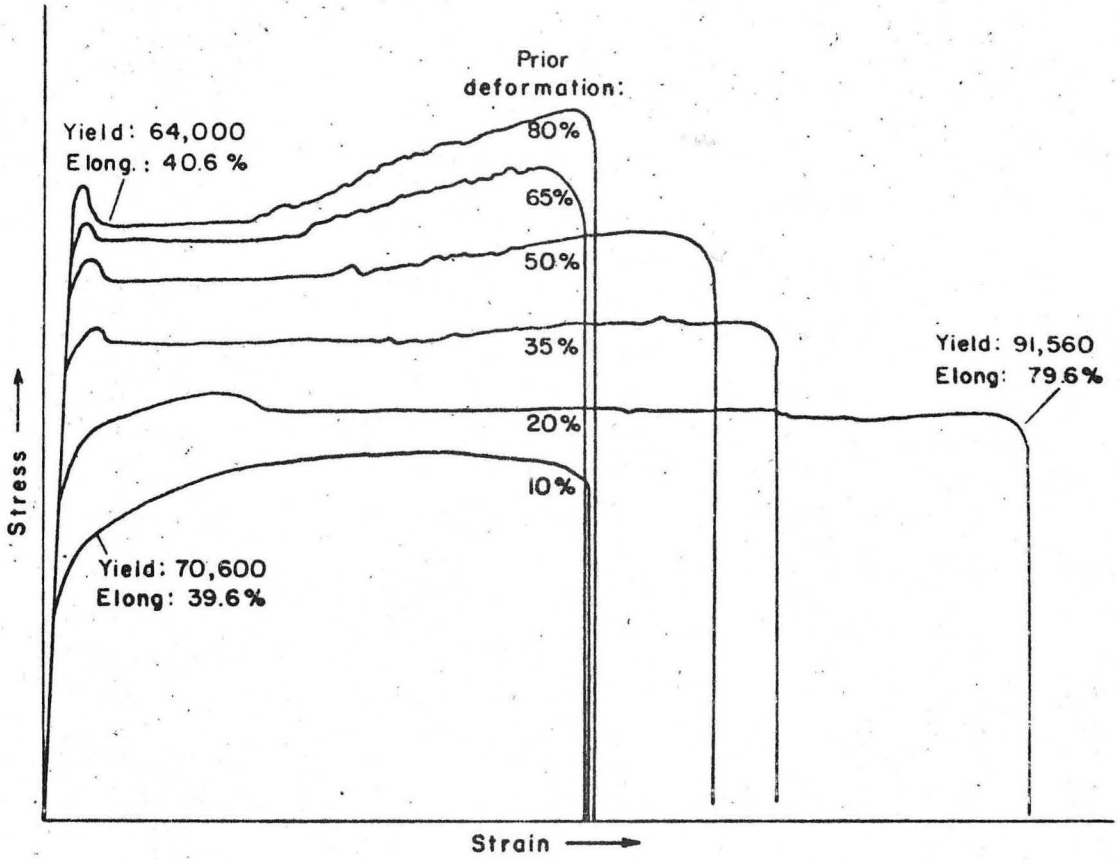
XBL 6911-6517

Figure 49



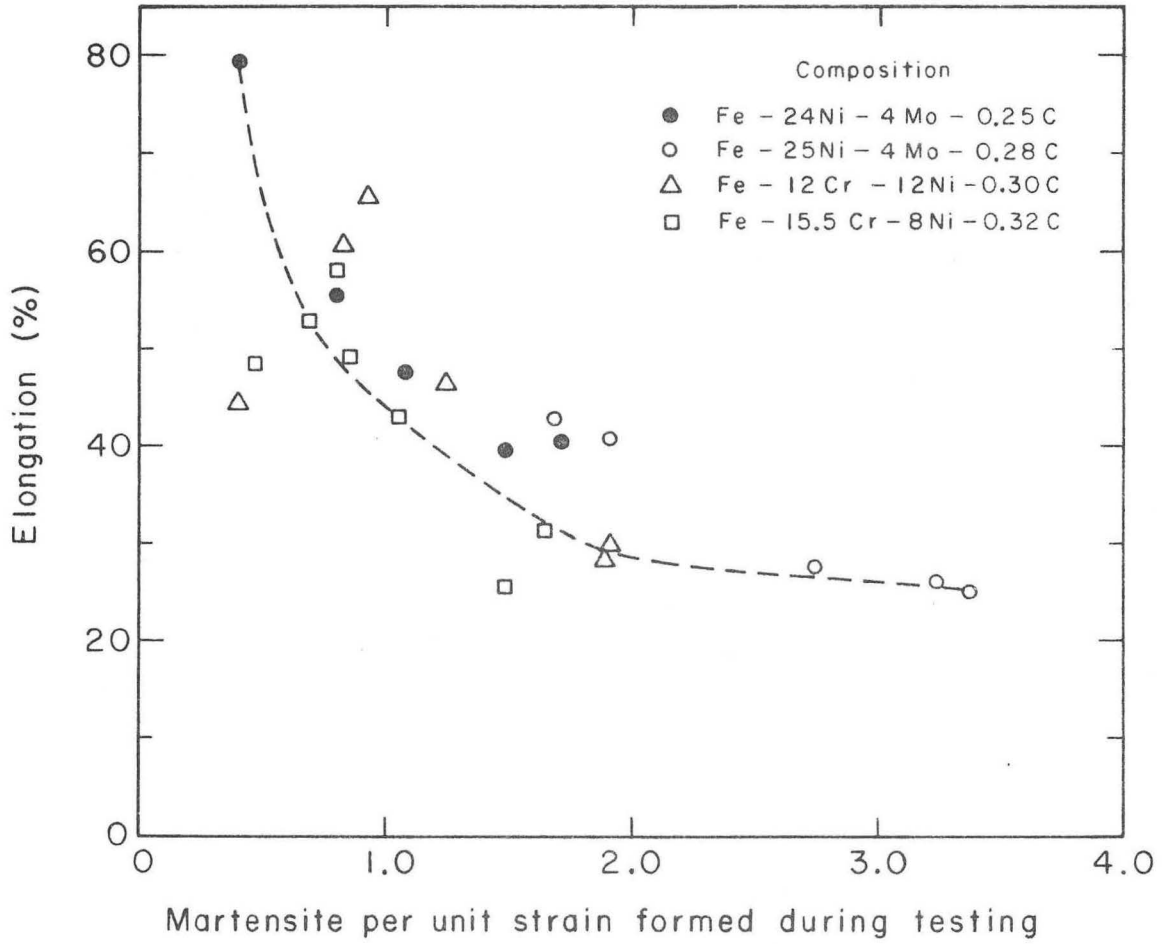
XBL 6911-6516

Figure 50



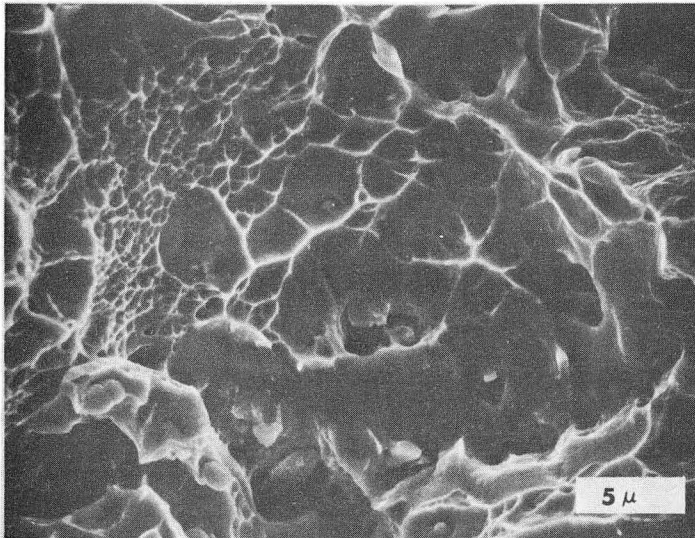
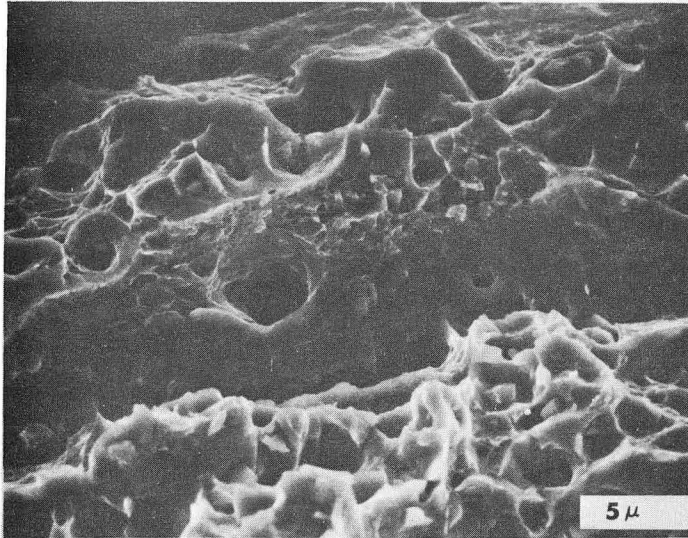
XBL 6911-6515

Figure 51



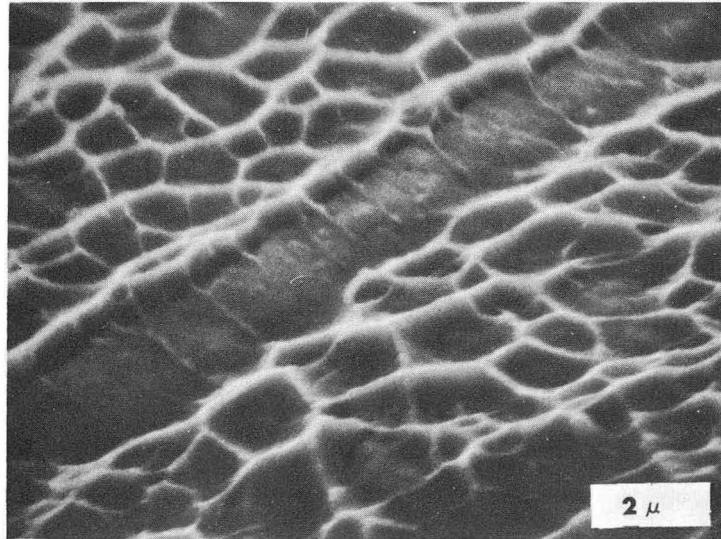
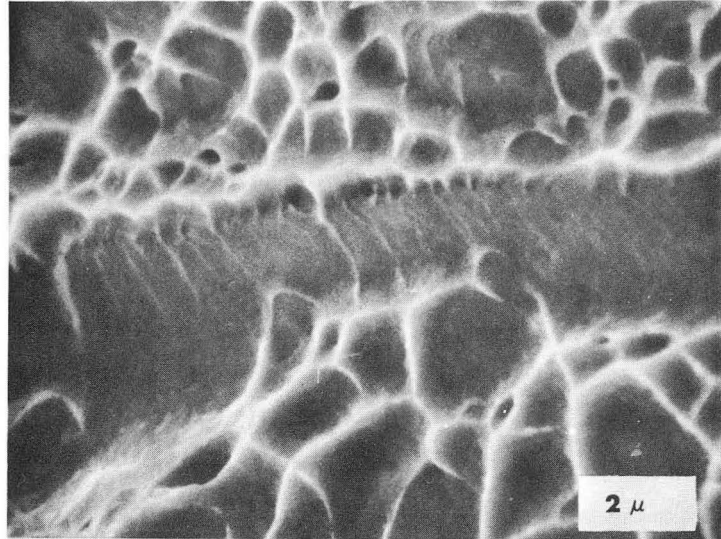
XBL695-2863

Figure 52



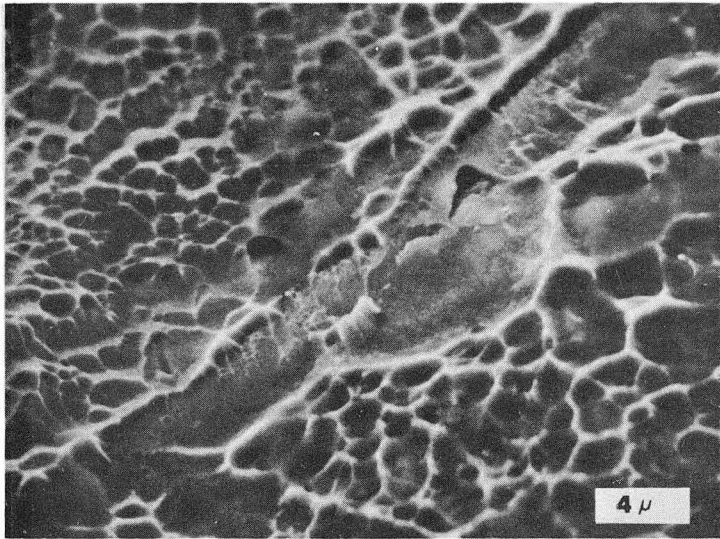
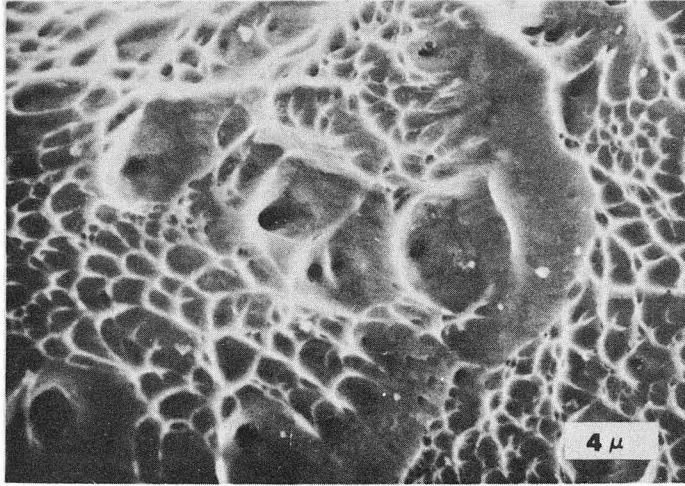
XBB 6911-7151

Figure 53



XBB 6911-7150

Figure 54



XBB 6911-7152

Figure 55

LEGAL NOTICE

This report was prepared as an account of Government sponsored work. Neither the United States, nor the Commission, nor any person acting on behalf of the Commission:

- A. Makes any warranty or representation, expressed or implied, with respect to the accuracy, completeness, or usefulness of the information contained in this report, or that the use of any information, apparatus, method, or process disclosed in this report may not infringe privately owned rights; or*
- B. Assumes any liabilities with respect to the use of, or for damages resulting from the use of any information, apparatus, method, or process disclosed in this report.*

As used in the above, "person acting on behalf of the Commission" includes any employee or contractor of the Commission, or employee of such contractor, to the extent that such employee or contractor of the Commission, or employee of such contractor prepares, disseminates, or provides access to, any information pursuant to his employment or contract with the Commission, or his employment with such contractor.